

Ingeniería e Investigación
Journal
Abbreviated Journal Title: **Ing. Investig.**

Editor-in-chief
Andrés Pavas, Ph.D.

Editorial Assistants
Fabián Hernando Ríos, B. Eng.
Ingri Gisela Camacho

Editorial Board
Paulo César Narváez Rincón, Ph.D.
Universidad Nacional de Colombia - Bogotá
Julio Esteban Colmenares, Ph.D.
Universidad Nacional de Colombia - Bogotá
Luis Fernando Niño, Ph.D.
Universidad Nacional de Colombia - Bogotá
Óscar Germán Duarte, Ph.D.
Universidad Nacional de Colombia - Bogotá
Jaime Salazar Contreras, M.U.
Universidad Nacional de Colombia - Bogotá
Ignacio Pérez, Ph.D.
Escuela Colombiana de Ingeniería - Colombia
Nelly Cecilia Alba, Ph.D.
Universidad Autónoma de Occidente - Colombia
Heberto Tapias García, Ph.D.
Universidad de Antioquia - Colombia
Ricardo Llamasa Villalba, Ph.D.
UIS - Bucaramanga - Colombia
Gustavo Bolaños, Ph.D.
Universidad del Valle - Colombia
Dora Ángela Hoyos Ayala, Ph.D.
Universidad de Antioquia - Colombia
Lourdes Zumalacárregui, Ph.D.
Ciudad Universitaria José Antonio Echeverría -
Cujae, Cuba
Federico Méndez Lavielle, Ph.D.
Universidad Nacional Autónoma de México -
México
Mauricio Camargo, Ph.D.
Université de Lorraine - France
Laure Morel, Ph.D.
Université de Lorraine - France
Andrés Romero Quete, Ph.D.
Universidad Nacional de San Juan
San Juan - Argentina
Víctor Berrera Núñez, Ph.D.
Data Analytics Senior Manager - PwC
México D.F. - México

Frequency
Quarterly, 3 issues per year
April, August and December

Cover Layout
Carlos Andrés Ortiz Valle

Proofreader
José Daniel Martínez

Layout Artist
Patricia Chávez R.

Photography
Mauricio Morales Pérez

For additional information contact
revii_bog@unal.edu.co
Bogotá - Colombia
August - 2021

Table of Contents

Editorial

Agricultural Engineering

Effect of Storage Temperature and Maturity Stage on the Postharvest Period of 'Horvin'
Plums (*Prunus domestica* L.)
Javier G. Álvarez-Herrera, Yuli Alexandra Deaquiz, and Ximena Rozo-Romero

Chemical Engineering / Food Engineering / Environmental Engineering

Study of Carbohydrate Hydrolysis From Arracacha Roots (*Arracacia Xanthorrhiza* Bancroft)
to Produce Fermentable Sugars
*Darwin Carranza-Saavedra, Jorge A. Alvarado-Núñez, José F. Solanilla-Duque, and
Claudia P. Valenzuela-Real*
Phenolic Compounds, Antioxidant Capacity, and Protein Content of Three Varieties of
Germinated Quinoa (*Chenopodium quinoa* Willd)
*David Choque-Quispe, Carlos A. Ligarda-Samanez, Betsy S. Ramos-Pacheco, Saida
Leguía-Damiano, Miriam Calla-Florez, Lourdes M. Zamalloa-Puma, and Luisa
Colque-Condeña*
Removal of Pb(II) in Aqueous Solutions Using Synthesized Zeolite X from Ecuadorian Clay
*Daniel F. Medina-Rodríguez, Dely M. San Martín-Torres, Carmen M. López de
García, Luis V. García-Berfon, Silvio D. Aguilar-Ramírez, Ximena V. Jaramillo-Fierro,
Daniel J. Rosado-Alcarria, and Adriana L. García-López*

Civil Engineering / Sanitary Engineering

Comparative Study of Theoretical and Real Deflection of Simple and Reinforced Concrete
Joists
*Socrates P. Muñoz-Perez, Angel A. Ruiz-Pico, Juan M. Anton-Perez, and Dandy B.
Roca-Loayza*

Industrial Engineering

A Novel Dynamic and Fuzzy Value Stream Mapping (DFVSM): System Dynamics and
Fuzzy Logic Integration
Roberto Baeza-Serrato
Selection Criteria for Sustainable Suppliers in the Supply Chain of Copper Mining in Chile
Orlando Gahona-Flores

Mechanical Engineering, Mechatronics, and Materials Science

Multimetric Analysis of a Simulated Mixed Traffic of Motorcycles and Automobiles: Flow,
Energy, CO₂, and Costs
*Fábio Santana Magnani, Paulo D'Ávila Garcia Neto, Fernando Wesley Cavalcanti de
Araújo, Alcides Luiz dos Anjos Hora, and Daniel Arraes de Alencar Valença*

Education in Engineering

The Gender Gap in Engineering Programs in Colombia
Nancy E. Hamid-Betancur and María C. Torres-Madronero

Instructions for Authors

**Facultad de Ingeniería
Universidad Nacional de Colombia**

María Alejandra Guzmán Dean
Camilo Andrés Cortés Guerrero
Vice Dean of Research and Extension
Jesús Hernán Camacho Tamayo
Vice Dean of Academic Affairs
Sandra Liliana Rojas Martínez
Director of the Students Welfare Service

Scientific Committee

Fabio González, Ph.D.
Universidad Nacional de Colombia, Bogotá
Miguel J. Bagajewicz, Ph.D.
University of Oklahoma, USA
Jayant Rajgopal, Ph.D.
University of Pittsburgh, USA

Ethical Committee

Óscar Fernando Castellanos, Ph.D.
Universidad Nacional de Colombia - Bogotá
Jullio César Cañón, Ph.D.
Universidad Nacional de Colombia - Bogotá

**Papers published in *Ingeniería e Investigación*
journal are abstracted/indexed in**

- Science Citation Index Expanded (SciSearch®), Clarivate Analytics
- Scopus - Elsevier
- Scientific Electronic Library Online - SciELO, Colombia
- Chemical Abstract
- Índice de Revistas Latinoamericanas en Ciencias Periódica
- Redalyc-Red de Revistas Científicas de América Latina y el Caribe, España y Portugal
- Dialnet
- Sistema Regional de Información en Línea para Revistas Científicas de América Latina, El Caribe, España y Portugal - Latindex
- Ebsco Publishing
- DOAJ - Directory of Open Access Journals
- Redib - Red Iberoamericana de Innovación y Conocimiento Científico

Ingeniería e Investigación journal was created in 1981. This is an entity in charge of spreading the teaching, scientific and technical research developed in the Universidad Nacional de Colombia's Engineering Faculty and other national and international institutions. *Ingeniería e Investigación journal* deals with original, unedited scientific research and technological developments in the various disciplines related to engineering. *Ingeniería e Investigación journal* contributes towards the development of knowledge, generating a global impact on academia, industry and society at large, through an exchange of knowledge and ideas maintaining a set of serious and recognized quality standards.

The content of the articles published in this journal does not necessarily reflect the opinions of the Editorial Team. These texts can be totally or partially reproduced provided a correct citation of the source.

Ingeniería e Investigación journal publications are developed for the academic community who is interested in research and engineering knowledge development. We invite readers to be part of this journal and participate either as authors, peer reviewers or subscribers.

For additional information contact:
www.revistas.unal.edu.co/index.php/ingenv
E-mail: revii_bog@unal.edu.co
Tel: 57(1) 3 16 5000 Ext. 13674

Tabla de Contenido

Editorial

Ingeniería Agrícola

Efecto de la temperatura de almacenamiento y el estado de madurez sobre la poscosecha de ciruela 'Horvin' (*Prunus domestica* L.)

Javier G. Álvarez-Herrera, Yuli Alexandra Deaquiz y Ximena Rozo-Romero

Ingeniería Química, Ambiental, y de Alimentos

Estudio de hidrólisis de carbohidratos en raíces de Arracacha (*Arracacia Xanthorrhiza* Bancroft) para producir azúcares fermentables

Darwin Carranza-Saavedra, Jorge A. Alvarado-Núñez, José F. Solanilla-Duque y Claudia P. Valenzuela-Real

Compuestos fenólicos, capacidad antioxidante y contenido proteico de tres variedades de quinoa germinada (*Chenopodium quinoa* Willd)

David Choque-Quispe, Carlos A. Ligarda-Samanez, Betsy S. Ramos-Pacheco, Saida Leguía-Damiano, Miriam Calla-Florez, Lourdes M. Zamalloa-Puma y Luisa Colque-Condeña

Remoción de Pb(II) en soluciones acuosas usando zeolita X sintetizada a partir de arcilla ecuatoriana

Daniel F. Medina-Rodríguez, Dolly M. San Martín-Torres, Carmen M. López de García, Luis V. García-Berfon, Silvio D. Aguilar-Ramírez, Ximena V. Jaramillo-Fierro, Daniel J. Rosado-Alcarria y Adriana L. García-López

Ingeniería Civil y Sanitaria

Estudio comparativo de la deflexión teórica y real de viguetas de concreto simple y reforzado

Socrates P. Muñoz-Perez, Angel A. Ruiz-Pico, Juan M. Anton-Perez y Dandy B. Roca-Loayza

Ingeniería Industrial

Un novedoso Value Stream Mapping dinámico y difuso (DFVSM): integración de dinámica de sistemas y lógica difusa

Roberto Baeza-Serrato

Criterios de selección de proveedores sostenibles en la cadena de suministro de la minería del cobre en Chile

Orlando Gahona-Flores

Ingeniería Mecánica, Mecatrónica y Ciencia de los Materiales

Análisis multimétrico de un tráfico mixto simulado de motocicletas y automóviles: flujo, energía, CO₂ y costos

Fábio Santana Magnani, Paulo D'Ávila Garcia Neto, Fernando Wesley Cavalcanti de Araújo, Alcides Luiz dos Anjos Hora y Daniel Arraes de Alencar Valença

Educación en Ingeniería

La brecha de género en los programas de ingeniería en Colombia
Nancy E. Hamid-Betancur y María C. Torres-Madronero

Instrucciones para Autores (Inglés)

Effect of Storage Temperature and Maturity Stage on the Postharvest Period of 'Horvin' Plums (*Prunus domestica* L.)

Efecto de la temperatura de almacenamiento y el estado de madurez sobre la poscosecha de ciruela 'Horvin' (*Prunus domestica* L.)

Javier G. Álvarez-Herrera¹, Yuli Alexandra Deaquiz², and Ximena Rozo-Romero³

ABSTRACT

Plums are classified as a climacteric fruit with a high respiration rate between the end of their development and the start of the ripening process, thus making it necessary to apply techniques to preserve the organoleptic characteristics required for the product to have good market acceptance. The aim of this study was to evaluate the effect of harvest maturity (states 2, 3, 4, and 5) and storage temperature (2, 4, and 18 °C) on the organoleptic and physicochemical quality and post-harvest storage duration of 'Horvin' plums. The experimental design was completely randomized with a 4 x 3 factorial arrangement. The first factor corresponded to the stage of maturity, and the second one to refrigeration temperatures, for a total of 12 treatments. Every three or four days, fruit peel color, accumulated mass loss, respiratory intensity, firmness, pH, total titratable acidity, and total soluble solids were measured every during storage. Measurements were taken until the fruits lost their organoleptic quality. For most of the measured variables, the fruits stored at 2 °C and harvested in maturity stage 5 maintained the best post-harvest quality during storage. The fruits without refrigeration only reached 10 days, while the fruits stored at 4 °C and 2 °C maintained quality of consumption for 24 and 31 days, respectively. Maturity stage 5 presented the highest values of accumulated mass loss, pH, total soluble solids, color index, maturity index, and respiratory intensity.

Keywords: storage, firmness, climacteric, fruit quality, refrigeration

RESUMEN

La ciruela está clasificada como un fruto climatérico con una alta tasa de respiración entre el final de su desarrollo y el comienzo de la maduración, por lo que es necesario aplicar técnicas que permitan conservar las características organolépticas necesarias para que el producto tenga buena aceptación en el mercado. El objetivo de este estudio fue evaluar el efecto de la madurez de cosecha (estados 2, 3, 4 y 5) y la temperatura de almacenamiento (2, 4 y 18 °C) sobre la calidad organoléptica y fisicoquímica y el tiempo de duración postcosecha de ciruelas 'Horvin'. Se utilizó un diseño experimental completamente al azar con un arreglo factorial de 4 x 3. El primer factor correspondió al estado de madurez y el segundo a las temperaturas de refrigeración, para un total de 12 tratamientos. Cada tres o cuatro días se midieron color, pérdida de masa, intensidad respiratoria, firmeza, pH, acidez total titulable y sólidos solubles totales en almacenamiento. Se realizaron mediciones hasta que los frutos perdieron su calidad organoléptica. En la mayoría de las variables medidas, los frutos almacenados a 2 °C y cosechados en estado de madurez 5 conservaron las mejores características postcosecha durante el almacenamiento. Los frutos sin refrigeración tan solo alcanzaron 10 días, mientras que los frutos almacenados a 4 °C y 2 °C mantuvieron la calidad de consumo por 24 y 31 días, respectivamente. El estado de madurez 5 presentó los mayores valores de pérdida de masa, pH, sólidos solubles totales, índice de color, índice de madurez e intensidad respiratoria.

Palabras clave: almacenamiento, firmeza, climaterio, calidad del fruto, refrigeración

Received: September 29th, 2019

Accepted: March 2nd, 2021

¹Agricultural Engineer, M.Sc. in Agricultural Sciences and Ph.D. in Agricultural Sciences, Universidad Nacional de Colombia. Affiliation: Associate Professor, Universidad Pedagógica y Tecnológica de Colombia (Boyacá, Colombia), Grupo de Investigaciones Agrícolas, GIA, Colombia. E-mail: javier.alvarez@uptc.edu.co

²Agronomist Engineer and M.Sc. in Plant Physiology, Universidad Pedagógica y Tecnológica de Colombia (Boyacá, Colombia). Affiliation: Professor, Fundación Universitaria Juan De Castellanos, Tunja, Colombia, Grupo de Investigaciones Agrícolas, GIA, Colombia. E-mail: yulideaquiz@gmail.com

³Agronomist Engineer and M.Sc. in Plant Physiology, Universidad Pedagógica y Tecnológica de Colombia (Boyacá, Colombia). Affiliation: Coordinator, Institución educativa rural departamental Simón Bolívar, Lenguaque, Colombia. E-mail: ximenarozo1@gmail.com

How to cite: Álvarez-Herrera, J., Deaquiz, Y., and Rozo-Romero, X. (2021). Effect of Storage Temperature and Maturity Stage on the Postharvest Period of 'Horvin' Plums (*Prunus domestica* L.). *Ingeniería e Investigación*, 41(2), e82530. 10.15446/ing.investig.v41n2.82530

Introduction

'Horvin' plum fruits have great acceptance in markets because they have excellent organoleptic and nutritional characteristics. Because it is a climacteric fruit, it can be harvested at physiological maturity, given that maturation continues during the postharvest period (Parra, Hernández, and Camacho, 2008). There are currently very little studies that have determined the optimum harvest maturity of 'Horvin' plums. In most cases, these determinations have been carried out subjectively, based only on the size and peel color of the fruits, resulting in inconsistent organoleptic characteristics when marketing the product (Kaur, Sawhney, and Jawandha, 2018). This is the cause for the negative



perception of the cultivar in a market with high demands and requirements regarding fruit quality (Kader, 2008).

The ripening process in plums is closely related to quality because it involves a series of biochemical, physiological, and structural changes that make the fruits more attractive for consumers (Rozo-Romero, Álvarez-Herrera, and Balaguera López, 2015). These processes involve an increased production of ethylene and the permeability of cell membranes, as well as chemical transformations that affect phenolic compounds, organic acids, pigments, and pectins, which modify the organoleptic characteristics of the fruits (Saltveit, 2019).

Minas, Crisosto, Holcroft, Vasilakakis, and Crisosto (2013) reported that the postharvest shelf-life of plums is very short and hardly exceeds seven days in the absence of management, given its moderate respiratory rate (10 to $20 \text{ mg CO}_2 \cdot \text{kg}^{-1} \cdot \text{h}^{-1}$) and high production of ethylene, which accelerates the metabolic processes that affect maturation (Kader, 2002). Therefore, it is necessary to maintain an optimal temperature during the postharvest period, which delays ripening and preserves quality because the respiration rate increases with temperature, thus leading to the acceleration of ripening and senescence in fruits (Iqbal, Rodríguez, Mahajan, and Kery, 2009).

Similarly, the maturity stage of collected fruits has a great influence on their postharvest storage duration and marketing because fruits undergo internal and external changes triggered by the release of ethylene (Larsen and Vangdal, 2013). These changes are physical, chemical, and physiological, such as loss of mass and firmness and flesh softening, which expose the external structures to environmental conditions. A reduction also occurs in the contents of starch and organic acids, along with an increase in the contents of sugars (Saltveit, 2019).

In this regard, Álvarez Herrera *et al.* (2015) stated that the market conditions of 'Horvin' plums and fresh consumption define the degree of maturation (color) at the time of harvest because the eating quality of the fruit depends on the degree of maturation at this point. The greater the degree of maturation, the shorter the shelf-life, thus resulting in the need for refrigeration to maintain quality in the postharvest period (Guerra and Casquero, 2008).

Therefore, the objective of this study was to evaluate the effect of harvest maturity (states 2, 3, 4, and 5) and storage temperature (2, 4, and 18°C) on the organoleptic and physico-chemical quality of 'Horvin' plums (*Prunus domestica* L.).

Materials and Methods

Location: This study was carried out in the plant physiology laboratory of the Universidad Pedagógica y Tecnológica de Colombia (Boyacá, Colombia), Tunja branch. The fruits were collected from a commercial crop in the municipality of Tuta, located at an altitude of 2600 masl, $05^\circ 41' 36''$ north latitude and $73^\circ 13' 51''$ west longitude, with an average rainfall of 935 mm and a temperature ranging between 12 and 14°C , as well as an average relative humidity of 70%.

Ecotype: 'Horvin' plums (*Prunus domestica* L.) were used. The fruits were collected at four maturity stages (2, 3, 4, and 5) according to their color (Álvarez-Herrera, Rozo-Romero, and Reyes, 2015). Fruits of uniform size, free of mechanical damage, and in good phytosanitary conditions were chosen. Two cold refrigerators with controlled temperatures and relative humidity (SuperNórdico, 9, and 12 cubic feet) were used for the storage. Temperature in the refrigerators was verified with a thermometer during the experiment.

Experimental Design: a completely randomized design with a 4×3 factorial arrangement was used. The first factor corresponded to the stage of maturity (2: 75% green - 25% red; 3: 50% green - 50% red; 4: 25% green - 75% red; and 5: 100% red), and the second factor to the refrigeration temperatures (2°C , 4°C , and ambient 18°C). Hence, a total of 12 treatments, each with 4 replications corresponding to 48 experimental units. Each unit had 900 g of fruits (45 fruits of 18 g, approximately), which were disinfected with a solution of 1% sodium hypochlorite after harvest. Then, they were air-dried for 30 minutes and packed in two Styrofoam containers with a capacity of up to 450 g of fruit for each experimental unit.

Response variables: Every three or four days, mass loss, color, and respiratory intensity, firmness, pH, total titratable acidity, and total soluble solids were measured. The measurements were taken until the fruits lost their organoleptic quality.

Mass loss was determined by measuring the fresh mass with a 0,01g precision electronic scale, an Acculab VIC 612 (Sartorius Group, Germany). Fruit firmness was measured with a PCE-PTR200 (PCE-Iberica, Spain) digital penetrometer, with an accuracy of 0,05 N. Peel color was determined with a CR 300 Minolta digital colorimeter (Minolta Co., Japan) according to the CIELab system parameters L^* , a^* , and b^* . Three readings were taken on the equatorial axis of two fruits per evaluation date at the same point. L^* indicates lightness, where 0 is black and 100 white; a^* values < 0 indicate a trend towards green and values > 0 indicate red; b^* has the same range, but values < 0 indicate a tendency towards blue, and values > 0 towards yellow (Pathare *et al.*, 2013). The color index (CI) was calculated with Equation 1.

$$CI = (1000 \times a^*) / (L^* \times b^*) \quad (1)$$

To determine the pH, approximately 1 mL of juice was diluted to 50 mL with distilled water, and the pH was measured with a HANNA HI8424 potentiometer (Hanna Instruments, Spain), previously calibrated with buffer solutions of pH 7,0 and 4,0. In a juice sample extracted from three fruits of each EU, the total soluble solids (TSS) were measured in degrees Brix with a HANNA HI 96803 digital refractometer (Hanna Instruments, Spain), with a range of 0-85% and 0,1 $^\circ\text{Brix}$ accuracy. The total titratable acidity (TTA) was determined following the methodology used by Rozo-Romero *et al.* (2015). The maturity index (MI) was expressed as the TSS/TTA ratio.

Additionally, the respiratory rate was determined (RR; $\mu\text{L CO}_2 \text{ kg}^{-1} \text{ h}^{-1}$) by placing approximately 200 g of plum fruits in 250 cm^3 SEE BC-2000 airtight chambers for 1 hour. Subsequently,

CO₂ evolution was determined with a VER CO₂-BTA sensor and a LabQuest2 interface system (Vernier Software and Technology, United States).

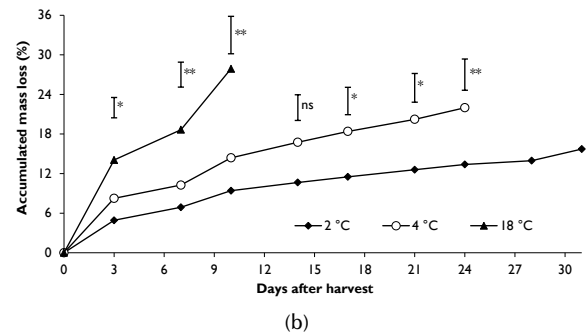
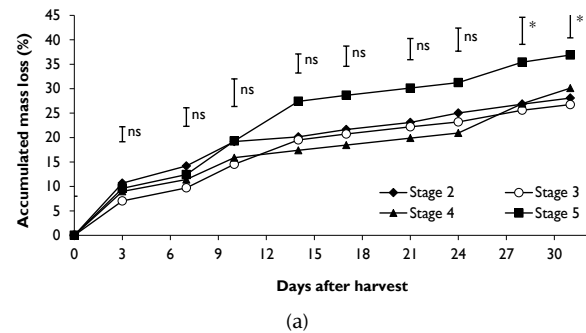
Data analysis: A Shapiro-Wilk normality test was carried out on the data, followed by an analysis of variance. Atypical and outlier values were removed from the data set. The Tukey comparison test ($p \leq 0,05$) was used to determine statistical differences between treatments in order to classify them. The analyses were performed using the statistical software SAS v. 9,2e (SAS Institute Inc., Cary, NC).

Results and Discussion

Loss of mass: significant differences were only observed towards the end of the storage period, at 28 and 31 days after harvest (dah) (Figure 1a). Maturity state 5 had the highest loss of mass after 10 dah, and reached 36,8%, compared to the other maturity stages, which, at the end of the postharvest period, had loss of mass ranging from 28,1% to 30,1%. The loss of mass increased almost linearly throughout the postharvest period, and fruits harvested in the earliest maturity stage had the lowest rates, similar to those found by Guerra and Casquero (2008). However, they obtained lower values of mass loss (12%) due to the fact that all the fruits were refrigerated.

As for the storage temperature, significant differences were seen between the fruits stored at 18 °C, with a mass loss of 27,9% at 10 dah, and those with 9,4% and 14,3% when stored at 2 and 4 °C, respectively (Figure 1b), which means that the loss of mass in the fruits stored at high temperatures resulted from the fruits' regulating the temperature through water evaporation, leading to severe dehydration and deterioration in their external appearance, thereby reducing their commercial value (Minas *et al.*, 2013). In this regard, Parra *et al.* (2008) reported mass loss values of 23% in Horvin plums stored at 18 °C at 11 dah, while the fruits subjected to 4 °C obtained a cumulative mass loss of 3,2% at 31 dah. Nevertheless, the evaluated plums stored at 4 °C only reached 24 days, where their mass loss was higher, probably due to the low relative humidity, causing the fruits to dehydrate and lose their commercial quality.

Mass loss was greater as the storage temperature increased, probably due to the increase in the vapor pressure deficit (VPD), which caused greater moisture loss (Díaz-Pérez, 2019). When the fruits were refrigerated, they maintained a very low loss of mass rate, with reductions of 15% and 12% for 'President' and 'Royal Rosa' plums, respectively (Martínez-Romero *et al.*, 2019). Likewise, the respiration process was not inhibited, and the low relative humidity directed the exchange of water from the fruits to the environment (Palou, Crisosto, Garner, and Basinal, 2003), which coincides with Larsen and Vangdal (2013), who reported a decrease in the respiration rate of 9 plum cultivars stored at 2 °C and, consequently, a loss of mass lower than that of fruits stored at 6 °C.



Note: The vertical bars indicate the minimum significant difference according to the Tukey test ($p \leq 0,05$). *statistical differences at 5%, **statistical difference at 1%, ns: no differences.

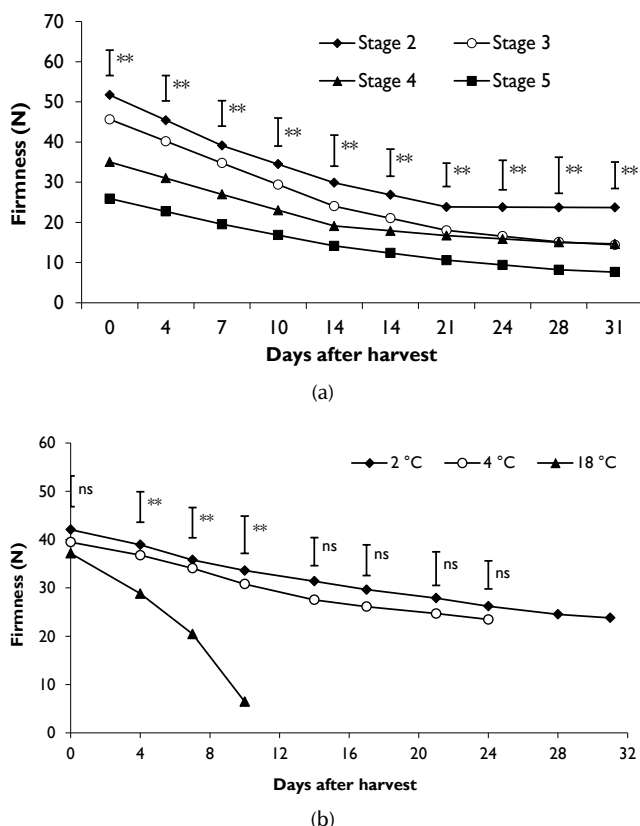
Figure 1. Effect of a) the maturity stage and b) storage temperatures on the accumulated loss of mass of plum fruits during postharvest cold-storage.

Source: Authors

Firmness: for the maturity factor, it was observed that, as the storage time elapsed, the fruits of all the treatments showed loss of firmness, possibly due to the action of hydrolase enzymes, which are induced by ethylene (Botton, Tonutti, and Ruperti, 2019). This occurs naturally in climacteric fruits such as 'Horvin' plums. These enzymes, such as polygalacturonase (PG), pectinmethylesterase (PME), β -galactosidase, and pectatelyase (PL), degrade the polymeric carbon hydrates, mainly pectin and hemicellulose (Sañudo-Barajas *et al.*, 2019), thus weakening of cell walls. In all maturity stages, the firmness decreased considerably until 14 dah, and, from this day, the loss of firmness was slower, (Figure 2a), which is probably due to the intensive loss of water in the cells of the fruit during the first days of storage. The fruits that maintained the firmness for the longest time were those stored in maturity state 2, while the loss of firmness was highest in maturity stage 5 because, during the postharvest period, the production of ethylene is greater, as it accelerates the maturation and senescence process.

As for the effect of the temperature on fruit firmness, significant differences were observed between the fruits stored at 18 °C and the refrigerated fruits (2 and 4 °C) from 7 dah, with an average value of 20,46 N for the first, as compared to higher data for the refrigerated fruits (35,79 N at 2 °C and 34,07 N at 4 °C). This difference could be observed throughout the experiment (Figure 2b). At 10 dah, there were firmness values of 30,81 N for the fruits stored at 4 °C, as well

as 6,46 N for the fruits stored at 18 °C. These results agree with those reported by Parra *et al.* (2008) for 'Horvin' plums stored at 18 °C, where firmness decreased drastically during the postharvest period. Likewise, Wang, Pan, Wang, Hong, and Cao (2016) found that plum fruits stored at 0 and 2 °C managed to maintain firmness for a longer time, while fruits stored at higher temperatures showed a drastic softening.



Note: The vertical bars indicate the minimum significant difference according to the Tukey test ($p \leq 0,05$). *statistical differences at 5%, **statistical difference at 1%, ns: no differences.

Figure 2. Effect of a) the maturity stage and b) storage temperatures on the firmness of plum fruits during postharvest.

Source: Authors

Skin color: color showed significant differences in almost all sampling points with respect to the stage of maturity, since it was the parameter by which the fruits were classified. Therefore, maturity stage 2 plums demonstrated the highest lightness values, with the lowest value in maturity stage 5 at all sampling points (Table 1). This happens because, as fruits ripen, they lose lightness due to the oxidation process of tissues and water loss (Singh, Singh, and Swinny, 2012). As for the a^* values, stage 4 had the highest (28,3) 28 days after harvesting, compared to stage 2, where a value of -17,29 was obtained, indicating that the color change from green to red was more noticeable in stage 4 than in the other stages, which probably occurred because, during the ripening of fruits, chloroplasts and thylakoid membranes disintegrate, a process that generates a rapid loss of chlorophyll and green color in plum tissues, which is increased by temperature (Wu *et al.*, 2011), thus resulting in the synthesis of red pigments

or anthocyanins in the plums. This change occurs in greater proportion in fruits in advanced stages of maturity because it takes longer for physiological changes to occur, such as degradation of chlorophylls and the unmasking of pigments.

As for the temperature factor, there were significant differences in most of the sampling points for the lightness of the plum fruits (Table 1), which showed higher values in the fruits stored at 2 °C. In plums, the most representative value for the coloring of the epidermis is the a^* value, for which there were no significant differences in most of the sampling points. A significant difference was only observed at 10 dah between the fruits stored at room temperature (which had lost commercial quality at this time) and the refrigerated fruits, demonstrating that refrigerated storage delays the color change from green to red, although there was no difference between the two refrigeration temperatures, according to Xu *et al.* (2020), who state that treatments with low temperatures reported the highest values of anthocyanins. In addition, refrigeration delays the respiratory process and, therefore, the production of ethylene, which in turn produces changes in pH and thus promotes the action of chlorophyllases (Singh and Singh, 2013).

In general, the color index was higher in stage 5 (100% red) and in the fruits stored at ambient temperature (Table 1), although only significant differences were obtained in the refrigerated fruits after 24 dah with CI values of 29,9 and 16,5, for 4 and 2 °C treatments, respectively. Then the 4 °C treatment lost commercial quality, indicating that, after 24 days, the color index becomes similar and independent of the storage temperature, according to what was reported by Pan *et al.* (2016) in three plum varieties subjected to ethylene applications under storage conditions. These data show the typical tendency of ripening fruit because, as the storage time progresses, degreening occurs, which, in some fruits, is related to the degradation of chlorophyll during maturation (Hussain, Suradkar, Wani, and Dar, 2015).

pH: the highest values were obtained in plum fruits harvested at maturity stage 5, with significant differences throughout the entire storage (Table 2), contrary to what was found by Álvarez-Herrera *et al.* (2015) in plum fruits treated with ethylene, where the different maturity stages had similar pH values. This implies that the maturity state in which the fruits are harvested is important for their organoleptic properties, even during the postharvest life of the fruits.

As for the temperature factor, a pH of 4,81 was observed at 10 dah in the fruits stored at 18 °C, as compared with values of 4,16 and 4,27 obtained in fruits stored at 2 and 4 °C, respectively, indicating that the fruits had higher pH when stored at ambient temperature (Table 2), in comparison with their refrigerated counterparts.

Table 1. Effect of maturity stage and storage temperature on skin color of 'Horvin' plum fruits

Parameters	dah	Maturity Stage				Storage Temperature (°C)		
		2	3	4	5	2	4	18
L	0	73,13a	53,59b	35,27c	24,81d	48,68a	46,79a	44,63a
	3	51,28a	36,30b	25,85c	17,13c	35,34a	37,72a	24,86b
	7	49,34a	36,70b	24,08c	19,35c	38,98a	37,03a	21,10b
	10	46,95a	37,69b	23,55c	19,02c	43,12a	35,63b	16,66c
	14	55,36a	39,42b	24,30c	17,39c	36,51a	31,72b	N
	17	27,19a	44,64a	34,29a	42,08a	41,46a	32,64a	N
	21	62,33a	42,09b	27,60c	22,06c	43,07a	33,97b	N
	24	52,44a	40,62b	23,89c	16,58c	35,97a	30,80b	N
	28	63,30a	54,03a	31,00b	18,09b	41,60	N	N
	31	50,82a	32,04b	22,38b	23,84b	32,27	N	N
a*	0	-17,29c	16,96a	28,31a	13,96b	11,70a	10,33a	9,43a
	3	-1,25c	22,79ab	25,26a	12,77b	16,95a	11,93a	15,80a
	7	-2,80c	18,12ab	24,05a	11,19b	11,93a	12,10a	13,89a
	10	-0,02b	15,81a	19,29a	12,46ab	12,84a	14,41a	8,41b
	14	-2,20c	20,61ab	24,99a	13,19b	14,09a	14,20a	N
	17	2,32b	17,50a	20,10a	15,74a	13,88a	13,43a	N
	21	-1,16c	21,40a	23,52a	12,18b	13,18a	14,97a	N
	24	3,00c	22,49a	21,99a	11,03b	13,16a	16,10a	N
	28	1,67c	19,91a	25,16a	11,90b	14,66	N	N
	31	3,49c	18,70a	23,13a	12,07b	14,35	N	N
b*	0	47,15a	30,96b	18,04c	7,53d	28,02a	26,11a	23,62a
	3	32,02a	23,46b	15,31c	6,31d	23,15a	23,00a	11,67b
	7	33,81a	25,43ab	14,71bc	6,27c	27,63a	23,89a	8,64b
	10	29,84a	22,31ab	10,42bc	4,58c	24,64a	23,67a	2,07b
	14	38,67a	26,34b	14,76c	6,19d	23,20a	19,78b	N
	17	13,56a	19,66a	7,97a	12,67a	15,49a	11,44a	N
	21	39,34a	24,92b	13,70c	6,41c	23,46a	18,73a	N
	24	35,28a	25,70b	13,27c	5,07d	22,17a	17,49b	N
	28	38,75a	30,70a	16,71b	5,89b	23,01	N	N
	31	34,12a	15,74b	14,04b	9,03b	18,23	N	N
CI	0	-5,01d	10,22c	44,48b	74,74a	8,58a	8,46a	8,95a
	3	-0,76d	26,76c	63,85b	118,09a	20,72b	13,75b	54,46a
	7	-1,68d	19,42c	67,88b	92,28a	11,08b	13,68b	76,19a
	10	-0,01d	18,80c	78,61b	143,10a	12,08b	17,09b	243,87a
	14	-1,03d	19,85c	69,66b	122,51a	16,63a	22,63a	N
	17	6,29c	19,94bc	73,54a	29,53b	21,61a	35,97a	N
	21	-0,47c	20,40bc	62,21a	86,13a	13,04b	23,53a	N
	24	1,62c	21,54c	69,35b	131,24a	16,50a	29,89a	N
	28	0,68c	12,0c	48,56b	111,71a	15,32	N	N
	31	2,01c	37,08b	73,61a	56,07b	24,39	N	N

Note: dah: days after harvest; L: Lightness; a*: range from green to red; b*: range from blue to yellow; CI: color index; pH: potential hydrogen; TTA: Total titratable acidity; TSS: Total solids soluble; MI: Maturity index. N: no data for the loss of organoleptic quality. Means with different letters in the same row and classified by factor indicate significant differences between the factor levels according to the Tukey mean test ($p \leq 0,05$).

Source: Authors

Table 2. Effect of maturity stage and storage temperature on physical variables measured in 'Horvin' plum fruits

Parameters	dah	Maturity Stage				Storage Temperature (°C)		
		2	3	4	5	2	4	18
pH	0	3,42b	3,33b	3,99b	4,37a	3,53a	4,10a	4,11a
	3	3,59b	3,59b	4,06a	4,59a	3,93a	4,15a	4,32a
	7	3,71b	3,74b	4,12b	4,74a	4,14a	4,19a	4,47a
	10	4,04b	4,11b	4,24b	4,81a	4,16b	4,27b	4,81a
	14	4,22b	4,31b	4,33b	4,88a	4,19b	4,33a	N
	17	4,35a	4,40a	4,07b	4,63a	4,32a	4,17a	N
	21	4,45a	4,48a	3,46a	3,95a	4,42a	3,93b	N
	24	4,19a	4,23a	3,57b	4,06a	4,21a	3,89a	N
	28	3,42b	3,62ab	3,71ab	4,14a	3,81a	N	N
	31	3,40b	3,64b	3,80ab	4,19a	3,86a	N	N
TTA*	0	1,10a	1,22a	0,75b	0,76b	0,92a	0,96a	1,00a
	3	1,15ab	1,26a	0,97ab	0,96b	1,11ab	1,23a	0,92b
	7	1,21a	1,30a	1,19a	1,16a	1,30a	1,50a	0,85b
	10	0,99a	1,04a	1,03a	1,04a	1,14a	1,25a	0,52b
	14	0,77b	0,78b	0,86ab	0,93a	0,98a	1,01a	N
	17	0,91a	0,89a	0,96a	0,96a	1,01a	1,02a	N
	21	1,06a	1,00a	1,06a	0,99a	1,03a	1,03a	N
	24	1,00a	0,92a	0,99a	0,95a	0,98a	0,92a	N
	28	0,93a	0,84a	0,92a	0,90a	0,92	N	N
	31	0,96a	0,85a	0,93a	0,90a	0,90	N	N
TSS*	0	10,29bc	9,14c	11,69b	13,68a	11,01a	11,28a	11,32a
	3	10,83b	10,23b	11,85ab	13,63a	10,99a	11,85a	12,06a
	7	11,38b	11,33b	12,00ab	13,58a	10,98b	12,43a	12,81a
	10	11,79b	11,66b	12,08b	13,65a	11,34b	12,48a	13,31a
	14	12,21b	12,00b	12,15b	13,71a	11,70b	12,54ab	N
	17	12,60b	12,20b	12,41b	13,92a	12,21a	12,96a	N
	21	12,99a	12,39a	12,68a	14,14a	12,71a	13,38a	N
	24	12,66a	12,69a	13,46a	14,44a	13,14a	13,56a	N
	28	12,33a	12,98a	14,25a	14,75a	13,57	N	N
	31	12,37a	13,05a	14,39a	14,83a	13,75	N	N
MI	0	9,38b	7,46b	15,50a	17,91a	11,99a	11,69a	11,35a
	3	9,39b	8,09b	12,20a	14,18a	9,90a	9,63a	13,07a
	7	9,40a	8,68a	10,10a	11,72a	8,43b	8,31b	15,10a
	10	11,89a	11,17a	11,77a	13,08a	9,93b	9,98b	25,45a
	14	15,80a	15,31a	14,06a	14,76a	11,91b	12,46b	N
	17	13,77a	13,65a	12,89a	14,51a	12,14a	12,74a	N
	21	12,29a	12,36a	11,93a	14,27a	12,36a	13,02a	N
	24	12,71a	13,79a	13,57a	15,28a	13,45a	14,80a	N
	28	13,18a	15,49a	15,45a	16,39a	14,67	N	N
	31	12,93a	15,35a	15,40a	16,45a	15,23	N	N

Note: dah: days after harvest; L: Lightness; a*: range from green to red; b*: range from blue to yellow; CI: color index; pH: potential hydrogen; TTA: Total titratable acidity; TSS: Total solids soluble; MI: Maturity index. N: no data for the loss of organoleptic quality. Means with different letters in the same row and classified by factor indicate significant differences between the factor levels according to the Tukey mean test ($p \leq 0,05$).

Source: Authors

In this regard, it is known that, as fruits ripen, acids function as respiratory substrates (Saltveit, 2019). Therefore, pH changes match the variations in the coloration of the fruits, considering that hydrogen ions contribute to the degradation of chlorophyllases of plum fruits. The pH values showed an average correlation for the different treatments of 0,57, 0,55, 0,37 and 0,37 with the variables b^* , L^* , a^* , and CI , respectively. Furthermore, the state of ripeness of the fruits changed, with a consequent increase in pH that promoted the action of chlorophyllase, which generally contributes to the degradation of the chlorophyll (Koca, Karadeniz, and Burdurlu, 2007).

Total titratable acidity (TTA): a normal tendency was observed in the fruits at different stages of maturity, as shown in Table 2. Although the differences were not always statistically significant, the acidity was generally lower in the fruits harvested at maturity stage 5 (0,95%) than in the other states, as observed in all of the measuring points. The higher TTA average values were generally seen in maturity stages 2, 3, and 4 (1,00%, 1,01% and 0,96%, respectively), which may indicate that fruits that have lower maturity and a higher amount of organic acids for use as respiratory substrates have a better postharvest behavior and, therefore, a longer shelf-life (Batista-Silva *et al.*, 2018).

Highly significant differences were seen at all the sampling points from 3 dah for the temperature factor (Table 2), and there were no significant differences between the treatments with refrigeration at 2 and 4 °C. The TTA values ranged between 1,03% and 1,12% in fruits stored at 2 and 4 °C, respectively, which were higher than the average value obtained for the fruits stored at room temperature (0,80%), which confirmed the reduction in the metabolic processes due to the cooling effect (Larrigaudière, Candan, Ubach, and Graell, 2009).

As for the interaction between the temperature and stage of maturity, significant differences were only observed during the first 10 dah, since the less mature fruits have more TTA, as well as the aforementioned cooling effect, to maintain the pH in plum fruits. The TTA remained constant in the refrigerated fruits, whereas, in the fruits stored at 18 °C, it decreased by 48% during their postharvest life, which is due to the fact that organic acids present in the cells are degraded by the synthesis of other substances and the oxidation in the respiratory metabolism, a reaction that results in an increase in the respiratory rate (Saltveit, 2019). In this regard, Parra *et al.* (2008) found TTA decreases in plums stored at 4, 12, and 18 °C, showing differences between the refrigerated fruits and those stored at room temperature.

Total soluble solids (TSS): there were significant differences between the stages of maturity at all sampling points up to 17 dah (Table 2). The highest values were obtained in the fruits harvested at maturity stage 5 (14,03 °Brix), which matches the data reported by Ndou, Tinyani, Slabbert, and Sultanbawa (2019), who stated that fruits harvested in later stages of maturation have a higher TSS concentration than those collected in the early stages.

Regarding the temperature factor, there were significant differences between the fruits stored at 2 °C and the fruits stored at 4 and 18 °C from 7 to 14 dah. From 17 dah on, the refrigerated fruits did not show differences between temperatures of 2 and 4 °C. This behavior indicates that the TSS of the fruits remained constant for longer at a storage temperature of 2 °C. However, at the end of the postharvest period, these values increased slightly, similar to those found by Singh and Singh (2013) with plum fruits stored at 0 °C and a TSS increase only occurring on the fourth postharvest week. This increase in sugars was a product of the hydrolysis of starch and the synthesis of sucrose and gluconeogenesis (Farcuh, Rivero, Sadka, and Blumwald, 2018).

The results of this study are consistent with those reported by Parra *et al.* (2008), where the TSS values of plums stored at 4, 12, and 18 °C did not vary significantly throughout the storage period. There were no significant differences between treatments, which was attributed to the effect of the temperature, which decreases the speed of change in fruits, thus affecting the accumulation of sugars (Hussain *et al.*, 2015).

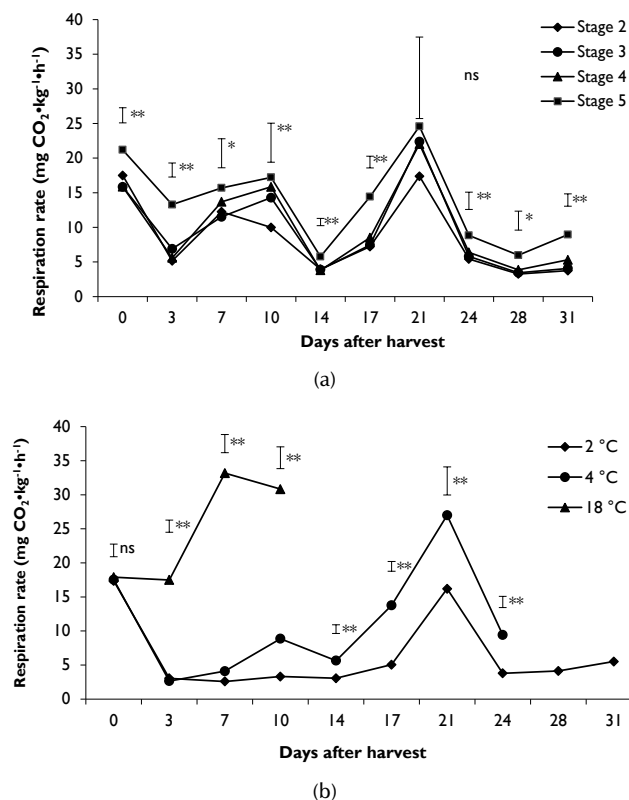
Maturity Index (MI): this variable showed significant differences for the maturity stages at the first two sampling points (Table 2). In general, the highest values were observed in the fruits at maturity stage 5, with an average of 14,20, while stages 2, 3, and 4 presented an average MI of 11,6, 12,04, and 13,95, respectively. This occurred because the fruits harvested in an immature state took longer to reach consumption maturity than those harvested closer to the optimum harvest point (Ndou *et al.*, 2019). The MI increased as the storage time passed in the fruits harvested in stages 2 and 3, while, in the stages 3 and 4, the MI remained constant during their postharvest life. This decrease in stages 2 and 3 was caused by the reduction in TTA during storage.

The effect of the storage temperature showed a similar trend, in which there were significant differences between 7 and 14 dah. We could observe differences between the fruits stored at 18 °C (14,85) and the fruits refrigerated at 2 (12,07) and 4 °C (12,13), where the values were much lower (Table 2). These results agree with those reported by Parra *et al.* (2008) for 'Horvin' plums, where the smallest increase in the MI was in a treatment at 4 °C, which supports the study by Kader (2008), who claimed that the reduction in temperature decreased the effect of ethylene on fruit ripening, like respiration, which therefore slows the process.

The fruits that maintained commercial quality for longer periods of time were stored at 2 °C (31 days), followed by storage at 4 °C (24 days) and, finally, those stored at 18 °C, which only reached 10 days. This behavior can be explained by the fact that temperature increases the respiration process. This factor may be influential because the fruits stored at ambient temperature had a shorter shelf-life than the refrigerated fruits (Minas *et al.*, 2013).

Respiration rate (RR): this variable showed highly significant differences for the stage of maturity factor at most of the sampling points, as shown in Figure 3a, since the plum, as a climacteric fruit, presents a marked increase in the production

of CO₂ and ethylene during ripening (Kader, 2002), so the respiration rate was greater at all sampling points for stage 5, which had a more advanced maturation process.



Note: The vertical bars indicate the minimum significant difference according to the Tukey test ($p \leq 0,05$). *statistical differences at 5%, **statistical difference at 1%, ns: no differences.

Figure 3. Effect of a) the maturity stage and b) storage temperatures on the respiration rate (RR) of plum fruits during postharvest.

Source: Authors

By analyzing the storage temperature factor, it was clear that the fruits stored at 18 °C had the highest value when compared to the values obtained in the fruits stored at 2 and 4 °C (Figure 3b). At 10 dah, the biggest difference was observed, with values of 3,31, 8,87, and 30,83 mg CO₂·kg⁻¹·h⁻¹ for fruits stored at 2, 4 and 18 °C, respectively. Similarly, a decrease in RR was only observed in the fruits stored at room temperature (18 °C), indicating that, at this sampling point (10 dah), the senescence of fruits and loss of consumption quality began, so this treatment was discontinued.

In this regard, Kader (2002) classified plum fruits as having a moderate RR (10 to 20 mg CO₂·kg⁻¹·h⁻¹), but a high production of ethylene, which accelerates the metabolic processes that induce maturation. Similarly, Iqbal *et al.* (2009) stated that RR increases at high temperatures, in all combinations of concentrations of O₂ and CO₂. Therefore, temperatures of 18 °C, to which the plums were subjected, increased the RR. This shortened the product's shelf-life, considering that respiration causes oxidative degradation of materials such as starch, sugars, and organic acids due to energy production and other molecules used in synthesis

reactions (Saltveit, 2019). The fruits stored at 15,6 °C had more intense respiration than the fruits stored at 0 °C, which only released at 10% to 20% of the heat of respiration when stored at 15,6 °C, allowing to preserve the fruits for longer periods of time, as indeed occurred in this study; the fruits stored at 2 °C managed to preserve their commercial quality for 31 days.

The results of this study are consistent with those reported by Parra *et al.* (2008), where the RR of the 'Horvin' plum showed the typical behavior of a climacteric product due to its continuous increase in the RR, reaching the highest level with the climacteric peak and then decreasing with senescence, which occurred at 31 days with fruits that had a RR of 22,02 mg CO₂·kg⁻¹·h⁻¹. Likewise, these results match those reported by Sharma and Sharma (2016), who found that ethylene absorbers decreased the respiration of plum fruits of the *Santa Rosa* variety. However, the fruits reached climacteric peaks of up to 54 mg CO₂·kg⁻¹·h⁻¹.

Conclusions

The fruits in maturity stage 5 had higher pH, TSS, CI, MI, and RR values, but they also had a greater loss of firmness. The most suitable refrigeration temperature for the 'Horvin' plum fruits was 2 °C, at which they maintained consumption quality for longer (31 days). Refrigeration decreased the loss of TTA during postharvest. The fruits in maturity stage 5 had higher pH, TSS, CI, MI, and RR values, but they also had greater loss of firmness. The highest RR for fruit stored at 2 and 4 °C occurred after 21 days of cold-storage. The fruits without refrigeration only maintained the quality of consumption for 10 dah.

References

- Álvarez-Herrera, J. G., Rozo-Romero, X., and Reyes, A. J. (2015). Comportamiento poscosecha de frutos de ciruela (*Prunus salicina* Lindl.) en cuatro estados de madurez tratados con etileno. *Revista Colombiana de Ciencias Hortícolas*, 9(1), 46-59. 10.17584/rcch.2015v9i1.3745
- Batista-Silva, W., Nascimento, V. L., Medeiros, D. B., Nunes-Nesi, A., Ribeiro, D. M., Zsögön, A., and Araújo, W. L. (2018). Modifications in organic acid profiles during fruit development and ripening: correlation or causation? *Frontiers in Plant Science*, 9(1689), 1-20. 10.3389/fpls.2018.01689
- Botton, A., Tonutti, P., and Ruperti, B. (2019). Biology and biochemistry of ethylene. In: Yahia, E. M., and Carrillo-López, A. (Eds.) *Postharvest physiology and biochemistry of fruits and vegetables* (pp. 93-112). First edition. Kidlington, UK: Elsevier. 10.1016/B978-0-12-813278-4.00005-1
- Díaz-Pérez, M.E. (2019). Transpiration. In: Yahia, E. M., and Carrillo-López, A. (Eds.) *Postharvest physiology and biochemistry of fruits and vegetables* (pp. 157-173). 1st ed. Kidlington, UK: Elsevier. 10.1016/B978-0-12-813278-4.00008-7

- Farcuh, M., Rivero, R. M., Sadka, A., and Blumwald, E. (2018). Ethylene regulation of sugar metabolism in climacteric and non-climacteric plums. *Postharvest Biology and Technology*, 139, 20-30. 10.1016/j.postharvbio.2018.01.012
- Guerra, M. and Casquero, P. A. (2008). Effect of harvest date on cold storage and postharvest quality of plum cv. Green Gage. *Postharvest Biology and Technology*, 47, 325-332. 10.1016/j.postharvbio.2007.07.009
- Hussain, P., Suradkar, P., Wani, A., and Dar, M. (2015). Retention of storage quality and post-refrigeration shelf-life extension of plum (*Prunus domestica* L.) cv. Santa Rosa using combination of carboxymethyl cellulose (CMC) coating and gamma irradiation. *Radiation Physics and Chemistry*, 107, 136-148. 10.1016/j.radphyschem.2014.10.007
- Iqbal, T., Rodríguez, F. A. S., Mahajan, P. V., and Kery, J. P. (2009). Mathematical modeling of the influence of temperature and gas composition on the respiration rate of shredded carrots. *Journal of Food Engineering*, 91, 325-332. 10.1016/j.jfoodeng.2008.09.012
- Kader, A. (2002). *Postharvest technology of horticultural crops*. University of California (System). Division of Agriculture and Natural Resources. Third edition. Davis, CA: ANR Publications.
- Kader, A. (2008). Flavor quality of fruits and vegetables. *Journal of the Science of Food and Agriculture*, 88, 1863-1868. 10.1002/jsfa.3293
- Kaur, H., Sawhney, B. K., and Jawandha, S. K. (2018) Evaluation of plum fruit maturity by image processing techniques. *Journal of Food Science and Technology*, 55(8), 3008-3015. 10.1007/s13197-018-3220-0
- Koca, N., Karadeniz, F., and Burdurlu, H. S. (2007). Effect of pH on chlorophyll degradation and colour loss in blanched green peas. *Food Chemistry*, 100(2), 609-615. 10.1016/j.foodchem.2005.09.079
- Larrigaudière, C., Candan, A. P., Ubach, D., and Graell, J. (2009). Physiological response of 'Larry Ann' plums to cold storage and 1-MCP treatment. *Postharvest Biology and Technology*, 51, 56-61. 10.1016/j.postharvbio.2008.07.005
- Larsen, H. and Vangdal, E. (2013). Variation in ethylene production and respiration rate for Norwegian grown plums (*Prunus domestica* L.) in relation to packaging parameters. *Scientia Horticulturae*, 154, 109-114. 10.1016/j.scienta.2013.02.029
- Martínez-Romero, D., Castillo, S., Guillén, F., Paladine, D., Zapata, P., Valero, D., and Serrano, M. (2019). Rosehip oil coating delays postharvest ripening and maintains quality of European and Japanese plum cultivars. *Postharvest Biology and Technology*, 151, 29-36. 10.1016/j.postharvbio.2019.05.005
- Minas, I. S., Crisosto, G. M., Holcroft, D., Vasilakakis, M., and Crisosto, C. H. (2013). Postharvest handling of plums (*Prunus salicina* Lindl.) at 10 °C to save energy and preserve fruit quality using an innovative application system of 1-MCP. *Postharvest Biology and Technology*, 76, 1-9. 10.1016/j.postharvbio.2012.08.013
- Ndou, A., Tinyani, P. P., Slabbert, R. M., and Sultanbawa, Y. (2019). An integrated approach for harvesting Natal plum (*Carissa macrocarpa*) for quality and functional compounds related to maturity stages. *Food Chemistry*, 293, 499-510. 10.1016/j.foodchem.2019.04.102
- Palou, L., Crisosto, C., Garner, D., and Basinal, L. (2003). Effect of continuous exposure to exogenous ethylene during cold storage on postharvest decay development and quality attributes of stone fruits and table grapes. *Postharvest Biology and Technology*, 27, 243-254. 10.1016/S0925-5214(02)00112-6
- Pan, H., Wang, R., Li, L., Wang, J., Cao, J., and Jiang, W. (2016). Manipulation of ripening progress of different plum cultivars during shelf life by post-storage treatments with ethylene and 1-methylcyclopropene. *Scientia Horticulturae*, 198, 176-182. 10.1016/j.scienta.2015.11.007
- Parra, A., Hernández, J., and Camacho, J. (2008). Estudio fisiológico poscosecha y evaluación de la calidad de la ciruela variedad Horvin (*Prunus domestica* L.) bajo tres condiciones de almacenamiento refrigerado. *Revista Ingeniería e Investigación*, 28(1), 99-104. 10.15446/inginvestig.v28n1.14872
- Pathare, P. B., Opara, U. L., and Al-Said, F. (2013). Colour measurement and analysis in fresh and processed foods: A review. *Food and Bioprocess Technology*, 6, 36-40. 10.1007/S11947-012-0867-9
- Rozo-Romero, X., Álvarez-Herrera, J. G., and Balaguera López, H. E. (2015). Ethylene and changes during ripening in 'Horvin' plum (*Prunus salicina* Lindl.) fruits. *Agronomía Colombiana*, 33(2), 228-237. 10.15446/agron.colomb.v33n2.49856
- Saltveit, M. E. (2019). Respiratory metabolism. In: Yahia, E.M., and Carrillo-López, A. (Eds.) *Postharvest physiology and biochemistry of fruits and vegetables* (pp. 228-237). First edition. Kidlington, UK: Elsevier. 10.1016/B978-0-12-813278-4.00004-X
- Sañudo-Barajas, J., Lipan, L., Cano-Lamadrid, M., Vélez, R., Noguera-Artiaga, L., Sanchez-Rodríguez, L., Carbonell-Barrachina, A. A., and Hernández, F. (2019). Texture. In: Yahia, E.M., and Carrillo-López, A. (Eds.) *Postharvest physiology and biochemistry of fruits and vegetables* (pp. 293-314). First edition. Kidlington, UK: Elsevier. 10.1016/B978-0-12-813278-4.00014-2
- Sharma, S. and Sharma, R. R. (2016). Impact of staggered treatments of novel molecules and ethylene absorbents on postharvest fruit physiology and enzyme activity of 'Santa Rosa' plums. *Scientia Horticulturae*, 198, 242-248. 10.1016/j.scienta.2015.11.043
- Singh, S. and Singh Z. (2013). Dynamics of enzymatic and non-enzymatic antioxidants in Japanese plums during storage at safe and lethal temperatures. *LWT-Food Science and Technology*, 50, 562-568. 10.1016/j.lwt.2012.08.008
- Singh, S., Singh, Z., and Swinny, E. (2012). Climacteric level during fruit ripening influences lipid peroxidation and enzymatic and non-enzymatic antioxidative systems in Japanese plums (*Prunus salicina* Lindl.). *Postharvest Biology and Technology*, 65, 22-32. 10.1016/j.postharvbio.2011.10.007

- Wang, J., Pan, H., Wang, R., Hong, K., and Cao, J. (2016). Patterns of flesh reddening, translucency, ethylene production and storability of 'Friar' plum fruit harvested at three maturity stages as affected by the storage temperature. *Postharvest Biology and Technology*, 121, 9-18. 10.1016/j.postharvbio.2016.07.009
- Wu, F., Zhang, D., Zhang, H., Jiang, G., Su, X., Qu, H., Jiang, Y., and Duan, X. (2011). Physiological and biochemical response of harvested plum fruit to oxalic acid during ripening or shelf-life. *Food Research International*, 44, 1299-1305. 10.1016/j.foodres.2010.12.027
- Xu, Y., Li, S., Huan, C., Jiang, T., Zheng, X., and Brecht, J. K. (2020). Effects of 1-methylcyclopropene treatment on quality and anthocyanin biosynthesis in plum (*Prunus salicina* cv. Taoxingli) fruit during storage at a non-chilling temperature. *Postharvest Biology and Technology*, 169, 111291. 10.1016/j.postharvbio.2020.111291

Study of Carbohydrate Hydrolysis From Arracacha Roots (*Arracacia Xanthorrhiza* Bancroft) to Produce Fermentable Sugars

Estudio de hidrólisis de carbohidratos en raíces de Arracacha (*Arracacia Xanthorrhiza* Bancroft) para producir azúcares fermentables

Darwin Carranza-Saavedra¹, Jorge A. Alvarado-Núñez², José F. Solanilla-Duque³, and Claudia P. Valenzuela-Real⁴

ABSTRACT

In Colombia, approximately 855 840 tons of arracacha are produced each year. The unsalable post-harvest arracacha root (*Arracacia xanthorrhiza* Bancroft) is not commercialized, mainly due to mechanical damage or small and misshapen roots. In this work, dry samples were characterized and subjected to two treatments: one using thermal hydrolysis, applying saturated steam at pressures of 0,1034 MPa, 0,2068 MPa, and 0,4137 MPa; and another one using hydrolysis with sulfuric acid in concentrations between 0,25-2,00 M. Then, the cake resulting from the hydrolysis and filtration process was enzymatically hydrolyzed (Liquozyme SC DS, Novozymes) at 1,5, 5 and 10 KNU/g (pH 6, 80 °C, 2 h). Fermentation inhibitors (acetic acid and furfural) were evaluated in the best pretreatment. The results showed that the treatment with sulfuric acid at 1,00 M (2 h) has high yields in reducing sugars added to enzymatic hydrolysis. The maximum level of fermentable carbohydrates per gram of dry sample (1,04 g/g) was also reached. Regarding the fermentation inhibitors of the reducing sugar, a higher concentration of acetic acid was found with a lower furfural content. Therefore, arracacha discards are a promising raw material to increase the supply of bioethanol.

Keywords: chemical hydrolysis, enzymatic hydrolysis, fermentation inhibitors, reducing sugars

RESUMEN

En Colombia se producen aproximadamente 855 840 toneladas anuales de arracacha. La raíz de arracacha postcosecha no vendible (*Arracacia xanthorrhiza* Bancroft) no se comercializa, principalmente debido a daños mecánicos o raíces pequeñas y deformadas. En este trabajo, las muestras secas fueron caracterizadas y sometidas a dos tratamientos: uno con hidrólisis térmica aplicando vapor saturado a presiones de 0,1034 MPa, 0,2068 MPa y 0,4137 MPa; y el otro de hidrólisis con ácido sulfúrico en concentraciones entre 0,25-2,00 M. Luego, la torta resultante del proceso de hidrólisis y filtración se hidrolizó enzimáticamente (Liquozyme SC DS, Novozymes) a 1,5, 5 y 10 KNU/g (pH 6, 80 °C, 2 h). Se evaluaron los inhibidores de fermentación (ácido acético y furfural) en el mejor pretratamiento. Los resultados mostraron que el tratamiento con ácido sulfúrico a 1,00 M (2 h) tiene altos rendimientos en azúcares reductores adicionados a hidrólisis enzimática. También se alcanzó el nivel máximo de carbohidratos fermentables por gramo de muestra seca (1,04 g/g). En cuanto a los agentes inhibidores de la fermentación del azúcar reductor, se encontró una mayor concentración de ácido acético con contenido furfural menor. Por tanto, los residuos de arracacha son una materia prima prometedora para incrementar la oferta de bioetanol.

Palabras clave: hidrólisis química, hidrólisis enzimática, inhibidores de fermentación, azúcares reductores

Received: May 17th, 2020

Accepted: January 22nd, 2021

¹Agroindustrial Engineer, M.Sc. in Agri-food Sciences, Universidad del Tolima. Affiliation: Researcher, Departamento de Producción y Sanidad Vegetal, Facultad de Ingeniería Agronómica, Universidad del Tolima. E-mail: dcarranzas@ut.edu.co

²Agroindustrial Engineer, Universidad Del Tolima. Affiliation: Researcher, Departamento de Producción y Sanidad Vegetal, Facultad de Ingeniería Agronómica, Universidad del Tolima. E-mail: andrejo75@gmail.com

³Agroindustrial Engineer, Universidad del Quindío, Ph.D. Ciencia y Tecnología en Coloides e Interfaces, Universidad Pablo De Olavide. Affiliation: Associate Professor, Departamento de Agroindustria, Facultad de Ciencias Agrarias, Universidad del Cauca. E-mail: jsolanilla@unicauca.edu.co

⁴Food Engineer, Fundación Universidad Incca de Colombia, M.Sc. Agricultural engineering, Universidad Nacional de Colombia, sede Bogotá. Affiliation: Full Professor, Departamento de Producción y Sanidad Vegetal, Facultad de Ingeniería Agronómica, Universidad Del Tolima. E-mail: cpvalenz@ut.edu.co

Introduction

Arracacha roots (AR) or creole celery (*Arracacia xanthorrhiza* Bancroft.), are a tuber with high nutritional value that offers large amounts of minerals and carbohydrates compared to cassava (Londoño-Restrepo, Rincón-Londoño, Contreras-Padilla, Millan-Malo, and Rodríguez-García, 2018; Otache, Ubwa, and Godwin, 2017). Furthermore, Colombia is

How to cite: Carranza-Saavedra, D., Alvarado, J. A., Solanilla J. F., Valenzuela, and C. P. (2021). Study of Carbohydrate Hydrolysis in Arracacha Roots (*Arracacia Xanthorrhiza* Bancroft) to Produce Fermentable Sugars. *Ingeniería e Investigación*, 41(2), e87365. 10.15446/ing.investig.v41n2.87365



Attribution 4.0 International (CC BY 4.0) Share - Adapt

currently the world's largest producer of arracacha with an annual production of 855 840 t/year in 2018 (MinAgricultura and Agronet, 2018).

Moreover, an arracacha crops are characterized by having productive cycles throughout the year, and their quality is definitely affected by pre-harvest, harvest, and post-harvest processes. Poor implementations stemming from cultural habits influence arracacha in terms of sprout decomposition, production heterogeneity, and the frequency of crop diseases (Rana and Kumar, 2017), thus generating a higher volume of non-quantified waste in post-harvest, as well as creating low production yields, poor product quality, and, in turn, environmental emissions problems such as nitrous oxide, carbon monoxide, among others; these compounds contribute to the greenhouse effect (Galford *et al.*, 2020; D. Huang *et al.*, 2019).

Likewise, the use of these agricultural residues is quite extensive and highly studied, including the extraction of compounds of pharmaceutical interest (Didaskalou, Buyuktiryaki, Kecili, Fonte, and Szekely, 2017), fertilizers (Lupton, 2017), and fermentable sugars for the production of biofuels (C. Huang, Jeuck, and Yong, 2017; Nair, Lennartsson, and Taherzadeh, 2017).

Obtaining biofuel from vegetable waste is an alternative to solve issues with oil dependency that come from the 1970s energy crisis, where the fossil fuel supply decreased considerably, and the ensuing riots created the necessity to contribute to environmental management (Venn, 2016).

Even though there was a collapse in crude oil prices, which fell to negative values due to the current COVID-19 pandemic (Aloui, Goutte, Guesmi, and Hchaichi, 2020), there is still an interest in modifying oil-powered engines. This has led to research on the topic of ethanol as a fuel source for the automotive, energetic and agroindustry industry since the mid-nineteenth century until now (Awad *et al.*, 2018).

Bioethanol increases gasoline octane, improving its combustion and efficiency in the conversion to mechanical energy. At the same time, it reduces fuel consumption by means of a higher release of free radicals (H, OH, and O) and reducing emissions of hydrocarbons (HC), carbon monoxide (CO), and nitrogen oxides (NO_x) (Aditiya, Mahlia, Chong, Nur, and Sebayang, 2016; Awad *et al.*, 2018). This complies with Colombian law nr. 693 of 2001 (Colombian Congress, 2001), which states that the automotive industry has to contain oxygenated components such as fuel alcohols, with the purpose of controlling air pollution.

Concerning the above, the ethanol production process is developed in four steps: pretreatment, fermentation, separation, and post-treatment of the liquid fraction (Zabed, Sahu, Suely, Boyce, and Faruq, 2017). As for pretreatments, benefits depend on the kind of material. They could be physical (increasing the surface area and pore volume) or chemical (alkali and acid). Their function is to decrease the degree of cellulose polymerization and its crystallinity, thus allowing for a major production of reducing sugars (Sarkar, Ghosh, Bannerjee, and Aikat, 2012). However, there are

some significant disadvantages in the use of physical methods, such as high energy consumption, which is environmentally unfriendly and non-viable for a commercial process.

Chemical pretreatments have the presence of inhibitors in each of the mentioned stages (Zabed *et al.*, 2017), which causes the delay of yeast activity and an extension of fermentation time. Due to hydrolytic pretreatments applied to vegetable material (like furfural, hydroxymethylfurfural, and acetic acid, among other compounds) (Maiti *et al.*, 2018) it has a major negative effect on enzymes (Wojtusik, Villar, Zurita, Ladero, and Garcia-Ochoa, 2017).

In this context, the purpose of this paper is to study the hydrolysis of the carbohydrates present in the post-harvest agricultural discards of arracacha (unsalable roots) to obtain fermentable sugars, assessing inhibiting compounds (acetic and furfural acid), despite AR having phenolic compounds (Leja *et al.*, 2013), which are major enzyme and microbial inhibitors that can potentially affect the production of ethanol during fermentation.

Methodology

Sample conditioning

AR samples were purchased from a crop in Cajamarca, Tolima, Colombia. Only roots that were not marketable, malformed, or with mechanical or pest damage were used in the tests. Samples were dried to an average humidity of 13% in a convection oven (60 °C, 72 h), and then the particle size was reduced to 1 mm using a hammermill.

Analytical techniques

The contents of moisture (method 925.10), crude protein (method 955.04), ether extract (method 963.15), crude fiber (method 962.09), and ash (method 941.12) were determined for each residue by means of the official methodology (AOAC, 2000). Also, neutral detergent fiber (NDF), acid detergent fiber (ADF), cellulose, hemicellulose, and lignin were all quantified according to the Van Soest methodologies (P. Van Soest and Wine, 1968; P. J. Van Soest, 1963).

Total and reducing carbohydrate quantification were performed by extraction with absolute ethanol in dilution 1:3 (w/v), filtered on quantitative paper and refrigerated until use. The quantification of both total carbohydrates (TC) and reducing sugars was carried out using the Antrona (Leyva *et al.*, 2008) and DNS (Miller, 1959) spectrophotometric methods using a UV-Vis Helios Gamma spectrophotometer (Thermo Fisher Scientific, Waltham, MA, USA) at 620 nm and 540 nm, respectively.

Physicochemical pretreatment

The AR was submitted to pressures of 0,1034 MPa (100,55 °C), 0,2068 MPa (121,28 °C), and 0,4137 MPa (144,83 °C) (saturated steam), and it diluted in distilled water to a ratio of 1:15 for one hour. The steam supply was generated in a 2-inch vertical, pirotubular boiler with

a capacity of 2 BHP (Equipos y Calderas Industriales E U, Bogotá) (Carranza Saavedra, Alvarado Núñez, Méndez Reyes, Valenzuela Real, and Solanilla Duque, 2015).

Chemical pretreatment

The samples were hydrolyzed with sulfuric acid (H_2SO_4) at concentrations of 0,25, 0,50, 1,00, and 2,00 M in 1:15 dilution at a temperature of 60 °C, refluxing at the atmospheric pressure of Ibagué, in the department of Tolima, Colombia (Carranza Saavedra *et al.*, 2015).

Residence time

The resistance time for sugar splitting in every case was performed during 1 h. Then, in order to observe the effect of residence time on the samples, the best pretreatment (physical or chemical) was selected, and the residence time was increased to 2 h of hydrolysis. Next, the contents of total and reducing carbohydrates were analyzed.

Enzymatic pretreatment

From the best pretreatment, the samples were submitted to enzymatic hydrolysis to increase their reducing carbohydrates (RC) with Novozymes' Liquezyme SC DS α -amylase at 1,5, 5, and 10 kilo Novo units (KNU)/g (one KNU was defined as the amount of enzyme that hydrolyzed 5,26 g of starch (soluble starch) per hour under Novozymes's standard conditions for α -amylase determination) with diacid phosphate buffer pH 6 at temperature of 80 °C and 2 h with constant agitation (150 rpm).

Samples were taken every 30 minutes. The enzyme was inactivated at 95 °C for 5 min, and the samples were later centrifuged at 5 000 rpm for 10 min, determining RC immediately (Rathore, Paulsen, Vidal Jr., and Singh, 2009). The rate constant for the formation of first-order fermentable sugars was also evaluated, which is directly proportional to the concentration of the substrate and can be evaluated at different concentrations of enzyme. It is described using Equation (1):

$$\frac{drc}{dt} = k * rc \quad (1)$$

Where, rc is the concentration of RC, k is the first order kinetic constant, and t is time. Additionally, the solution of the linearized Equation (1), where k is the slope, is described using Equation (2):

$$\ln [rc] = kt + \ln [rc_0] \quad (2)$$

Where rc_0 is the concentration of initial RC.

Inhibiting Compounds in Pretreated Liquid Fractions

Determination of acetic acid content: Acetic acid was quantified through titratable acidity (Cheng *et al.*, 2008). The results are expressed as equivalent milligrams of acetic acid per milliliter (mgEAA/mL).

Furfural quantitative determination: Furfural quantification was implemented according to the methodology described by

the AOAC (2000). 25 mL of pretreatment liquid were taken to be distilled through a fractionating column. The fraction was collected at boiling temperature (161,20 °C). Later, 1 mL of the distilled result was taken and gauged with alcohol (99,80%) to complete 10 mL. Sample absorbance, alcohol white, and the standard (furfural) 277 nm were determined in a spectrophotometer. The results are expressed as equivalent furfural milligrams per milliliter (FEmg/mL).

Statistical Analysis

The results obtained in the study were expressed as the mean and the standard deviation of three determinations for each pretreatment. Analysis of Variance (ANOVA) and Multivariate Analysis of Variance (MANOVA) at a 95% confidence level were used to compare the mean values of each determination among the different pretreatments.

The STATGRAPHICS Centurion XV statistical package was used for the analysis of the obtained results. The treatments were executed through randomized complete block design (RCBD) and averaged differences using the least significant difference (LSD) for each one. The coefficient of determination (Equation 3) was used to assess the goodness of fit of the linearization of Equation (1).

$$R^2 = 1 - \frac{\sum (y_i - f_i)^2}{\sum (y_i - \bar{y})^2} \quad (3)$$

Where f_i , y_i , and \bar{y} are the model data, experimental data, and the mean of the experimental data, respectively.

Results and Discussion

Bromatological and carbohydrates analysis

Table 1 shows the results of the bromatological analysis, as well as the composition of cell walls in AR. The protein content in the studied samples was higher than in other types of arracacha (Londoño-Restrepo *et al.*, 2018), and did not exceed the range between 4,00% and 8,00%. When added to the TC content, it represents a significant amount of calories that partly support the conversion of energy in animals that are fed with these residues.

The ethereal extract found to have the greatest amount was the yellow and purple arracacha plant (Londoño-Restrepo *et al.*, 2018; Palacios, Morales, and Arias, 2011), with documented fat values of 0,90% (dry basis).

The crude fiber content was almost ten times higher than in other studies (Londoño-Restrepo *et al.*, 2018; Palacios *et al.*, 2011), which shows a promising composition for the extraction of RC. The ash contents had similar values as the reported cases of arracacha flour, which means it is an important source of minerals in use for human and animal food.

Table 1 shows the values of the study of the cell wall (ADF, NDF, hemicellulose, cellulose, and lignin) which evinces a small amount of lignocellulosic material in its structure, as well as the fact that, according to studies, it contains between

75% and 90% starch on dry basis (Londoño-Restrepo *et al.*, 2018; Palacios *et al.*, 2011). Therefore, it was not necessary to carry out tests with sodium hydroxide. It was also observed that it did not contain detectable lignin in its structure.

The carbohydrates in unprocessed AR (control) were characterized in order to evaluate the increase or decrease in present sugars during the pretreatments. The studies reported 27,39% and 1,63% of total and reducing carbohydrates, respectively, a considerable amount compared to cane cachaza, penelera cane chuff, rice shell, Tahití lime (*Citrus latifolia*), and common lemon (*Citrus aurantifolia*), which are reported as feedstock to obtain ethanol, especially by way of fermentation (Sánchez-Riaño, Barrero, and Murillo, 2010).

Table 1. Physicochemical analysis of AR

Parameters	% w/w
Moisture	13,50 ± 1,4 ^a
Ash	4,30 ± 0,8 ^{bc}
Ethereal extract	2,50 ± 1,7 ^c
Raw fiber	13,20 ± 0,7 ^a
Crude protein	8,00 ± 0,7 ^b
ADF	5,80 ± 0,5 ^b
NDF	2,30 ± 1,6 ^c
Hemicellulose	8,60 ± 2,1 ^b
Cellulose	3,50 ± 1,0 ^c
Lignin	0,00 ^d
Total available carbohydrates	27,39 ± 1,5
Reducing carbohydrates	1,63 ± 0,1

Results are the mean of three determinations ($n = 3$), \pm represent standard deviation. Similar lower-case letters indicate that there is no statistical difference between treatments ($p < 0,05$).

Source: Authors

Pretreatments

Physicochemical pretreatment: Figure 1 shows the different pressures at which the AR were treated to obtain reductive carbohydrates at different temperatures. The MANOVA reported significant differences ($p < 0,05$) between the total and reducing carbohydrates by physicochemical treatment with a 95% level of significance.

Now, elevating the temperature of the starchy material proved its sensitiveness, which showed an increase in the quantification of TC with a significant pressure differences ($p < 0,05$) between 0,10 MPa ($0,52 \pm 0,03$ g/g), 0,20 MPa ($0,53 \pm 0,01$ g/g), and 0,41 MPa ($0,67 \pm 0,05$ g/g) with respect to the control sample. However, the pressure at 0,41 MPa allows an upper splitting of high molecular weight carbohydrates, attributed to hydrolyzed starch by the action of water molecules, which speed up the absorption at high temperatures, causing the swelling of the starch and breaking the granule; releasing the amylose and amylopectin molecules; and later, breaking their glycosidic bonds (Kong *et al.*, 2016).

On the other hand, the variability of the results in terms of RC is shown in Figure 1, indicating that there are significant

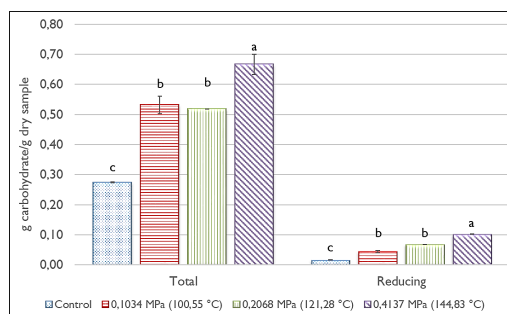


Figure 1. Total and reducing carbohydrate contents of arracacha obtained at different pressures with saturated steam. Vertical bars represent standard deviation. Similar lower-case letters indicate that there is no statistical difference between treatments ($p < 0,05$).

Source: Authors

differences ($p < 0,05$) in the RC obtained at 0,41 psi in comparison with the control sample. Moreover, the simple sugars do not exceed $0,10 \pm 0,01$ g/g because of amylose and amylopectin molecules are released only in the rupture of starch granule, causing the breakup of 1,4 and 1,6 glycosidic bonds, respectively, but in small proportions (Shigematsu *et al.*, 2017).

Chemical pretreatment: Figure 2 shows the sugar content (total and reducing) of arracacha when submitted to chemical hydrolysis. There seems to be a proportional or consequent behavior with the increase in acid concentration during the pretreatment. However, the 2,0 M acid concentration had an observed decline of total and reducing carbohydrates with a significant statistical effect ($p < 0,05$). TC reached their highest hydrolysis point at 1,0 M ($0,73 \pm 0,03$ g/g). A similar behavior was observed in RC at an acid concentration of 1,0 M with a $0,33 \pm 0,03$ g/g quantification. This phenomenon could be due to the degradation of amylose chains, and even amylopectin chains by H_2SO_4 , which, as a consequence, releases total and reducing sugars (Li *et al.*, 2020).

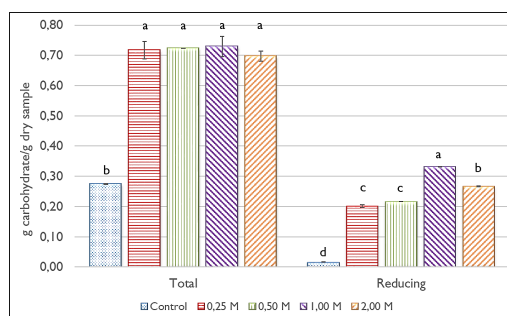


Figure 2. Total and reducing carbohydrate contents of arracacha obtained at different concentrations of H_2SO_4 . Vertical bars represent standard deviation. Similar lower-case letters indicate that there is no statistical difference between treatments ($p < 0,05$).

Source: Authors

Furthermore, the increase of H_2SO_4 concentration for the hydrolysis of arracacha samples was harmful, because carbohydrates began to degrade, turning into unwanted compounds for fermentation (phenols and furfurals) (Guerrero, Ballesteros, and Ballesteros, 2017).

Increase in residence time: In pretreatments (physicochemical and chemical), it was evident that hydrolysis with H_2SO_4 at a 1,0 M concentration is the most effective method to obtain RC from arracacha discards.

Judging from the assessment of the residence time, higher yields were obtained at two hours with $0,52 \pm 0,09$ g/g (RC) compared to the one-hour treatment. This confirms a decrease in TC ($0,56 \pm 0,1$ g/g), possibly due to the rupture of the hydroxyl groups present in starchy materials (Peñaranda Contreras, Perilla Perilla, and Algecira Enciso, 2008).

Enzymatic pretreatment: The enzymatic hydrolysis for arracacha residues was implemented with α -amylase after choosing the best acid hydrolysis pretreatment (H_2SO_4 1,0 M, 2 h). Figure 3A shows the enzyme kinetics when it reacts with the substrate. An ANOVA revealed a statistic interaction ($p < 0,05$) with a 95,0% level of confidence between the fermentable sugar concentrations present in the hydrolyzed sample (g/g) and the enzyme concentration, showing a considerable increase in the monomeric sugars, due to the action that the enzyme exerts along any point of the carbohydrate chain (1-4 glucosidic bonds), hydrolyzing them in dextrin from amylose (Oliveira, Pinheiro, Fonseca, Cabrita, and Maia, 2019).

Therefore, the maximum conversion from substratum to dextrose is obtained within 2 hours, and in absence of a significant difference, according to Fisher's LSD method, between 1,5 and 5,0 KNU/g of concentration of the α -amylase enzyme, it is understood that 1,5 KNU/g is the concentration at which the enzyme works better, and the best results from enzymatic hydrolysis ($0,56 \pm 0,05$ g/g) are obtained. Also, the highest concentration of the α -amylase enzyme might not have been attained because it could have been inhibited by the relation between enzyme and substrate, *decreasing the hydrolysis speed of starch to glucose* (Zhang et al., 2020).

Low values were obtained for corn starch hydrolysate with a reducing sugar content of 12-14% with the same enzyme and operation time, but without pretreatment (Z. Li, Wang, and Shi, 2019). Thus, it is possible that the enzyme conversion with pretreatment could find suitable applications in productions of sugars and chemicals made by the fermentation of sugars.

Alternatively, it is important to characterize the reaction kinetics for a reducing sugar gain. Contents of RC increase as part of the aging process, as shown in Figure 3A. First-order kinetics correctly described an increase in reducing sugars ($R^2 > 0,95$, 1,5 KNU/g in Equation (1)), as shown Figure 3B.

Chemical compounds react and convert to other species, and the rate constant indicates the speed of the change in concentration. The half-life time of each chemical species is an indicator of the time that a given compound increases its concentration by a factor of 0,02 (k) to 1,5 (NKU/g). Therefore, it is a standardized parameter that indicates the time at which a compound is degraded to simple sugars.

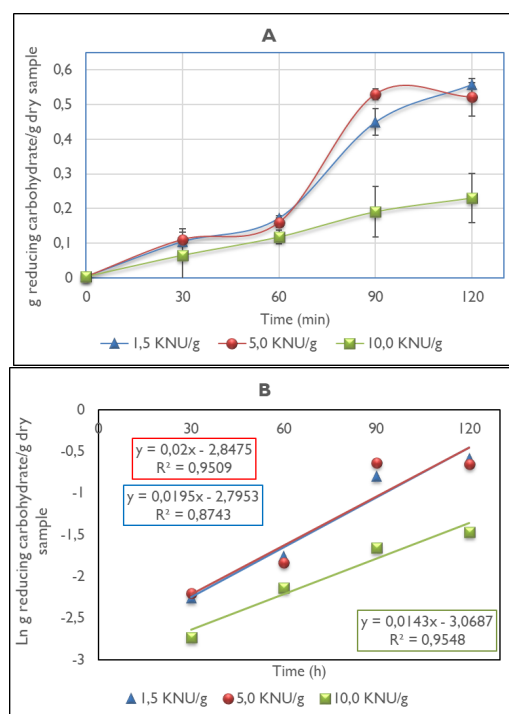


Figure 3. Hydrolysis of carbohydrates in AR with α -amylase enzyme. A: Enzymatic kinetics of reducing carbohydrate B: Kinetic analysis of the reducing sugar content. Vertical bars represent standard deviation. Lines in A are a guide for the eye and in B represent first-order fitting according to Equation 1.

Source: Authors

Evaluation of inhibiting agents

The assessment of the inhibiting compounds present in starchy material was made from AR hydrolysates. It was then concluded that this is the most efficient method to obtain reducing sugars using the chemical pretreatment with H_2SO_4 at 1,0 M and 2 h of residence time. In the hydrolyzed samples, an acetic acid formation was observed, due to the conditions of the chemical pretreatment applied to the roots ($3,12 \pm 0,11$ mgEAA/mL). This result is associated with presence of acetyl groups by deacetylation of hemicelluloses during the pretreatment. These are not degraded despite the prolonged storage time, and they were possibly entirely hydrolyzed to form acetic acid by the action of the acid environment in which the pretreatment was carried out (Maiti et al., 2018), regardless of the residence time at which it was submitted.

There was also an effect ($0,28 \pm 0,002$ mgEF/mL) of H_2SO_4 concentration, temperature, and residence time in the formation of the environment that fosters pentose dehydration, until their degradation to furfural in pre-treated starchy waste. This could be explained by the way in which many monomeric sugars (pentoses) were possibly hydrolyzed during the process of acid pretreatment in AR; these sugars would be degraded to this inhibiting compound (furfural) (Maiti et al., 2018). Lastly, AR have phenolic compounds within their structure, which act well as major enzymes and microbial inhibitors.

Conclusions

The physicochemical pretreatment with distilled water under high pressures turns out to be a soft method of carbohydrate hydrolysis compared to chemical pre-treatment in H₂SO₄ at 1,0 M with quantification of 51,8% of RC by dry sample of roots and a residence time of 2 h.

A further pretreatment with α -amylase increases the fermentable sugar yield with arracacha discards, reaching a conversion of 1,04 g of fermentable sugars per gram of dry vegetable material.

The fermentation of non-detoxified hydrolysates is characterized by a limited productivity and yield, due to the presence of a variety of compounds that act as potential inhibitors of the cellular metabolism, such as furfural and acetic acid found in AR after the hydrolysis with diluted H₂SO₄. Therefore, the use of mechanisms that remove most of these toxic compounds in the hydrolysates is necessary, thus improving the metabolism of the microorganisms responsible for starchy material fermentation.

Furthermore, the identification of the RC type that is generated in the hydrolysis is used to establish the appropriate biological mechanism for fermenting ethanol, considering the detoxification tests before the fermentation.

This study of carbohydrate hydrolysis in non-marketable food significantly shows the ease of taking advantage of agricultural waste and converting it into clean energy, thereby contributing to the continuous development of producing fermentable sugars as a workhorse in the production of bioethanol.

Acknowledgements

The authors want to thank the laboratory LASEREX of the Universidad del Tolima and its Central Research Committee and the Universidad del Cauca, as well as engineers John Rincon and Daniel Bernier for their technical support in the quantification of inhibitors.

References

- Aditiya, H., Mahlia, T. M. I., Chong, W., Nur, H., and Sebayang, A. (2016). Second generation bioethanol production: A critical review. *Renewable Sustainable Energy Reviews*, 66, 631-653. 10.1016/j.rser.2016.07.015
- Aloui, D., Goutte, S., Guesmi, K., and Hchaichi, R. (2020). COVID 19's impact on crude oil and natural gas S&P GS Indexes. SSRN. 10.2139/ssrn.3587740
- AOAC. (2000). Official Methods of Analysis. (17th. ed.). Gaithersburg, USA: Association of Official Analytical Chemists.
- Awad, O. I., Mamat, R., Ali, O. M., Sidik, N., Yusaf, T., Kadirgama, K., and Kettner, M. (2018). Alcohol and ether as alternative fuels in spark ignition engine: A review. *Renewable Sustainable Energy Reviews*, 82(3), 2586-2605. 10.1016/j.rser.2017.09.074
- Carranza Saavedra, D., Alvarado Núñez, J. A., Méndez Reyes, D. A., Valenzuela Real, C. P., and Solanilla Duque, J. F. (2015). Pretratamiento de residuos de plátano (*Musa paradisiaca* (L.) AAB) y arracacha (*Arracacia xanthorrhiza* Bancroft) para la obtención de azúcares fermentables. *Revista Venezolana de Ciencia y Tecnología de Alimentos*, 6(1), 019-035. <http://oaji.net/articles/2017/4924-1495586231.pdf>
- Cheng, K.-K., Cai, B.-Y., Zhang, J.-A., Ling, H.-Z., Zhou, Y.-J., Ge, J.-P., and Xu, J.-M. (2008). Sugarcane bagasse hemicellulose hydrolysate for ethanol production by acid recovery process. *Biochemical Engineering Journal*, 38(1), 105-109. 10.1016/j.bej.2007.07.012
- Congreso de Colombia (2001). LEY 693 de 2001. Por la cual se dictan normas sobre el uso de alcoholes carburantes, se crean estímulos para su producción, comercialización y consumo, y se dictan otras disposiciones. September 27, 2001. D.O. Nr. 44564. http://www.secretariassenado.gov.co/senado/basedoc/ley_0693_2001.html
- Didaskalou, C., Buyuktiryaki, S., Kecili, R., Fonte, C. P., and Szekely, G. (2017). Valorisation of agricultural waste with an adsorption/nanofiltration hybrid process: from materials to sustainable process design. *Green Chemistry*, 19(13), 3116-3125. 10.1039/c7gc00912g
- Galford, G. L., Peña, O., Sullivan, A. K., Nash, J., Gurwick, N., Pirolli, G., Richards, M., White, J., and Wollenberg, E. (2020). Agricultural development addresses food loss and waste while reducing greenhouse gas emissions. *Science of The Total Environment*, 699, 134318. 10.1016/j.scitotenv.2019.134318
- Guerrero, A. B., Ballesteros, I., and Ballesteros, M. (2017). Optimal conditions of acid-catalysed steam explosion pretreatment of banana lignocellulosic biomass for fermentable sugar production. *Journal of Chemical Technology Biotechnology*, 92(9), 2351-2359. 10.1002/jctb.5239
- Huang, C., Jeuck, B., and Yong, Q. (2017). Using pretreatment and enzymatic saccharification technologies to produce fermentable sugars from agricultural wastes. In Kalla, V. C. and Singh, L. (Eds.) *Waste Biomass Management—A Holistic Approach* (pp. 15-38) Berlin, Germany: Springer.
- Huang, D., Cao, G., Geng, Y., Wang, L., Chen, X., and Liang, A. (2019). Impact of agricultural waste return on soil greenhouse gas emissions. *Applied Ecology Environmental Research*, 17(1), 1321-1335. 10.15666/aeer/1701_13211335
- Kong, W., Zhang, T., Feng, D., Xue, Y., Wang, Y., Li, Z., Yang, W., and Xue, C. (2016). Effects of modified starches on the gel properties of Alaska Pollock surimi subjected to different temperature treatments. *Food Hydrocolloids*, 56, 20-28. 10.1016/j.foodhyd.2015.11.023
- Leja, M., Kamińska, I., Kramer, M., Maksylewicz-Kaul, A., Kammerer, D., Carle, R., and Baranski, R. (2013). The content of phenolic compounds and radical scavenging activity varies with carrot origin and root color. *Plant Foods for Human Nutrition*, 68(2), 163-170. 10.1007/s11130-013-0351-3

- Leyva, A., Quintana, A., Sánchez, M., Rodríguez, E. N., Cremata, J., and Sánchez, J. C. (2008). Rapid and sensitive anthrone-sulfuric acid assay in microplate format to quantify carbohydrate in biopharmaceutical products: Method development and validation. *Biologicals*, 36(2), 134-141. 10.1016/j.biologicals.2007.09.001
- Li, H., Yan, S., Mao, H., Ji, J., Xu, M., Zhang, S., Wang, J., Yingli, L., and Sun, B. (2020). Insights into maize starch degradation by sulfuric acid from molecular structure changes. *Carbohydrate polymers*, 229, 115542. 10.1016/j.carbpol.2019.115542
- Li, Z., Wang, D., and Shi, Y. C. (2019). High-Solids Bio-Conversion of Maize Starch to Sugars and Ethanol. *Starch-Stärke*, 71(1-2), 1800142. 10.1002/star.201800142
- Londoño-Restrepo, S. M., Rincón-Londoño, N., Contreras-Padilla, M., Millan-Malo, B. M., and Rodríguez-García, M. E. J. I. (2018). Morphological, structural, thermal, compositional, vibrational, and pasting characterization of white, yellow, and purple Arracacha lego-like starches and flours (*Arracacia xanthorrhiza*). *Journal of Biological Macromolecules*, 113, 1188-1197. 10.1016/j.jbiomac.2018.03.021
- Lupton, S. (2017). Markets for waste and waste-derived fertilizers. An empirical survey. *Journal of Rural Studies*, 55, 83-99. 10.1016/j.jrurstud.2017.07.017
- Maiti, S., Gallastegui, G., Suresh, G., Sarma, S. J., Brar, S. K., Drogui, P., LeBihan, Y., Buelna, G., Verna M., and Soccol, C. R. (2018). Hydrolytic pre-treatment methods for enhanced biobutanol production from agro-industrial wastes. *Bioresource Technology*, 249, 673-683. 10.1016/j.biortech.2017.09.132
- Miller, G. L. (1959). Use of dinitrosalicylic acid reagent for determination of reducing sugar. *Analytical Chemistry*, 31(3), 426-428. 10.1021/ac60147a030
- MinAgricultura and Agronet. (2018). Reporte: Área, Producción y Rendimiento Nacional por Cultivo. <https://www.agronet.gov.co/estadistica/Paginas/home.aspx?cod=1>
- Nair, R., Lennartsson, P. R., and Taherzadeh, M. J. (2017). Bioethanol production from agricultural and municipal wastes. In Pandey, A., Larroche, C., Angeles Saronman, M., and Du, G. (Eds.) *Current developments in biotechnology and bioengineering* (pp. 157-190). Amsterdam, Netherlands: Elsevier.
- Oliveira, H. M., Pinheiro, A. Q., Fonseca, A. J., Cabrita, A. R., and Maia, M. R. (2019). Flexible and expeditious assay for quantitative monitoring of alpha-amylase and amyloglucosidase activities. *MethodsX*, 6, 246-258. 10.1016/j.mex.2019.01.007
- Otache, M. A., Ubwa, S. T., and Godwin, A. K. (2017). Proximate analysis and mineral composition of peels of three sweet cassava cultivars. *Asian Journal of Physical Chemical Sciences*, 3(4), 1-10. 10.9734/AJOPACS/2017/36502
- Palacios, R., Morales, M., and Arias, G. C. (2011). Evaluación químico bromatológica de tres variedades de Arracacia xanthorrhiza "arracacha". *Ciencia e Investigación*, 14(2), 12-14. 10.15381/ci.v14i2.3161
- Peñaranda Contreras, O. I., Perilla Perilla, J. E., and Algecira Enciso, N. A. (2008). Revisión de la modificación química del almidón con ácidos orgánicos. *Ingeniería e Investigación*, 28(3), 47-52. 10.15446/ing.investig.v28n3.15119
- Rana, M., and Kumar, S. (2017). Arracacha. In M. K. Rana (Ed.), *Vegetable Crop Science* (pp. 923-932). Boca Raton, FL: CRC Press.
- Rathore, S., Paulsen, M. R., Vidal Jr, B., and Singh, V. (2009). Monitoring liquefaction unit operation in dry-grind ethanol process: Factors affecting hydrolysis and methods for analysis. *Transactions of the ASABE*, 52(5), 1639-1647. 10.13031/2013.29115
- Sánchez-Riaño, A., Barrero, C. R., and Murillo, E. (2010). Perspectivas de uso de subproductos agroindustriales para la producción de bioetanol. *Scientia et Technica*, 3(46), 232-235. <https://revistas.utp.edu.co/index.php/revistaciencia/article/view/259>
- Sarkar, N., Ghosh, S. K., Bannerjee, S., and Aikat, K. J. R. e. (2012). Bioethanol production from agricultural wastes: an overview. *Renewable Energy*, 37(1), 19-27. 10.1016/j.renene.2011.06.045
- Shigematsu, T., Furukawa, N., Takaoka, R., Hayashi, M., Sasao, S., Ueno, S., . . . Iguchi, A. (2017). Effect of high pressure on the saccharification of starch in the tuberous root of sweet potato (*Ipomoea batatas*). *Biophysical Chemistry*, 231, 105-110. 10.1016/j.bpc.2017.04.012
- Van Soest, P. and Wine, R. (1968). Determination of lignin and cellulose in acid-detergent fiber with permanganate. *Journal of the association of official analytical chemists*, 51(4), 780-785. 10.1093/jaoac/51.4.780
- Van Soest, P. J. (1963). Use of detergents in the analysis of fibrous feeds. 2. A rapid method for the determination of fiber and lignin. *Journal of the Association of Official Agricultural Chemists*, 46(5), 829-835. 10.1093/jaoac/46.5.829
- Venn, F. (2016). *The oil crisis*. New York, NY: Routledge.
- Wojtusik, M., Villar, J. C., Zurita, M., Ladero, M., and García-Ochoa, F. (2017). Study of the enzymatic activity inhibition on the saccharification of acid pretreated corn stover. *Biomass Bioenergy*, 98, 1-7. 10.1016/j.biombioe.2017.01.010
- Zabed, H., Sahu, J., Suely, A., Boyce, A., and Faruq, G. (2017). Bioethanol production from renewable sources: Current perspectives and technological progress. *Renewable Sustainable Energy Reviews*, 71, 475-501. 10.1016/j.rser.2016.12.076
- Zhang, B., Li, H., Wang, S., Junejo, S. A., Liu, X., and Huang, Q. (2020). In Vitro Starch Digestion: Mechanisms and Kinetic Models. In Wang, S. (Ed.), *Starch Structure, Functionality and Application in Foods* (pp. 151-167). Singapore: Springer Singapore.

Phenolic Compounds, Antioxidant Capacity, and Protein Content of Three Varieties of Germinated Quinoa (*Chenopodium quinoa* Willd)

Compuestos fenólicos, capacidad antioxidante y contenido proteico de tres variedades de quinua germinada (*Chenopodium quinoa* Willd)

David Choque-Quispe¹, Carlos A. Ligarda-Samanez², Betsy S. Ramos-Pacheco³, Saida Leguía-Damiano⁴, Miriam Calla-Florez⁵, Lourdes M. Zamalloa-Puma⁶, and Luisa Colque-Condeña⁷

ABSTRACT

Quinoa (*Chenopodium quinoa* Willd) is a pseudocereal with a high nutritional potential and a significant content of bioactive compounds, which is consumed mainly by the inhabitants of the South American Andes. The aim of this study was to evaluate the protein content, total phenols, and antioxidant activity of quinoa grains of the *Salcedo INIA*, *Pasankalla*, and *Negra collana* varieties, germinated for 24 and 48 hours at 35 °C. Organic quinoa grains were grown in the Andahuaylas province in Peru, at an altitude of 3582 m. The protein content was determined through the Kjeldahl method, total phenols, in turn, by spectrophotometry with the Folin-Ciocalteu reagent, and the antioxidant activity of the DPPH type were registered. The data were analyzed through an Analysis of Variance (ANOVA), a Tukey test, and Pearson's correlation at 5% significance. The germinated quinoa grains showed a considerable increase ($p < 0,05$) in their protein content, total phenolic compounds, and antioxidant activity, as well as a strong positive correlation with the size of sprouts during the germination time. Therefore, germinated quinoa could be considered as a promising product for human nutrition and health.

Keywords: quinoa, bioactives, antioxidant activity, proteins, germinated quinoa

RESUMEN

La quinua (*Chenopodium quinoa* Willd) es un pseudocereal con alto potencial nutricional y un contenido significativo de compuestos bioactivos, el cual es consumido principalmente por los habitantes de los Andes sudamericanos. El objetivo del presente estudio fue evaluar el contenido de proteínas, fenoles totales y actividad antioxidante de granos de quinua de las variedades Salcedo INIA, Pasankalla y Negra collana, germinados a 24 y 48 horas y 35 °C. Los granos de quinua orgánica fueron cultivados en la provincia de Andahuaylas, Perú, a 3582 m de altitud. Se determinaron el contenido proteico a través del método Kjeldahl, los fenoles totales por espectrofotometría con el reactivo Folin-Ciocalteu, y la actividad antioxidante del tipo DPPH. Los datos fueron analizados a través de un análisis de la varianza (ANOVA), un test de Tukey y la correlación de Pearson al 5 % de significancia. Los granos de quinua desaponificados y germinados presentaron un incremento considerable ($p < 0,05$) en contenido proteico, compuestos fenólicos totales y actividad antioxidante, así como una fuerte correlación positiva con el tamaño de brotes durante el tiempo de germinación. Por lo tanto, la quinua germinada podría considerarse un producto prometedor para la nutrición y salud humana.

Palabras clave: quinua, bioactivos, actividad antioxidante, proteínas, quinua germinada

Received: August 9th, 2020

Accepted: January 18th, 2021

¹Chemical Engineer, UNSAAC, Peru. Ph.D. Candidate in Environmental and Water Resources Engineering, UFPR, Brazil. Affiliation: Research Professor, UNAJMA, Andahuaylas, Peru. E-mail: dchoque@unajma.edu.pe

²Food Engineer, UNSCH, Peru. Ph.D. Candidate in Environment and Sustainable Development, UAC, Peru. Affiliation: Research Professor, UNAJMA, Andahuaylas, Peru. E-mail: caligarda@unajma.edu.pe

³Agroindustrial Engineer, UNAJMA, Peru. Ph.D. Candidate in Environment and Sustainable Development, UAC, Peru. Affiliation: Research Professor, UNAJMA, Andahuaylas, Peru. E-mail: bsramos@unajma.edu.pe

⁴Agroindustrial Engineer, UNAJMA Peru. Affiliation: Research student, UNAJMA, Andahuaylas, Peru. E-mail: saidleguia@gmail.com

⁵Agroindustrial Engineer, UNSAAC, Peru. Affiliation: Associate Professor, UNSAAC, Cusco, Peru. E-mail: miriam.calla@unsaac.edu.pe

⁶Agroindustrial Engineer, UNSAAC, Peru. M.Sc. in Food Science and Technology, UAP, Peru. Affiliation: Research Professor, UNSAAC, Cusco, Peru. E-mail: lourdes.zamalloa@unsaac.edu.pe

⁷Agroindustrial Engineer, UNSAAC, Peru. M.Sc. in Food Science and Technology, UAP, Peru. Affiliation: Professor, UNSAAC, Cusco, Peru. E-mail: luisa.colque@unsaac.edu.pe

Introduction

Quinoa (*Chenopodium quinoa* Willd) is an endemic South American plant typical, domesticated thousands of years ago by the Inca people of the Andes of Peru and Bolivia, as well as parts of Ecuador, Argentina, and Chile. It comes with a diversity of forms, genotypes, and wild progenitors (Navruz-Varli, and Sanlier, 2016), as well as a high resistance and

How to cite: Choque-Quispe, D., Ligarda-Samanez, C. A., Ramos-Pacheco, B. S., Leguía-Damiano, S., Calla-Florez, M., Zamalloa-Puma, L. M., and Colque-Condeña, L. (2021). Phenolic Compounds, Antioxidant Capacity, and Protein Content of Three Varieties of Germinated Quinoa (*Chenopodium quinoa* Willd). *Ingeniería e Investigación*, 41(2), e89831. 10.15446/ing.investig.v41n2.89831



Attribution 4.0 International (CC BY 4.0) Share - Adapt

adaptability to climatic and edaphic conditions (Jacobsen, Mujica, and Jensen, 2003; Filho *et al.*, 2015).

Quinoa grain is considered to be a pseudocereal with a high nutritional value, mainly due to its high protein content and essential amino acids, which are higher than traditionally consumed cereals (Filho *et al.*, 2015; Dakhili, Abdolalizadeh, Hosseini, Shojaee-Aliabadi, and Mirmoghtadaie, 2019), whose importance is increasingly recognized in food safety, since it considerably replaces and complements the diet, especially for people who rarely consume meat and dairy products (Elsahaimy, Refaay, and Zaytoun, 2015; Navruz-Varli, and Sanlier, 2016). It is one of the main sources of protein in developing countries (Repo-Carrasco-Valencia, and Serna, 2011).

Quinoa grains have been found to contain numerous phytochemical compounds such as phytosterols, phytoecdysteroids, and phenols, which provide health benefits with their metabolic, cardiovascular, gastrointestinal, and anticarcinogenic aspects (Navruz-Varli and Sanlier, 2016; Vilcacundo and Hernández-Ledesma, 2017), and therefore have a high antioxidant activity, especially associated with phenolic compounds (Contreras-Jiménez, Torres-Vargas, and Rodríguez-García, 2019; Repo-Carrasco-Valencia, 2020), with up to 27 types of free and conjugated phenols (Abderrahim, Huanatico, Segura, Arribas, Gonzalez, Condezo-Hoyos, 2015), mostly phenolic acids (Repo-Carrasco-Valencia, and Serna, 2011; Tang, *et al.*, 2015; Tang *et al.*, 2016).

Quinoa grains are consumed in different forms by the inhabitants of the American Andes: in soups, extruded, instant breakfasts, flour, as a constituent of cookies, flour, bread, tortillas, among others (Bhargava, Shukla, and Ohri, 2006). This is due to their content of fiber, starch, and sugars such as maltose, D-galactose and D-ribose, fructose and glucose (Zhu, 2018; Piñuel *et al.*, 2019), which makes them ideal even for the production of fermented beverages such as beer and chicha (FAO, 2011).

The digestibility of quinoa protein is a limiting factor in their use in food (Elsahaimy *et al.*, 2015), but it improves considerably when subjected to germination, fermentation, and thermal treatments, thus increasing the bioavailability of its amino acids (Graf *et al.*, 2014; Navruz-Varli and Sanlier, 2016; Nickel, Spanier, Botelho, Gularte, and Helbig, 2016).

The germination process allows obtaining grains with high biological activity after enzymatic hydrolysis, thus enabling the accumulation of bioactive compounds such as polyphenols (Gan, Wang, Lui, Wu, and Corke, 2016; Televiciute *et al.*, 2020), which improves antioxidant activity (Banchuen, Thammarutwasik, Ooraikul, Wuttijumnong, and Sirivongpaisal, 2009; Sani, Iqbal, Chan, and Ismail, 2012). Thus, the germination process makes quinoa a more functional food (Dávila, Sangronis, and Granito, 2003; Graf *et al.*, 2014; Mariod and Salama, 2020), which implies a new way of sell a nutraceutical food, with good acceptance, especially in people who cannot consume food from animal sources (Piñuel *et al.*, 2019).

The aim of this research was to evaluate the effect of the germination of quinoa (*Chenopodium quinoa* Willd) of the *Salcedo INIA*, *Pasankalla*, and *Negra collana* varieties on phenolic compounds, antioxidant capacity, and protein content.

Materials and methods

Vegetable material

Organic quinoa grains (grown without the addition of pesticides and synthetic fertilizers) of the *Salcedo INIA*, *Pasankalla*, and *Negra collana* varieties were provided by the Machu Picchu agrarian cooperative in the province of Andahuaylas, Perú. These grains were cultivated during the vegetative period of 2017-2018, in fields located at 13° 39'26" S, 73° 17'32" W, and 3 682 m of altitude.

Obtaining germinated quinoa

Quinoa grains were washed with abundant treated water (pH 7.5), generating friction between grains to eliminate saponin. The washing continued until an evident absence of foam was reached. Then, they were subjected to a humidity between 43% and 45%, and packed in a wet gauze at 35 °C, for periods of 24 and 48 h, in order to cause germination, and the size of the sprout was measured with a Vernier. The sprouts were taken to a horizontal dryer at 60 °C, until constant humidity was reached, and then they were ground to 250 microns in an Agate mortar.

Protein quantification

The nitrogen content was determined through AOAC method 984.13 (AOAC, 2016). The protein content was calculated by $N \times 6.25$, and the results were expressed as percentage on dry basis (d.b).

Total phenol quantification

The spectrophotometric method used by Ah-Hen *et al.* (2012) was followed with some modifications. 1.0 g of sample was taken (germinated quinoa ground) and mixed with 10 ml of acidified methanol with 1% HCl. The homogenate was stored for 24 hours at 4 °C in darkness. Then, it was centrifuged for 15 min at 7000 rpm. An aliquot of the supernatant was taken in a test tube, thus obtaining a germinated quinoa extract, which was stored in a dark refrigerator.

100 µL of the extract were taken and caused to react under agitation with 750 µL of the reagent 1.0 N and 750 µL of sodium carbonate (60 g/L). The mixture was stored for 30 minutes in darkness at room temperature. In the same way, a blank was prepared using distilled water, which served to calibrate the spectrophotometer. Then, the absorbance was read at 755 nm in a spectrophotometer, model T80+ from PG Instruments.

The total phenolic compounds (TP) were estimated from a standard curve made with an aqueous gallic acid solution

($R^2 = 0,96$). The results were expressed as the mg gallic acid equivalent (GAE) per 100 g sample on dry basis (d.b.).

Antioxidant capacity quantification

The method of Brand-Williams, Cuvelier, and Berset, (1995) was followed with some modifications. 5,0 g of sample (germinated quinoa ground) were weighed, and 20 ml of 80% methanol were added and mixed for 15 min at 800 rpm. The extract was stored for 24 hours at 4 °C in darkness. Then, it was centrifuged at 3000 rpm for 20 minutes, taking an aliquot of the supernatant (extract) and placed in the darkness at 4 °C lined with aluminum foil.

150 μ L of the extract were taken and 2850 μ L of diluted DPPH solution (24 mg/100 ml methanol) were added. Identically, a blank was prepared with 150 μ L of 80% methanol to obtain a correction factor due to the dilution. The mixture was left to react in darkness for 30 min at 20 °C and then taken to the spectrophotometer; the absorbance was read at 515 nm.

The antioxidant capacity was calculated using a standard Trolox curve (0,5 mM) and expressed as the μ mol Trolox equivalent (TE)/g sample on dry basis (d.b.).

Statistic analysis

The data were collected in triplicate, and an analysis of variance (ANOVA) and Tukey test were applied. Correlations between variables were determined by the Pearson correlation coefficient (R_s) at 5% significance.

Results and discussion

Sprout size

In Figure 1, the size of the sprouts during germination can be observed. After 24 h, sprouts of around 6,4 mm are seen for the *Salcedo INIA* and *Pasankalla* varieties, and 8,8 mm for the *Negra collana* varieties, respectively; after 48 h of germination, these increased significantly ($p < 0,05$) in 175%, 232%, and 214% for *Salcedo INIA*, *Pasankalla*, and *Negra collana*, respectively (Figure 2). Similar results were reported by Bravo, Reyna, Gómez, and Huapaya (2013) for the Blanca de Junín variety. The difference in sprout size between varieties is due to genotypic differences (Piñuel *et al.*, 2019) and by grain color (Televičiutė *et al.*, 2020), as well as composition (sugars, proteins, minerals, lipids, among others) (Han *et al.*, 2019; Piñuel *et al.*, 2019).

Protein content

The protein contents of the ungerminated quinoa grains were between 13,73% and 15,61% (Table 1), with *Negra collana* being the variety that reported the highest content $15,61 \pm 0,23\%$. These results were similar to those reported by Pereira *et al.*, (2019), and Dakhili *et al.*, (2019).

On the other hand, it was observed that the protein content in the germinated quinoa increased significantly ($p < 0,05$) for the *Salcedo INIA* and *Pasankalla* varieties, unlike the *Negra*

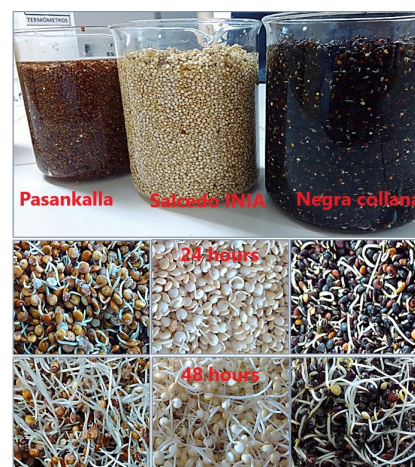


Figure 1. Quinoa varieties germinated at 24 and 48 h.

Source: Authors

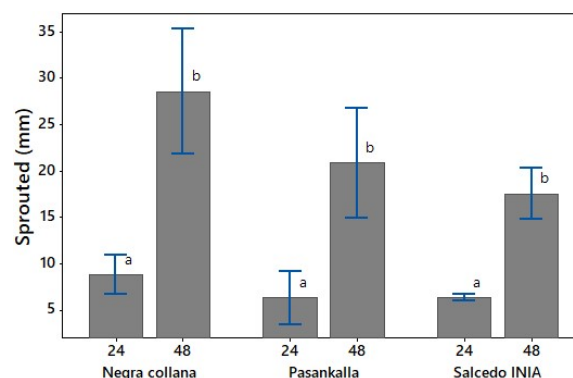


Figure 2. Sprout size of quinoa varieties germinated at 24 and 48 h.

Source: Authors

Table 1. Protein percentage variation in germinated quinoa

Time (h)	Salcedo INIA	Increase (%)	Pasankalla	Increase (%)	Negra collana	Increase (%)
0	13,73 \pm 0,17a		14,71 \pm 0,17a		15,61 \pm 0,23a	
24	14,75 \pm 0,23b	7,5	15,25 \pm 0,18b	3,7	15,70 \pm 0,24a	0,6
48	15,18 \pm 0,23b	10,6	15,60 \pm 0,23b	6,1	16,13 \pm 0,17a	3,4

Evaluated through a Tukey test at 5% significance.

Source: Authors

collana ($p > 0,05$). Likewise, it was observed that *Salcedo INIA* reported the greatest increase in protein content, from 13,73% to 14,75% in 24 hours (7,5%), and it increased to 15,18% in 48 hours, which represented 10,6%. On the other hand, *Pasankalla* and *Negra collana* reported a 6,1% and 4,8% increase from the initial value after 48 hours of germination, respectively. The same behavior was observed by Chaparro, Pismag, and Elizalde (2010), Bravo *et al.* (2013), and Piñuel *et al.* (2019).

During the germination process, the enzymatic systems are activated, mobilizing reserve proteins located in the cotyledons of the quinoa grain. In the same way, changes in the amino acid composition occur due to enzymatic activity (Gan *et al.*, 2016; Televičiutė *et al.*, 2020), which

allows the production of peptides of intermediate molecular weight due biological activity (Torres, Cova, and Valera *et al.*, 2018; Banchuen *et al.*, 2009). This also happens with the mobilization of nitrogen stored in the quinoa grain, which allows a significant increase in protein, as observed by El-Safy, Mukhtar, and Salem (2013), Graf *et al.* (2014), and Li, *et al.* (2014). However, this depends on the humidity and temperature of the environment.

Total phenol content

Polyphenolic compounds are beneficial for human health due to their antioxidant potential, which reduces the risk of cardiovascular diseases, neurodegenerative disorders, and diabetes (Gawlik-Dziki *et al.*, 2013; Navruz-Varli and Sanlier, 2016; Vilcacundo, and Hernández-Ledesma, 2017; Anngeli *et al.*, 2020).

The TP for the quinoa grains was between 159,69 and 198,23 mg GAE/100 g on dry basis (Table 2). These values are similar to those reported by Abderrahim *et al.* (2015), Nickel *et al.* (2016), and Saad-Allah and Youssef (2018). The differences in the total phenol content are due to growing conditions such as soil type (Nsimba, Kikuzaki, and Konishi, 2008; Liberal, Calhelha, Pereira, and Adegá, 2016; Huang, Qin, Shi, and Wen, 2017), as well as the variety, since the colored varieties have a higher TP, as reported by Tang *et al.* (2015), Abderrahim *et al.* (2015), and Han *et al.* (2019). *Pasankalla* (red coloration) reported the highest content, followed by the *Negra collana* variety (shiny black coloration).

Table 2. TP variation (mg GAE/100 g d.b) in germinated quinoa

Time (h)	Salcedo INIA	Increase (%)	Pasankalla	Increase (%)	Negra collana	Increase (%)
0	172,56 ± 0,51a		198,23 ± 1,46a		159,69 ± 4,89a	
24	278,27 ± 3,80b	61,3	307,64 ± 3,66b	55,2	233,78 ± 4,29b	46,4
48	308,82 ± 3,93c	79,0	417,75 ± 1,78c	110,7	403,30 ± 4,74c	152,6

Evaluated through a Tukey test at 5% significance.

Source: Authors

It was observed that, after 24 h of germination, the TP for the *Salcedo INIA* variety had an increase of 61,3% and, 79,0% after 48 h. The *Pasankalla* variety increased to 55,2% and 110,7% after 24 and 48 h, respectively (Table 2). It could also be observed that *Negra collana* reported the highest increase (152,6% after 48 h), which is due to its genotypic differences; since this variety is darker, it releases a greater amount of phenolic compounds due to the leaching effect during germination (Televičiutė *et al.*, 2020; Piñuel *et al.*, 2019).

The TP increase during the germination process of quinoa has been observed by Alvarez-Jubete, Wijngaard, Arendt, and Gallagher (2010), Filho *et al.* (2015), Gan *et al.* (2016), and Piñuel *et al.* (2019). It is due to the fact that quinoa grains suffer biotic and abiotic stress during germination, which induces the generation mainly of oxygen-reactive species (ROS). These compounds are vital to protecting the grains during germination (Shulaev, Cortes, Miller, and Mittler,

2008; Televičiutė *et al.*, 2020) and for the biochemical and physiological functions of the sprouts, releasing aglycones due to enzymatic activity, which translates into an increase in phenols (Shetty, 2004; Sani *et al.*, 2012). Another critical aspect is the germination temperature, which was 35 °C for this research. The recommended standard is between 35 and 45 °C (Televičiutė *et al.*, 2020).

Thus, germination is used as a strategy to increase the presence of bioactive compounds such as phenols, anthocyanins, flavonoids and others in legumes, cereals, and pseudocereals such as quinoa (Mbithi, Van, Rodríguez, and Huyghebaert, 2001; Fernandez-Orozco *et al.*, 2008; Sarvajeet, and Narendra, 2010; Oghbaei, and Prakash, 2017; Televičiutė *et al.*, 2020).

Antioxidant capacity (AA)

AA is an aspect that evaluates the ability of a compound to reduce the impact of ROS, and quinoa grains are an excellent source of antioxidants, being superior to many cereals, pseudocereals, and legumes (Pasko *et al.*, 2009; Tang and Tsao, 2017).

In Table 3, it is observed that the ungerminated quinoa grains reported antioxidant activity between 3,18 to 5,65 µmol TE/g d.b. The *Pasankalla* variety reported the highest antioxidant activity, followed *Negra collana*. This behavior is common for colored quinoa grains (Tang *et al.*, 2014; Abderrahim *et al.*, 2015; Escribano *et al.*, 2017; Mariod and Salama, 2020). The results were similar to those reported by other authors (Pasko *et al.*, 2009; Tang *et al.*, 2015; Nickel *et al.*, 2016; Repo-Carrasco-Valencia, 2000). However, the variation in antioxidant activity is due to genetic, agrotechnological, and environmental factors (Nsimba *et al.*, 2008).

Table 3. A variation (µmol TE/g d.b.) in germinated quinoa

Time (h)	Salcedo INIA	Increase (%)	Pasankalla	Increase (%)	Negra collana	Increase (%)
0	3,18 ± 0,05a		5,65 ± 0,04a		4,96 ± 0,04a	
24	3,81 ± 0,05b	19,8	6,66 ± 0,02b	17,8	5,65 ± 0,04b	13,9
48	5,40 ± 0,13c	69,4	6,82 ± 0,01c	20,8	5,90 ± 0,06c	19,0

Evaluated through a Tukey test at 5% significance.

Source: Authors

It was observed that, during germination, the AA of the grains of the quinoa varieties showed a significant difference ($p < 0,05$). The *Salcedo INIA* variety reported the greatest increase (19,8% and 69,4% after 24 and 48 h of germination, respectively), while the colored varieties, *Pasankalla* and *Negra collana*, reported increases of 20,8 and 19,0% after 48 h, respectively (Table 3). This behavior is common in quinoa grains that germinate under light or darkness (Pasko *et al.*, 2009; Filho *et al.*, 2015; Piñuel *et al.*, 2019); or when subjected to some biotechnological modifications (Nickel *et al.*, 2016; Mariod and Salama, 2020).

The increase in antioxidant activity is due to the response of the seed to the physiological and biochemical changes to which they are subjected at the beginning of germination, so

germination is used as a strategy to increase this capacity (Banchuen *et al.*, 2009; Sani *et al.*, 2012; Filho *et al.*, 2015; Torres *et al.*, 2018).

Correlation between variables

It was observed that the size of shoots evinced a high positive correlation with proteins, total phenols, and antioxidant activity ($R_s > 0,81$) (Table 4), which indicates that germination time causes these variables to increase considerably. Likewise, it was observed that the germination process of the three varieties of quinoa showed a high correlation between the study variables.

The protein content reported high correlation with the total phenols, with values above 0,80, as well as with the antioxidant capacity. This indicates that quinoa grains, during the stress that occurs during germination, produce phenols and proteins in parallel to condition the sprouts of the grains (Li *et al.*, 2014; Televičiūtė *et al.*, 2020).

Table 4. Correlation of study variables

	SS	P	TP
Salcedo INIA			
P	0,90		
TP	0,90	0,96	
AA	0,99	0,84	0,86
Pasankalla			
P	0,87		
TP	0,96	0,91	
AA	0,81	0,89	0,93
Negra collana			
P	0,82		
TP	1,00	0,80	
AA	0,88	0,63	0,88

Sprout size (SS), Proteins (P), Total phenols (TP), Antioxidant activity (AA).

Source: Authors

In the same way, the TP shows a high positive correlation with the AA for the three quinoa varieties ($> 0,86$), which suggests that the phenol content is a good indicator of the antioxidant activity (Pasko *et al.*, 2009; Tang *et al.*, 2014; Contreras-Jiménez *et al.*, 2019), thus making germinated quinoa highly bioaccessible and bioavailable to human health (Tang *et al.*, 2015; Navruz-Varli, and Nevin Sanlier, 2016; Vilcacundo and Hernández-Ledesma, 2017).

Conclusions

The study showed that unsaponified quinoa grains of the *Salcedo INIA*, *Pasankalla*, and *Negra collana* varieties, subjected to germinations of 24 and 48 hours at 35 °C, increased their content of proteins and total phenolic compounds, as well as their antioxidant activity, presenting a strong positive correlation between them.

The results allow us to confirm that germinated quinoa is a promising product for human nutrition and health.

References

- Abderrahim, F., Huanatico, E., Segura, R., Arribas, S., Gonzalez, M. C., and Condezo-Hoyos L. (2015). Physical features, phenolic compounds, betalains and total antioxidant capacity of coloured quinoa seeds (*Chenopodium quinoa* Willd) from Peruvian Altiplano. *Food Chemistry*, 183, 83-90. 10.1016/j.foodchem.2015.03.029
- Ah-Hen, K., Fuenzalida, C., Hess, S., Contreras, A., Vega-Gálvez, A., and Lemus-Mondaca, R. (2012). Antioxidant capacity and total phenolic compounds of twelve selected potato landrace clones grown in southern Chile. *Chilean journal of agricultural research*, 72(1), 3-9. 10.4067/S0718-58392012000100001
- Alvarez-Jubete L., Wijngaard, H., Arendt, E. K., and Gallagher, E. (2010). Polyphenol composition and in vitro antioxidant activity of amaranth, quinoa, buckwheat and wheat as affected by sprouting and baking. *Food Chemistry*, 119(2): 770-778. 10.1016/j.foodchem.2009.07.032
- Angeli, V., Silva, P., Massuela, D., Khan, M. W., Hamar, A., Khajehei, F., and Piatti, C. (2020). Quinoa (*Chenopodium quinoa* Willd.): An Overview of the Potentials of the "Golden Grain" and Socio-Economic and Environmental Aspects of Its Cultivation and Marketization. *Foods*, 9(2), 216. 10.3390/foods9020216
- AOAC (2016). *Official Methods of Analysis* (20th Ed.). Washington DC: Association of Official Analytical Chemists.
- Banchuen, J., Thammarutwasik, P., Ooraikul, B., Wuttijumong, P., and Sirivongpaisal, P. (2009). Effect of germinating processes on bioactive component of sangyodmuang-phatthalung rice. *Thai Journal of Agricultural Science*. 42(4), 191-199. <http://www.thaiscience.info/Journals/Article/TJAS/10594529.pdf>
- Bhargava, A., Shukla, S., and Ohri, D. (2006). *Chenopodium quinoa* - An Indian perspective. *Industrial Crops and Products*, 23(1), 73-87. 10.1016/j.indcrop.2005.04.002
- Brand- Williams, W., Cuvelier, M. E., and Berset, C. (1995). Use of a free radical method to evaluate antioxidant activity. *Lebensmittel, Wissenschaft und Technologie*, 28(1), 25-30. 10.1016/S0023-6438(95)80008-5
- Bravo, M., Reyna, J., Gómez, I., and Huapaya, M. (2013). Estudio químico y nutricional de granos andinos germinados de quinua (*Chenopodium quinoa*) y kiwicha (*Amarantuscaudatus*). *Revista Peruana de química e Ingeniería Química*, 16(1), 54-60. <https://revistasinvestigacion.unmsm.edu.pe/index.php/quim/article/view/6558>
- Chaparro, D. C., Pismag, R. Y., and Elizalde, A. (2011). Efecto de la germinación sobre el contenido de hierro y calcio de amaranto, quinua, guandul y soya. *Biotecnología en el Sector Agropecuario y Agroindustrial*, 9(1), 51-59. <https://revistas.unicauca.edu.co/index.php/biotecnologia/article/view/763>
- Contreras-Jiménez, B., Torres-Vargas, O. L., and Rodríguez-García, M.E. (2019). Physicochemical characterization of quinoa (*Chenopodium quinoa*) flour and isolated starch. *Food Chemistry*, 298, 1-7. 10.1016/j.foodchem.2019.124982

- Dakhili, S., Abdolizadeh, L., Hosseini, S. M., Shojaei-Aliabadi, S., and Mirmoghtadaie, L. (2019). Quinoa protein: Composition, structure and functional properties. *Food Chemistry*, 299, 125161. 10.1016/j.foodchem.2019.125161
- Dávila, M. A., Sangronis, E., and Granito, M. (2003). Leguminosas germinadas o fermentadas: alimentos o ingredientes de alimentos funcionales. *Artículos latinoamericanos de nutrición*, 53(4), 348-354. <https://www.alanrevista.org/ediciones/2003/4/art-2/>
- El-Safy, S., Mukhtar, E., and Salem, R. (2013). The impact of soaking and germination on chemical composition, carbohydrate fractions, digestibility, antinutritional factors and minerals content of some legumes and cereals grain seeds. *Alexandria Science Exchange Journal*, 34(4), 499-513. 10.21608/ASEJAIQJSAE.2013.3112
- Elsohaimy, S. A., Refaay, T M., and Zaytoun, M. A. M. (2015). Physicochemical and functional properties of quinoa protein isolate. *Annals of Agricultural Science*, 60(2), 297-305. 10.1016/j.aos.2015.10.007
- Escribano, J., Cabanes, J., Jimenez-Atiénzar, M., Ibañez, M., Gomez-Pando, L., García-Carmona, F., and Gandía-Herrero, F. (2017). Characterization of betalains, saponins and antioxidant power in differently colored quinoa (*Chenopodium quinoa*) varieties. *Food Chemistry*, 234, 285-294. 10.1016/j.foodchem.2017.04.187
- FAO (2011). *Quinoa: An Ancient Crop to Contribute to World Food Security*. Santiago de Chile, Chile: FAO, Regional Office for Latin America and the Caribbean.
- Fernández-Orozco, R., Frías, J., Zielinski, H., Piskula, M. K., Kozłowska, H., and Vidal-Valverde, C. (2008). Estudio cinético de los compuestos antioxidantes y la capacidad antioxidante durante la germinación de *Vigna radiata* cv. Emerald, *Glycine max* cv. Jutro y *Glicina max* cv. Mérito. *Food Chemistry*, 111(3), 622-630. 10.1016/j.foodchem.2008.04.028
- Filho, A. M., Ribeiro, M., Da Silva, J T., Pinheiro, H. M. Santana, J. B., and Dos Reis, J. S. (2015): Quinoa: Nutritional, Functional and Antinutritional Aspects. *Critical reviews in Food Science and Nutrition*, 57(8), 1618-1630. 10.1080/10408398.2014.1001811
- Gan, R. Y., Wang, M. F., Lui, W. Y. Wu, K., and Corke, H. (2016). Dynamic changes in phytochemical composition and antioxidant capacity in green and black mung bean (*Vigna radiata*) sprouts. *International Journal of Food Science and Technology*, 51(9), 2090-2098. 10.1111/ijfs.13185
- Gawlik-Dziki, U., Swieca, M., Sułkowski, M., Dziki, D., Baraniak, B., and Czyż, J. (2013). Antioxidant and anticancer activities of *Chenopodium quinoa* leaves extracts - In vitro study. *Food Chemical Toxicology* 57, 154-160. 10.1016/j.fct.2013.03.023
- Graf, B. L., Poulev, A., Kuhn, P., Grace, M. H., Lila, M. A., and Raskin, I. (2014). Quinoa seeds leach phytoecdysteroids and other compounds with anti-diabetic properties. *Food Chemistry*, 163, 178-185. 10.1016/j.foodchem.2014.04.088
- Han, Y., Chi, J., Zhang, M., Zhang, R., Fan, S., Huang, F., Xue, K., and Liu, L. (2019). Characterization of saponins and phenolic compounds: antioxidant activity and inhibitory effects on α -glucosidase in different varieties of colored quinoa (*Chenopodium quinoa* Willd). *Bioscience, Biotechnology, and Biochemistry*, 83(11), 2128-2139. 10.1080/09168451.2019.1638756
- Huang, J., Qin, L., Shi, Q., and Wen, A. (2017). Effect of quinoa saponins extraction and sprouting on saponins content. *Journal of the Chinese Cereals and Oils Association*, 32(11), 34-39. https://en.cnki.com.cn/Article_en/CJFDTotat-ZLYX201711008.htm
- Jacobsen, S. E., Mujica, A., and Jensen, C. R., (2003). The resistance of quinoa (*Chenopodium quinoa* Willd) to adverse abiotic factors. *Food Reviews International*, 19(1-2), 99-109. 10.1081/FRI-120018872
- Li, Y. C., Qian, H., Sun, X. L., Cui, Y., Wang, H. Y., Du, C., and Xia, X. H. (2014). The Effects of Germination on Chemical Composition of Peanut Seed. *Food Science and Technology Research*, 20(4), 883-889. 10.3136/fstr.20.883
- Liberal, A., Calhella, R. C., Pereira, C., and Adegá, F. (2016). A comparison of the bioactivity and phytochemical profile of three different cultivars of globe amaranth: red, white, and pink. *Food and Function*, 7(2), 679-688. 10.1039/c5fo01342a
- Mariod, A. A., and Salama, S. M. (2020). The Efficacy of Processing Strategies on the Gastroprotective Potentiality of *Chenopodium quinoa* Seeds. *The Scientific World Journal*, 6326452, 1-16. 10.1155/2020/6326452
- Mbithi, S., Van Camp, J., Rodríguez, R., and Huyghebaert, A. (2001). Efectos de la germinación en la composición de nutrientes y antinutrientes de los frijoles (*Phaseolus vulgaris* var. Rose coco). *European Food Research and Technology*, 212, 188-191. 10.1007/s002170000200
- Navruz-Varli, S. and Sanlier, N. (2016). Nutritional and health benefits of quinoa (*Chenopodium quinoa* Willd). *Journal of Cereal Science*, 69, 371-376. 10.1016/j.jcs.2016.05.004
- Nickel, J., Spanier, L. P., Botelho, F. T., Gularte, M. A., and Helbig, E. (2016). Effect of different types of processing on the total phenolic compound content, antioxidant capacity, and saponin content of *Chenopodium quinoa* Willd grains. *Food Chemistry*, 209, 139-143. 10.1016/j.foodchem.2016.04.031
- Nsimba, R. Y., Kikuzaki, H., and Konishi, Y. (2008). Antioxidant activity of various extracts and fractions of *Chenopodium quinoa* and *Amaranthus* spp. seeds. *Food Chemistry*, 106(2), 760-766. 10.1016/J.FOODCHEM.2007.06.004
- Oghbaei M., and Prakash J. (2017). Nutritional properties of green gram germinated in mineral fortified soak water: I. Effect of dehulling on total and bioaccessible nutrients and bioactive components. *Journal of Food Science and Technology*, 54, 880-889. 10.1007/s13197-016-2460-0
- Pasko, P., Barton, H., Zagrodzki, P., Gorinstein, S., Foltá, M., and Zachwieja, Z. (2009). Anthocyanins, total polyphenols and antioxidant activity in amaranth and quinoa seeds and sprouts during their growth. *Food Chemistry*, 115(3), 994-998. 10.1016/j.foodchem.2009.01.037

- Pereira, E., Encina-Zelada, C., Barros, L., Gonzales-Barron, U., Cadavez, V., and Ferreira, I. (2018). Chemical and nutritional characterization of *Chenopodium quinoa* Willd (quinoa) grains: A good alternative to nutritious food. *Food Chemistry*, 280, 110-114. 10.1016/j.foodchem.2018.12.068
- Piñuel, L., Boeri, P., Zubillaga, F., Barrio, D. A., Torreta, J., Cruz, A., Vásquez, G., Pinto, A., and Carrillo, W. (2019). Production of White, Red and Black Quinoa (*Chenopodium quinoa* Willd Var. Real) Protein Isolates and Its Hydrolysates in Germinated and Non-Germinated Quinoa Samples and Antioxidant Activity Evaluation. *Plants*, 8(8), 257. 10.3390/plants8080257
- Repo-Carrasco-Valencia, R. (2020). Nutritional Value and Bioactive Compounds in Andean Ancient Grains. *Proceedings*, 53(1), 1-5. 10.3390/proceedings2020053001
- Repo-Carrasco-Valencia, R. A. M. and Serna, L. A. (2011). Quinoa (*Chenopodium quinoa* Willd) as a source of dietary fiber and other functional components. *Food Science and Technology*, 31(1), 225-230. 10.1590/S0101-20612011000100035
- Saad-Allah, K. M., and Youssef, M. S. (2018). Phytochemical and genetic characterization of five quinoa (*Chenopodium quinoa* Willd) genotypes introduced to Egypt. *Physiology and Molecular Biology of Plants*, 24(4), 617-629. 10.1007/s12298-018-0541-4
- Sani, I. M., Iqbal, S., Chan, K. W., and Ismail, M. (2012). Effect of acid and base catalyzed hydrolysis on the yield of phenolics and antioxidant activity of extracts from germinated brown rice (GBR). *Molecules*, 17(6), 7584-7594. 10.3390/molecules17067584
- Sarvajeet, S. G. and Narendra, T. (2010). Especies reactivas de oxígeno y maquinaria antioxidante en tolerancia al estrés abiótico en plantas de cultivo. *Plant Physiology and Biochemistry*, 48(12), 909-930. 10.1016/j.plaphy.2010.08.016
- Shetty, K. (2004). Papel de la ruta del fosfato de pentosa ligado a la prolina en la biosíntesis de fenoles vegetales para aplicaciones funcionales alimentarias y ambientales: una revisión. *Process Biochemistry*, 39(7), 789-804. 10.1016/S0032-9592(03)00088-8
- Shulaev, V., Cortes, D., Miller, G., and Mittler, R. (2008). Metabolómica para la respuesta al estrés de la planta. *Physiologia Plantarum*, 132(2), 199-208. 10.1111/j.1399-3054.2007.01025.x
- Tang, Y., Zhang, B., Li, X., Chen, P. X., Zhang, H., Liu, R., and Tsao, R. (2016). Bound phenolics of quinoa seeds released by acid, alkaline, and enzymatic treatments and their antioxidant and α -glucosidase and pancreatic lipase inhibitory effects. *Journal of Agricultural and Food Chemistry*, 64(8), 1712-1719. 10.1021/acs.jafc.5b05761
- Tang, Y. and Tsao, R. (2017). Phytochemicals in quinoa and amaranth grains and their antioxidant, anti-inflammatory, and potential health beneficial effects: a review. *Molecular Nutrition and Food Research*, 61(7), 1600767. 10.1002/mnfr.201600767
- Tang, Y., Li, X., Chen, P. X., Zhang, B., Hernandez, M., Zhang, H., Marcone, M. F., Liu, R., and Tsao, R. (2014). Characterisation of fatty acid, carotenoid, tocopherol/tocotrienol compositions and antioxidant activities in seeds of three *Chenopodium quinoa* Willd genotypes. *Food Chemistry*, 174, 502-508. 10.1016/j.foodchem.2014.11.040
- Tang, Y., Li, X., Zhang, B., Chen, P. X., Liu, R., and Tsao, R. (2015). Characterisation of phenolics, betanins and antioxidant activities in seeds of three *Chenopodium quinoa* Willd. genotypes. *Food Chemistry*, 166, 380-388. 10.1016/j.foodchem.2014.06.018
- Televičiūtė, D., Tarasevičienė, Ž., Danilčenko, H., Barčauskaitė, K., Kandaraitė, M., and Paulauskienė, A. (2020). Changes in chemical composition of germinated leguminous under abiotic stress conditions. *Food Science and Technology*, 40(2), 415-421. 10.1590/fst.23019
- Torres, A., Cova, A., and Valera, D. (2018). Efecto del proceso de germinación de granos de Cajanuscajan en la composición nutricional, ácidos grasos, antioxidantes y bioaccesibilidad mineral. *Revista chilena de nutrición*, 45(4), 323-330. 10.4067/S0717-75182018000500323
- Vilcacundo, R., and Hernández-Ledesma, B. (2017). Nutritional and biological value of quinoa (*Chenopodium quinoa* Willd). *Current Opinion in Food Science*, 14, 1-6. 10.1016/j.cofs.2016.11.007
- Zhu, F. (2018). Chemical composition and food uses of teff (*Eragrostis tef*). *Food Chemistry*, 239, 402-415. 10.1016/j.foodchem.2017.06.101

Removal of Pb(II) in Aqueous Solutions Using Synthesized Zeolite X from Ecuadorian Clay

Remoción de Pb(II) en soluciones acuosas usando zeolita X sintetizada a partir de arcilla ecuatoriana

Daniel F. Medina-Rodríguez¹, Delly M. San Martín-Torres², Carmen M. López de García³, Luis V. García-Berfón⁴, Silvio D. Aguilar-Ramírez⁵, Ximena V. Jaramillo-Fierro⁶, Daniel J. Rosado-Alcarria⁷, and Adriana L. García-López⁸

ABSTRACT

Zeolite X was synthesized from clay using the alkaline fusion method and hydrothermal treatment to remove Pb(II) in aqueous solutions. Clay and zeolite were characterized through X-ray diffraction and fluorescence (XRD, FRX), as well as through specific surface area (SSA). The adsorbents were prepared as cylindrical extrudates using clay and a clay-zeolite combination (60-40%, respectively). The effects of pH, isotherm, and adsorption kinetics on the removal of Pb(II) in solutions of 80 mg Pb(II)/L were studied. It was possible to obtain a zeolite X from clay, with an SSA of 376 m²/g, 30 times greater than that of clay (12 m²/g). In the combined extrudate was present the zeolitic structure, with an SSA 12 times higher compared to the clay extrudate. The adsorption capacity, at 30 °C and V/m ratio of 1 g/L, is almost double compared to the clay extrudate (24 mg Pb(II)/g vs. 13 mg Pb(II)/g). Adsorption follows second order kinetics, and the Langmuir isotherm equation showed a good fit with the experimental equilibrium data for the two extrudates. The Webber-Morris and Bangham-Burt's models suggest that pore and film diffusion influence the kinetic mechanism.

Keywords: Pb(II) removal, heavy metals, alkaline fusion, zeolite synthesis

RESUMEN

Se sintetizó zeolita X a partir de arcilla utilizando el método de fusión alcalina y tratamiento hidrotérmico para eliminar Pb(II) en soluciones acuosas. La arcilla y la zeolita se caracterizaron por difracción y fluorescencia de rayos X (XRD, FRX), así como por área específica (SSA). Los adsorbentes se prepararon como extruidos cilíndricos usando arcilla y una combinación de arcilla-zeolita (60-40%, respectivamente). Se estudiaron los efectos del pH, la isoterma y cinética de adsorción en la remoción de Pb(II) en soluciones de 80 mg Pb(II)/L. Fue posible obtener zeolita X a partir de la arcilla, con una SSA de 376 m²/g, 30 veces mayor que la de arcilla (12 m²/g). En el extrudado combinado estuvo presente la estructura zeolítica, con una SSA 12 veces mayor comparado con el extruido de arcilla. La capacidad de adsorción, a 30 °C y relación V/m de 1 g/L, es casi el doble comparada con el extruido de arcilla (24 mg Pb(II)/g frente a 13 mg de Pb(II)/g). La adsorción sigue la cinética de segundo orden, y la ecuación de isoterma de Langmuir mostró un buen ajuste con los datos experimentales de equilibrio para los dos extruidos. Los modelos de Webber-Morris y Bangham-Burt sugieren que la difusión en la película y en los poros influye en el mecanismo cinético.

Palabras clave: remoción de Pb(II), metales pesados, fusión alcalina, síntesis de zeolita

Received: August 3rd, 2020

Accepted: February 18th, 2021

¹Daniel Fernando Medina. Master in Applied Chemistry from the Universidad Técnica Particular de Loja. Affiliation: Universidad Técnica Particular de Loja, Ecuador. Email: dfmedina4@utpl.edu.ec

²Delly Maribel San Martín. Master in Applied Chemistry from the Universidad Técnica Particular de Loja. Affiliation: Universidad Técnica Particular de Loja, Ecuador. Email: maribel22sanmartin@gmail.com

³Carmen Milena López. Doctor of Science, Major in Chemistry from Universidad Central de Venezuela. Affiliation: Universidad Técnica Particular de Loja, Ecuador. Email: milena.lopez2009@gmail.com

⁴Luis Vicente García. Doctor of Science, Major in Chemistry from Universidad Central de Venezuela. Affiliation: Universidad Técnica Particular de Loja, Ecuador. Email: lvargarcia4@utpl.edu.ec

⁵Silvio David Aguilar. Master in Applied Chemistry from the Universidad Técnica Particular de Loja. Affiliation: Universidad Técnica Particular de Loja, Ecuador. Email: sdaguilar@utpl.edu.ec

⁶Ximena Verónica Jaramillo. Master in Applied Chemistry from the Universidad Técnica Particular de Loja. Affiliation: Universidad Técnica Particular de Loja, Ecuador. Email: xvjaramillo@utpl.edu.ec

⁷Daniel Jesús Rosado. Doctor in Chemical and Environmental Technology from Universidad de Sevilla (Spain). Affiliation: University of Kiel, Germany. Email: drosado@hydrology.uni-kiel.de

Introduction

Lead (Pb) is a natural element of the Earth's crust present in the air, water, and soil. Due to its unique characteristics, humans have used lead in different manufactured products that have become its main anthropogenic sources, such as leaded gasoline, paints, ceramics, solders, water tanks, hair

⁸Adriana Lucía García. Doctor of Engineering Sciences from Universidad Central de Venezuela. Affiliation: Universidad Central de Venezuela, Venezuela. Email: adriana.ucv@gmail.com

How to cite: Medina, D. F., San Martín, D. M., López, C. M., García, L. V., Aguilar, S. D., Jaramillo, X. V., Rosado, D. J., and García, A. L. (2021). Removal of Pb(II) In Aqueous Solutions using Synthesized Zeolite X from Ecuadorian Clay. *Ingeniería e Investigación*, 41(2), e89671. [10.15446/ing.investig.v41n2.89671](https://doi.org/10.15446/ing.investig.v41n2.89671)



Attribution 4.0 International (CC BY 4.0) Share - Adapt

dye, cosmetics, airplanes, agricultural machinery, armour for X-ray machines, etc. (Boskabady *et al.*, 2018). However, lead is also an environmental pollutant and a non-biodegradable toxic metal, with well-known toxic effects (Poma, 2008). Therefore, it poses a risk to public health and, as a result, the world health organization, as well as other international organizations, has established a Pb(II) limit for drinking water of 0,01 mg Pb(II)/L (Uddin, 2017).

To stop releasing of Pb(II) into the environment and improve public health, it is necessary to remove Pb(II) from industrial wastewater. It is common today to use a large number of techniques for this purpose, including ion exchange, reverse osmosis, precipitation, and adsorption (Carolin, Kumar, Saravanan, Joshiba, and Nau-shad, 2017). Adsorption is an efficient separation technique that has been in use for a long time to remove heavy metal ions. In aqueous solutions, a wide variety of solid adsorbents have been reported, such as natural zeolites (Belova, 2019), bentonite (Ramola, Belwal, Li, Wang, and Zhou, 2020), cassava peel (Albis, 2016), activated carbon (Zafarzadeh, Sadeghi, Golbini-Mofrad, and Beirami, 2018), carbon nanotubes (Wang, Zhou, Peng, Yu, and Yang, 2007) or clay monoliths (Ahrouch, Gatica, Draoui, Bellido, and Vidal, 2019), among others.

Zeolites are crystalline solids with pores of molecular dimensions that allow the passage of molecules below a certain size depending on the porous system of the material. Zeolites contain mainly silicon, aluminium, oxygen, and some metals, including titanium, tin, zinc, and others. They have applications in adsorption, catalysis, ion exchange, and biological processes (Montalvo, Huiliñir, Borja, Sánchez, and Hermann, 2020).

Clays have been used as a source of silicon and aluminium in zeolite synthesis (Ayele, Pérez-Pariente, Chebude, and Díaz, 2016; Luo, Lau, Wu, Zhu, and Yang, 2018), since they are abundant and cheap materials in many countries, as is the case of Ecuador. Clays are very abundant silicoaluminates worldwide. They are used mainly for to manufacture construction materials such as bricks and tiles, as well as in the ceramic sector (Wi, Yang, Park, Chang, and Kim, 2020; Moussi *et al.*, 2020).

Synthetic zeolites with a faujasite structure (FAU) have been effective for the removal of Pb(II) in wastewater (Pandey, Sharma, and Sambhi, 2015; Shariatnia and Bagherpour, 2018). In light of the above, this research aims to synthesize zeolite from Ecuadorian clay and evaluate its potential as an adsorbent for the removal of Pb(II). In this work, faujasite type X zeolite was synthesized from clay from southern Ecuador, and cylindrical extrudates were prepared to evaluate its performance as an adsorbent in the removal of Pb(II) using an aqueous solution prepared in the laboratory. It was compared the behaviour of extrudates prepared with clay and those prepared with zeolite-clay mixtures.

Methods and materials

Materials and reagents

The starting clay, collected in the province of Loja, Ecuador, was named PACL-029. This clay, available in lumps of relatively large size, was oven-dried at 90 °C overnight, then crushed and sieved to a No. 200 ASTM mesh (0,075 mm) (Gilson Co., n.d).

The following reagents were used:

- Sodium hydroxide in lentils, 98%, Merck, Germany.
- Sodium aluminate (solid), 50-56% Al_2O_3 -37-45% Na_2O , Sigma Aldrich, United States.

Zeolite synthesis

In summary, the synthesis conditions were set based on previous work on zeolite synthesis from aluminosilicate gels (García, López, García, Casanova, and Goldwasser, 2016). The composition set for the synthesis mixture was $\frac{\text{SiO}_2}{\text{Al}_2\text{O}_3} = 4$, $\frac{\text{Na}_2\text{O}}{\text{SiO}_2} = 1,65$, and $\frac{\text{H}_2\text{O}}{\text{Na}_2\text{O}} = 40$. Since the employed clay has a $\frac{\text{SiO}_2}{\text{Al}_2\text{O}_3}$ ratio equal to eight, it was necessary to add sodium aluminate as an additional aluminium source to decrease the molar $\frac{\text{SiO}_2}{\text{Al}_2\text{O}_3}$ ratio to four.

The detailed process consisted of the following steps:

- Mixing 30 g of clay with 35 g of NaOH dissolved in 50 ml of water to form a homogeneous mud;
- calcinating the clay-NaOH mud at 800 °C for 4 h;
- trituration of the calcined product and mixing with a solution prepared by dissolving 15 g of sodium aluminate in 390 ml of water and stirring the mixture at room temperature for 1 h to homogenize;
- keeping the mixture at room temperature for 24 h (aging);
- a hydrothermal treatment of the mixture in covered and heated containers at 90 °C for 24 h;
- separating the solid product by filtration, washing with water to remove excess alkali, and drying at 90 °C overnight; and
- packaging the solid for subsequent characterization (the zeolitic product obtained with this procedure is the sodic form).

Preparation of adsorbents

For the evaluation of the solids as adsorbents, cylindrical extrudates with approximate dimensions of 0,5 cm in length and 0,25 cm in diameter were prepared. The preparation of these solids consisted of the following steps:

- (i) mixing of the solid materials in zeolite (clay ratio 40:60) adding water (approximately 35%) to form a mixture with good plasticity;
- (ii) extruding the mixture using a syringe with a 2,5 mm diameter plunger (the mixture is expelled at a constant speed, thus achieving extrudate threads with a diameter equal to the opening of the syringe);
- (iii) drying the extrudates at 90 °C for 12 h;
- (iv) Calcining in a muffle furnace with the following heating program: from room temperature to 100 °C at a rate of 2 °C/min, maintaining this temperature for 40 min, and increasing to 550 °C at a rate of 3 °C/min, leaving 550 °C for 8 h.

Characterization of solids

X-Ray diffraction measurements of the clay, synthesized zeolite, and the extrudates were performed on a Bruker model D8 Advanced, equipped with a solid-state LynxEye detector, using Cu K α radiation ($\lambda = 1,5406 \text{ \AA}$), operated at 40 kV and 25 mA, with a step width of 0,02044 in a 2θ range of 4,0-60,0°. The chemical composition was determined through X-Ray Fluorescence (XRF) in a portable Bruker model S1-turbo^{SD}, using the Mining Light Elements measurement method.

The determination of the specific surface area of the solids (m²/g) was carried out in the ChemiSorb 2720 equipment from Micromeritics, by adsorption of nitrogen at the temperature of liquid nitrogen (-196 °C) with a 30% gas mixture of diluted N₂ in He. The Chemisoft TPxV1.03 software allows calculating the specific surface area by applying the BET equation and the single point method (Webb, Orr, Camp, Olivier, and Yunes, 1997). The scanning electron microscopy (SEM) micrographs were taken on a Hitachi S-500 at 20 keV and 50 mA.

Pb(II) removal studies

Effect of pH: With the extrudates prepared with clay and extrudates prepared with zeolite-clay, an experiment was carried out consisting of contacting 25 mg of adsorbent with 25 mL (1g of solid per liter of solution) of 80 mg Pb(II)/L solution at 30 °C for 24 h and 100 rpm. The pH was adjusted to 4,03, 4,97, 6,06 and, 6,99 with 0,1 M HCl or NaOH solutions. The pH interval was chosen based on Pandey's work (Pandey *et al.*, 2015).

Adsorption equilibrium studies: For this study, Pb(II) solutions of 20, 40, 60, 80, 110, 140, 180, and 240 mg/L were used. The solution was maintained at pH = 5 based on the results obtained from the studied pH interval. The extrudates and an amount of Pb(II) solution, with a ratio of 1 g of solid per liter of solution, were placed in an Erlenmeyer flask of 100 mL. The above recipients were placed in an orbital agitator (Thermo Scientific SHKA2000) at 30 °C for 24 h and 100 rpm.

Adsorption isotherm: The adsorption capacity of solids can be determined by analyzing the equilibrium data through

isotherm models. An equilibrium isotherm relates the amount adsorbed and the concentration remaining in the solution in equilibrium. The Langmuir, Freundlich, and Temkin isotherm models were applied in this research (Bhatt *et al.*, 2012).

The Langmuir isotherm assumes a surface with homogeneous adsorption sites, without interactions between adsorbed species. Equation (1) represents the linear form of this isotherm (Bhatt *et al.*, 2012):

$$\frac{C_e}{Q_e} = \frac{1}{Q_m} * C_e + \frac{1}{K_L Q_m} \quad (1)$$

where

Q_e = equilibrium adsorption capacity, mg Pb(II)/g of adsorbent

Q_m = maximum adsorption capacity, mg Pb(II)/g of adsorbent

C_e = equilibrium concentration, mg Pb(II)/g of adsorbent

K_L = Langmuir adsorption constant, L/mg Pb(II)

Plotting $\frac{C_e}{Q_e}$ against C_e obtains a straight line with slope and intercept of $\frac{1}{Q_m}$ and $\frac{1}{K_L Q_m}$ respectively. K_L is a tool to the calculation of the dimensionless equilibrium parameter (R_L) calculated using Equation (2) (Bhatt *et al.*, 2012).

$$R_L = \frac{1}{(1 + K_L C_0)} \quad (2)$$

where

C_0 = initial concentration, mg Pb(II)/g of adsorbent

The Freundlich isotherm is an empirical model that describes monolayer and multilayer adsorption, expressed mathematically as Equation (3) (Bhatt *et al.*, 2012).

$$\log Q_e = \frac{1}{n} \log C_e + \log K_f \quad (3)$$

K_f and n are Freundlich constants incorporating the factors affecting the adsorption capacity and adsorption intensity, respectively. Plotting $\log Q_e$ vs. $\log C_e$ results in a linear graph with slope $\frac{1}{n}$ and intercept $\log K_f$, from which n and K_f can be calculated.

The Temkin isotherm model assumes that the adsorption heat decreases linearly with the increase in coverage of the adsorbent surface and a uniform distribution of binding energies up to a maximum binding energy. Equation (4) describes the Temkin isotherm (Inyibor, Adekola and Olatunji, 2016):

$$Q_e = B \ln A + B \ln C_e \quad (4)$$

B is a constant related to the heat of adsorption, and A is the Temkin isotherm constant (L/g). From the plot of Q_e vs $\ln C_e$, B and A can be calculated from the slope (B) and intercept ($B \ln A$) (Inyibor, Adekola and Olatunji, 2016).

In all cases, the equilibrium adsorption capacity, Q_e , was determined through Equation (5) (Bhatt *et al.*, 2012).

$$Q_e = (C_0 - C_e) * \left(\frac{V}{m}\right) \quad (5)$$

$\frac{V}{m}$ is the relationship between the Volume of solution in L (V) and mass of solid in g (m) used in the experiment. In all experiments, the $\frac{V}{m}$ ratio was the unity.

Adsorption kinetics studies: A plot of sorption vs. time usually indicates the adsorption kinetics. For kinetics experiments, the $\left(\frac{V}{m}\right)$ ratio was kept equal to unity: 500 mg of solid in 500 mL of 80 mg Pb(II)/L solution at 100 rpm and 30 °C. The sampling was performed in triplicate from time zero to 180 minutes, taking the average value in each measurement. The adsorption capacity of the solid (q), expressed as mg of Pb(II)/g, was determined through Equation (6) (Tan and Hamed, 2017):

$$q = (C_0 - C) * \left(\frac{V}{m}\right) \quad (6)$$

where q is the adsorption capacity of the solid for any time t , expressed as mg Pb(II)/g extrudate; C_0 and C , represents the metal concentration initial and at time t , respectively. In all of the above experiments, the Pb content in the solutions was determined on a Perkin Elmer Analyst 400 atomic absorption spectrometer.

Adsorption kinetics were investigated using pseudo first order (PFO), pseudo second order (PSO), and Elovich models. The diffusion mechanism was studied applying the Bangham-Burt and Webber-Morris intra-particle diffusion models (Tan and Hamed, 2017).

The pseudo first order (PFO) model has the linear form given in Equation (7) (Tan and Hamed, 2017).

$$\ln(q_e - q) = \ln(q_e) - k_1 t \quad (7)$$

where q_e is the equilibrium adsorption capacity (mg/g) at time t (the process time), k_1 is the pseudo first order rate constant which is calculated from the slope of the plot of $\ln(q_e - q)$ vs. time.

The PSO model assumes that the sorption rate is of the second order with respect to accessible active sites. Equation (8) shows the linear form of this model, where k_2 is the rate constant. A plot of $\frac{t}{q}$ vs. t produces a straight line for conforming kinetics. The values of k_2 and q_e are obtained from the slope and the intercept (Tan and Hamed, 2017).

$$\frac{t}{q} = \frac{1}{k_2 q_e^2} + \frac{t}{q_e} \quad (8)$$

The linear form of the Elovich model is presented in Equation (9), where α is the initial adsorption rate (mg/g.min) and β is the desorption constant associated with surface coverage. Kinetic data obeying this model would produce a straight line from the plot of q vs. $\ln t$. The slope and intercept are equal to $\left(\frac{1}{\beta}\right)$ and $\left(\frac{1}{\beta}\right) \ln(\alpha\beta)$, respectively (Tan and Hamed, 2017).

$$q = \left(\frac{1}{\beta}\right) \ln(\alpha\beta) + \left(\frac{1}{\beta}\right) \ln t \quad (9)$$

Bangham's model is usually applied to verify if pore diffusion is the only rate-controlling mechanism during an adsorptive process. It is generally used in the following form

(Equation 10) (Tan and Hamed, 2017):

$$\lg\left(\log\left(\frac{C_0}{C_0 - q\bar{m}}\right)\right) = \log\left(\frac{k_0 \bar{m}}{2.303 V}\right) + \alpha \log t \quad (10)$$

where V is the volume of the solution (mL), \bar{m} is the amount of extrudate per volume of solution in g/L, and k_0 and α are constants. In order to check the Bangham-Burt model, a plot of $\log\left(\log\left(\frac{C_0}{C_0 - q\left(\frac{V}{m}\right)}\right)\right)$ vs. $\log t$ should produce a straight line.

The Webber-Morris model (Equation 11), is also used to describe adsorption kinetics controlled by intra-particle diffusion (Equation 11), (Tan and Hamed, 2017).

$$q = k_{id} \sqrt{t} + B \quad (11)$$

where k_{id} is the intra-particle diffusion rate constant $\left(\frac{\text{mg}}{\text{g min}^{1/2}}\right)$, while B is the initial adsorption capacity (mg/g). To validate the Webber-Morris model, a plot of q vs. \sqrt{t} should be linear with k_{id} and B obtained as the slope and intercept, respectively.

Results and discussion

Characterization of clay and synthesized zeolite

The XRD pattern of the original clay (Figure 1) indicates the presence of these phases: heulandite (9,80 and 11,11° 2 θ), cristobalite (22 and 36° 2 θ), quartz (26,6° 2 θ), and anorthite (28° 2 θ). The XRD lines of the clay have a low intensity, indicating a low proportion of the identified clay minerals. For the synthesis, the alkaline fusion method recommended by various authors was used to obtain zeolites from clays, porcelain, and ashes (Ayele *et al.*, 2016; Bai, Zha, Chang, Zhang, and Chu, 2018; Kongnoo, Tontisirin, Worathanakul, and Phalakornkule, 2017; Ke, Shen, and Yang, 2019; Boycheva, 2020; Wajima and Ikegami, 2009). It was possible to zeolitize the clay through the applied method, since the synthesis product has the characteristic XRD pattern of the Faujasite structure (Figure 2), without the presence of lines corresponding to other crystalline phases (Treacy and Higgins, 2001). However, it cannot rule out the presence of amorphous phases not detectable by XRD.

The cell parameter a_0 (Å) of the synthesized zeolite was determined from the XRD pattern of the solid (Figure 2) according to the equation of the cubic crystalline system of the FAU structure. This parameter was calculated for each of the XRD lines at positions 15,44, 23,35, 26,70, and 30,92 position 2 θ , Cu, taking the average value of the determinations. The number of structural Al atoms in the zeolite was determined using the Breck-Flanigen equation (Giannetto, Montes, and Rodríguez, 2000), and the structural Si/Al ratio of the synthesized zeolite was calculated with this value. The calculated value for a_0 was 24,99 Å with $\left(\frac{\text{Si}}{\text{Al}}\right)_{\text{DRX}} = 1,08$ (Table 1). These values classify the synthesized zeolite as type X Faujasite (FAU). Therefore, the nomenclature used for this zeolite was FAU-Na.

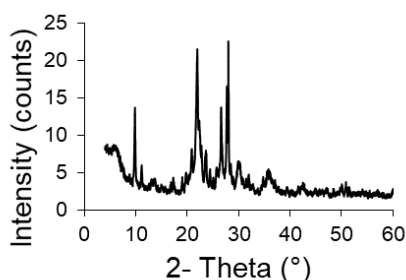


Figure 1. XRD pattern of PACL-029.

Source: Authors

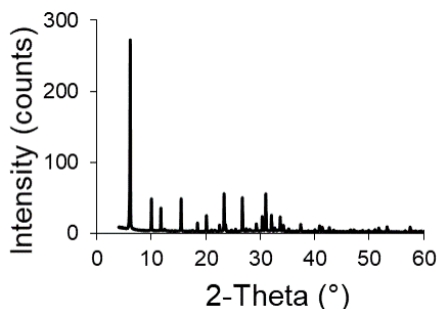


Figure 2. XRD pattern of FAU-Na.

Source: Authors

Figure 3 shows a SEM micrograph of the synthesized FAU-Na zeolite. The sample showed the typical morphology of octahedral crystalline aggregates, whose size aggregates can be lower than 1 μm .

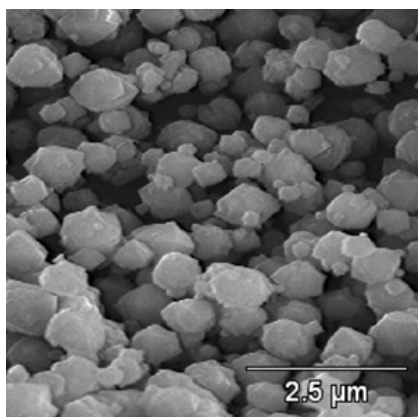


Figure 3. SEM micrograph of the FAU-Na zeolite.

Source: Authors

Table 1 shows the values of mass percentage of SiO_2 and Al_2O_3 , the molar $\left(\frac{\text{SiO}_2}{\text{Al}_2\text{O}_3}\right)$ ratio, and values of specific surface area (SSA) of the synthesized zeolite and clay. The synthesized zeolite has a SSA value 30 times higher than that of clay, due to the structural difference between the two solids. The dense phases that constitute the clay as cristobalite, quartz, and anorthite have low SSA values (about 3 m^2/g) (Bustillo, Fort, and Bustillo, 1993), whereas the synthetic Faujasite zeolite can have SSA values of up to 700 m^2/g (García et al 2016).

The chemical composition also changes with respect to the clay; the molar $\frac{\text{SiO}_2}{\text{Al}_2\text{O}_3}$ ratio in the zeolite is lower because it was changed in the synthesis mixture by the addition of the aluminium source. The determined value of the ratio $\left(\frac{\text{SiO}_2}{\text{Al}_2\text{O}_3}\right)_{\text{FRX molar}}$ in the zeolite was lower than that used in the synthesis mixture, which suggests that soluble silicate species formed during the alkaline fusion process remain in the synthesis mother liquor. On the other hand, the molar ratio $\left(\frac{\text{SiO}_2}{\text{Al}_2\text{O}_3}\right)_{\text{FRX molar}} > \left(\frac{\text{SiO}_2}{\text{Al}_2\text{O}_3}\right)_{\text{DRX molar}}$ indicated the difference between global molar and structural molar ratio; the first includes all present phases and the second refers only to zeolitic structure.

Table 1. Chemical composition and specific surface area of the synthesized clay and the zeolite

Solid	SSA (m^2/g)	Chemical composition (FRX)	(Si/Al) _{XRD}
Clay	12	% m SiO_2 = 65,90	—
		% m Al_2O_3 = 13,10	
		$\left(\frac{\text{SiO}_2}{\text{Al}_2\text{O}_3}\right)_{\text{molar}} = 8,55$	
zeolite	376	% m SiO_2 = 34,9	$a_0 = 24,99 \pm 0,01 \text{ \AA}$
		%m Al_2O_3 = 19,7	$\left(\frac{\text{Si}}{\text{Al}}\right)_{\text{XRD}} = 1,08$
		$\left(\frac{\text{SiO}_2}{\text{Al}_2\text{O}_3}\right)_{\text{FRX molar}} = 3,01$	$\left(\frac{\text{SiO}_2}{\text{Al}_2\text{O}_3}\right)_{\text{DRX molar}} = 2,16$

Source: Authors

Characterization of the prepared extrudates (solid adsorbents)

Despite the great industrial importance of producing structured adsorbents and catalysts from powders, few articles directly address structuring. Traditionally, the structuring of catalysts and adsorbents has been developed by companies and maintained as an internal know-how only disclosed in patents (Akthar, Anderson, Ogunwumi, Hedin, and Bergström, 2014).

Single-component clay extrudates and clay-zeolite extrudates were prepared with the synthesized zeolite. Table 2 shows the obtained SSA values. It is worth noting that the extrudates kept their shape after the adsorption experiments.

Table 2. Specific surface area values of extrudates

Solid	Specific surface area (m^2/g)
Extruded clay	10,0
Extruded clay-zeolite	120,0

Source: Authors

The XRD pattern of the extrudates prepared from the PACL-029 clay (Figure 4) is very similar to that of the original clay; only the lines under the 2θ angle are lost. In the XRD pattern of the clay-FAU-Na extrudates, the characteristic lines of the FAU structure are present with a high intensity (Figure 5), indicating that the structure is preserved. They also have all the DRX lines of the clay-only extrudates. The

SSA of the clay extrudates is very similar to the area of the original clay, indicating that the calcination treatment does not appreciably modify the structure of the solid. However, the slight difference in SSA values can be attributed to the lack of heulandite phase in the calcined clay, as indicated by the XRD pattern in Figure 4. The zeolite-clay extrudates reported a higher SSA value due to the contribution of the 40% of zeolite.

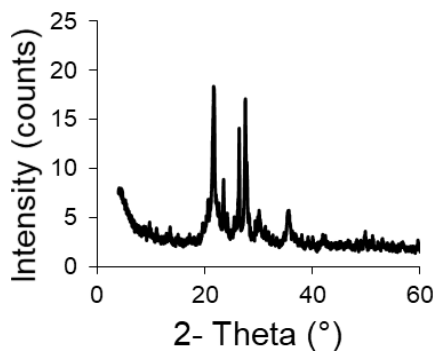


Figure 4. XRD pattern of clay extrudates.

Source: Authors

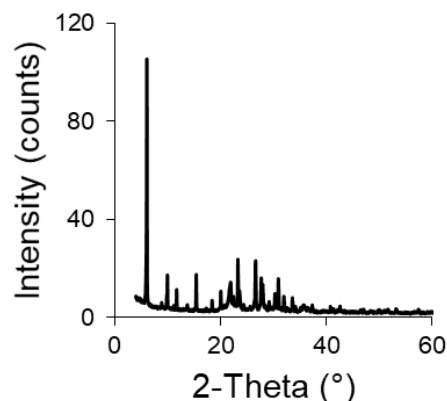


Figure 5. XRD pattern of clay-zeolite extrudates.

Source: Authors

Adsorption studies

Effect of pH on Pb(II) adsorption: With the combined adsorbent zeolite FAU Na-clay PACL-029, the maximum adsorption capacity is obtained at pH 4.97 (Figure 6), in accordance with what was reported by other authors (Pandey et al., 2015; Bai, Wang, and Zhu, 2020; Alsuhybani, Alshahrani, Algamdi, Al-Kahtani, and Alqadami, 2020; Yuan, Xie, Yan, Chen, and Wang, 2018). Figure 7, made with the chemical-equilibrium-diagram tool (Puigdomenech and Of, 2010), illustrates Pb(II) distribution vs pH. The Pb species present vary according to the pH of the solution. Considering only the influence of pH, Pb(II) dominates at low pH, whereas, at neutral-alkaline pH, the precipitation of $\text{Pb}(\text{OH})_2$ is dominant. Pb is amphoteric and, under extreme alkaline conditions ($\text{pH} > 12$), the negatively charged ion $\text{Pb}(\text{OH})_4^{2-}$ is dominant (Jensen, Ottosen, and Pedersen, 2006).

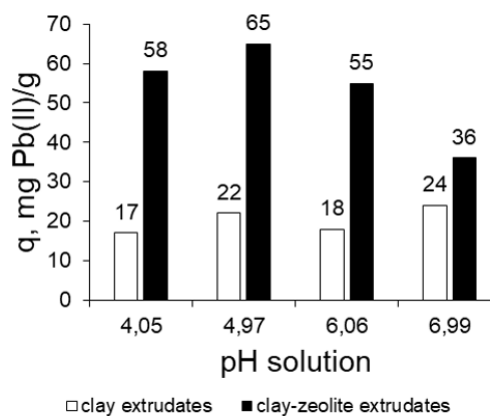


Figure 6. Variation of the adsorption capacity of Pb(II) with changes in pH of the solution.

Source: Authors

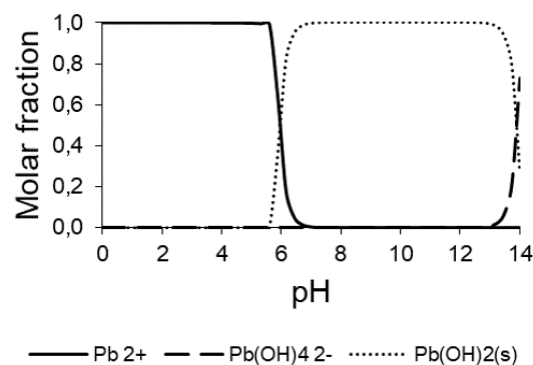


Figure 7. Predominance diagram Pb(II) in solution as a function of pH. Total concentration Pb(II) 80mg/L.

Source: Authors

Pandey et al. (2015) found that the removal of Pb(II) increased with increasing pH and recorded its minimum values at 4.0. The above behaviour was explained with the following argument: at lower pH values, the H^+ ions compete with the metal cation for the adsorption sites on the adsorbent, which in turn leads to partial release of the metal cation. At a higher pH level, the concentration of the H^+ ions as competing ion decreases, thus resulting in an increase in the amount of removed metal. Additionally, in the zeolite-containing adsorbent, the removal of Pb(II) can be carried out by adsorption and by ion exchange with the exchangeable cations of the zeolite. For a pH close to 5, it is likely that the concentration of interchangeable cations with Pb(II) such as H^+ and Na^+ is adequate to increase the adsorption capacity of the solid. With the PACL-029 adsorbent clay, little variation of the adsorption capacity of Pb(II) was obtained in the studied pH interval. In clay, the removal of Pb(II) could occur mainly by adsorption.

Equilibrium isotherm studies: The parameters obtained from isotherm model plots at 30 °C are tabulated in Table 3. Figure 8 shows plots of the linear form of the Langmuir, Freundlich and Temkin isotherm models.

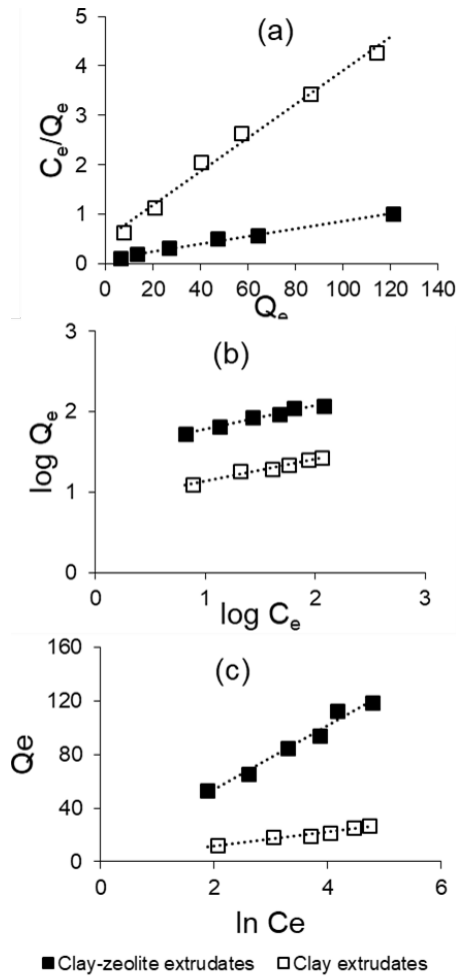


Figure 8. Representation of the isotherm linear forms for the extrudates: (a) Langmuir, (b) Freundlich, (c) Temkin.

Source: Authors

The best fit was obtained with the Langmuir model. For the determination of the constants of the Langmuir equation, the linear form of the Langmuir model, Equation (1) was employed obtaining acceptable adjustments (Figure 8a). The Langmuir model served to estimate the maximum metal uptake values where they could not be reached by the experiments. The separation factor (R_L) values, calculated through the Langmuir isotherm model for $C_0 = 80$ mg/L (Table 3), indicate that the adsorption is favourable for both adsorbents. The K_L values are comparable, but the maximum adsorption capacity Q_m according to the Langmuir equation is 4 times higher in the combined clay-zeolite extrudate. The representation of the linear Langmuir model in Figure 8a indicates a clear difference between the clay extrudates and the clay-zeolite combination. The zeolitization process remarkably improves the adsorption properties for Pb(II). Clay-zeolite extrudates have a higher adsorption capacity, which may be due to the higher specific surface area value of the extrudates, as well as to a difference in surface composition.

The parameters estimated from the Freundlich plot (Figure 8b) are presented in Table 3. The nature of the adsorptive process can be determined by the value of n (the process

is linear if $n = 1$, chemical if $n < 1$, and physical and favorable if $n > 1$). The values of n are > 1 , which indicates a favorable physisorption condition (Ohale, Onu, Ohale, N., and Oba, 2020).

Table 3. Isotherm parameters of the Langmuir, Freundlich and Temkin models

Langmuir Isotherm				
Extrudates	Qm (mg/g)	K _L (L/mg)	R _L	Linear regression equation
Clay	29,5	0,066	0,098	$\frac{C_e}{Q_e} = 0,034 \left(\frac{1}{C_e} \right) + 0,516$ $R^2 = 0,988$
Clay-zeolite	131,6	0,075	0,053	$\frac{C_e}{Q_e} = 0,0076 \left(\frac{1}{C_e} \right) + 0,101$ $R^2 = 0,994$
Freundlich Isotherm				
Extrudates	K _f (mg/g)	n	Linear regression equation	
Clay	7,23	3,61	$\log Q_e = 0,859 + 0,277 \log C_e$ $R^2 = 0,976$	
Clay-zeolite	31,33	3,45	$\log Q_e = 1,496 + 0,290 \log C_e$ $R^2 = 0,977$	
Temkin Isotherm				
Extrudates	A (L/g)	B	Linear regression equation	
Clay	1,37	5,17	$Q_e = 1,629 + 5,174 \ln C_e$ $R^2 = 0,974$	
Clay-zeolite	1,29	23,90	$Q_e = 6,119 + 23,90 \ln C_e$ $R^2 = 0,973$	

Source: Authors

The parameter B in the Temkin isotherm (Equation 4) is equal to $B = \frac{RT}{b_T}$, where R is the universal gas constant (J/mol K), T is the absolute temperature (K), and b_T (J/mol) is a factor that indicates the adsorbent-adsorbate interaction (Ohale *et al.*, 2020). Then from B , the parameter b_T was determined, obtaining the following values: b_T clay extrudate = 487 J/mol, and b_T clay – zeolite extrudate = 105 J/mol. These indicate a high interaction between adsorbent and the adsorbate, in disagreement with postulates from the Langmuir and Freundlich isotherm models. This model is probably not applicable in the present study. It is worth noting that the fit of the data is not very good.

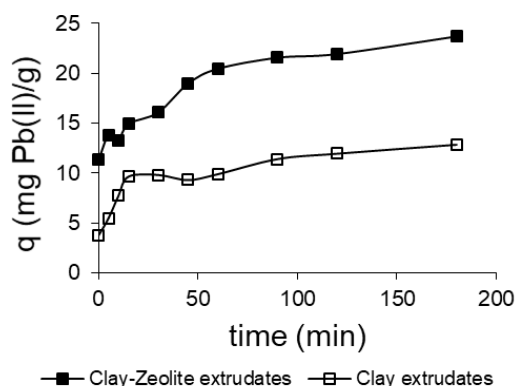
The data from the isotherms, adjusted according to the Langmuir model, indicate that the developed adsorbents are suitable for the adsorption of Pb(II). The maximum adsorption capacity values shown in Table 3 are comparable and even higher than other adsorbents reported in the literature. In Table 4, the maximum adsorption capacity and the adsorption constant according to the Langmuir model are compared for various solid adsorbents reported in previous works.

Adsorption kinetics studies: The kinetic behaviour is an important aspect to study the adsorption process of heavy metal ions in the solid adsorbent. The adsorption capacity q_t for each contact time represented in Figure 9 indicates that the combined adsorbent of the synthesized clay and FAU-Na zeolite has the highest Pb removal capacity.

Table 4. Comparison of the Q_m adsorption capacity and K_L adsorption constant of the Langmuir model with different solid adsorbents

Adsorbent	Q_m (mg/g)	K_L L/mg	Reference
Zeolite Na-X synthetic Si/Al = 1,37	14,22	0,0976	(Pandey <i>et al.</i> , 2015)
nFe@ZIF-8 (Zeolitic Imidazole Framework-8 modified with Fe)	182,0	2,87	(Zhou <i>et al.</i> , 2020)
ZCET-40 (material obtained from coal ash containing the zeolites NaP1, Hidroxisodalite and Analcima)	88,0	0,0002	(Visa, 2016)
Activated carbon with Fe	52,0	0,15	(Liu, Lai, and Wang, 2019)
FA24 adsorbent (synthesized from ashes consisting mainly of Hydroxisodalite)	38-40,5	0,11-0,16	(Kobayashi <i>et al.</i> , 2020)
Composite material Polyacrylonitrile/zeolite NaY, functionalized with Hydroxylamine	73,35	0,9015	(Elwakeel <i>et al.</i> , 2018)

Source: Authors

**Figure 9.** Adsorption capacity as a function of contact time for the two prepared adsorbents.

Source: Authors

The complete course of adsorption includes mass transfer and comprises three steps: (i) film diffusion (external diffusion), which is the transport of adsorptive from the bulk phase to the external surface of the adsorbent; (ii) pore diffusion (intra-particle diffusion), which is the transport of adsorptive from the external surface into the pores; and (iii) surface reaction, which is the attachment of adsorptive to the internal surface of sorbent (Tan and Hameed, 2017).

The surface reaction kinetics were studied with the pseudo first order, pseudo second order, and Elovich models stated in Equations (7), (8), and (9), respectively. Table 5 shows the parameters estimated from the plots of these models as described earlier in Experimentation section.

The graphs corresponding to the linear Equations (7), (8), and (9) are shown in Figure 10. The best fit was obtained by the second-order model. The q_e values obtained from pseudo first order and Elovich models were different from the actual q_e values obtained experimentally (Table 5). This suggests that these models were unsuitable to describe the adsorptive rate

processes. However, q_e values of the pseudo second order model showed good agreement with experimental q_e values. The evaluated regression coefficients were satisfactorily high ($R^2 \sim 0,99$) for the PSO model than for other sorption models.

Table 5. Adsorption kinetic parameters obtained by the PFO, PSO, and Elovich models

Pseudo first order model (PFO)			
Extrudates	$q_e \frac{mg Pb(II)}{g}$	$k_1 \min^{-1}$	Linear regression equation
Clay	6,55	0,0165	$\ln(q_e - q) = 1,880 - 0,0165 t$ $R^2 = 0,882$
Clay-Zeolite	11,35	0,0172	$\ln(q_e - q) = 2,429 - 0,0172 t$ $R^2 = 0,9655$
Pseudo second order model (PSO)			
Extrudates	$q_e \frac{mg Pb(II)}{g}$	$k_2 \left(\frac{g}{min \cdot mg Pb(II)} \right)$	Linear regression equation
Clay	12,94	0,0088	$\frac{t}{Q_e} = 0,6742 + 0,0773 t$ $R^2 = 0,989$
Clay-Zeolite	24,04	0,0055	$\frac{t}{Q_e} = 0,3434 + 0,0416 t$ $R^2 = 0,994$
Elovich model			
Extrudates	$\alpha \frac{mg Pb(II)}{g \min}$	β	Linear regression equation
Clay	3,16	0,466	$q = 1,061 + 2,143 \ln t$ $R^2 = 0,9201$
Clay-Zeolite	18,49	0,317	$q = 5,580 + 3,153 \ln t$ $R^2 = 0,9372$

Source: Authors

The values of the adsorption rate constant (k_2) are of the same order in the clay extrudates and in the combined extrudate, and the latter has twice the adsorption capacity. The pseudo second order kinetic model has been reported in several investigations on Pb(II) removal in aqueous systems. Table 6 shows the kinetic parameter values reported in other investigations. Like the data indicated by the adjustment with the Langmuir isotherm model, these data indicate that the two prepared adsorbents are suitable for the Pb(II) removal.

To determine whether pore diffusion was the only rate-limiting step in the adsorptive study of this system, experimentally obtained kinetic data was fitted to the Bangham-Burt model stated in Equation (10). The linear plot presented in Figure 11b and the corresponding R^2 values given in Table 7 suggest that pore and film diffusion influenced the kinetic mechanism.

The Webber-Morris intraparticle diffusion model (Equation 11) was used to examine the contributions of each diffusion step in the overall mass transfer mechanism: external and intra-particle (Robati, 2013; Chu *et al.*, 2019). Results of model plot are presented in Figure 11a. This Figure shows two linear segments, which implies that adsorptive mass transfer took place under two steps. The first segment signifies an external

surface adsorption associated with liquid film diffusion, while the second segment depicts an adsorption controlled by intra-particle diffusion. The intra-particle diffusion rate constant (k_{id1} and k_{id2}) estimated from both segments is presented in Table 7.

Table 6. Comparison of the kinetic parameters of the pseudo second order model reported in previous investigations

Solid adsorbent	$q_e \frac{mg Pb(II)}{g}$	$k_2 \left(\frac{g}{min \cdot mg Pb(II)} \right)$	Reference
Graphene oxide / alginate hydrogel membrane	163,0	0,324	(Bai et al., 2020)
Magnetic nanoparticles covered with benzoic acid functionalized with aminoguanidinopentanoic acid	19,53	0,0017	(Alsuhybani et al., 2020)
HCTMABr Modified Micronized Clinoptilolite	0,304	0,6536	(Shirzadi and Nezamzadeh-Ejehieh, 2017)
Zeolite USY with alkaline treatment	4,03	0,1070	(Sulaiman et al., 2020)
Clinoptilolite-glycine	4,14	0,032	(Nasiri-Ardali and Nezamzadeh-Ejehieh, 2020)

Source: Authors

Table 7. Parameters obtained from intra-particle diffusion kinetic models

Webber-Morris' model			
Extrudates	$k_{id} \frac{mg}{g \cdot min^{1/2}}$	$B \frac{mg}{g}$	Linear regression equation
Clay	$k_{id1} = 1,23$	$B_1 = 3,64$	$q_1 = 3,64 + 1,23t^{1/2} R^2 = 0,9017$
	$k_{id2} = 0,54$	$B_2 = 5,87$	$q_1 = 5,87 + 0,54t^{1/2} R^2 = 0,9615$
Clay-Zeolite	$k_{id1} = 11,39$	$B_1 = 0,84$	$q_1 = 11,69 + 0,85t^{1/2} R^2 = 0,927$
	$k_{id2} = 15,06$	$B_2 = 0,65$	$q_2 = 15,06 + 0,65t^{1/2} R^2 = 0,9582$
Bangham's model			
Extrudates	k_0	α	Linear regression equation
Clay	18,30	0,31	$\log \left(\log \left(\frac{C_0}{C_0 - q_m} \right) \right) = -1,80 + 0,31 \log t R^2 = 0,8667$
Clay-Zeolite	53,22	0,22	$\log \left(\log \left(\frac{C_0}{C_0 - q_m} \right) \right) = -1,34 + 0,22 \log t R^2 = 0,8667$

Source: Authors

Conclusions

Zeolite X with Si/Al = 1,08 ratio was synthesized from clay, using synthesis mixture compositions employed in synthesis from aluminosilicate gels. The characterization carried out indicated adequate properties in the synthesized zeolite, such as purity, crystallinity, and specific area. The zeolite in the

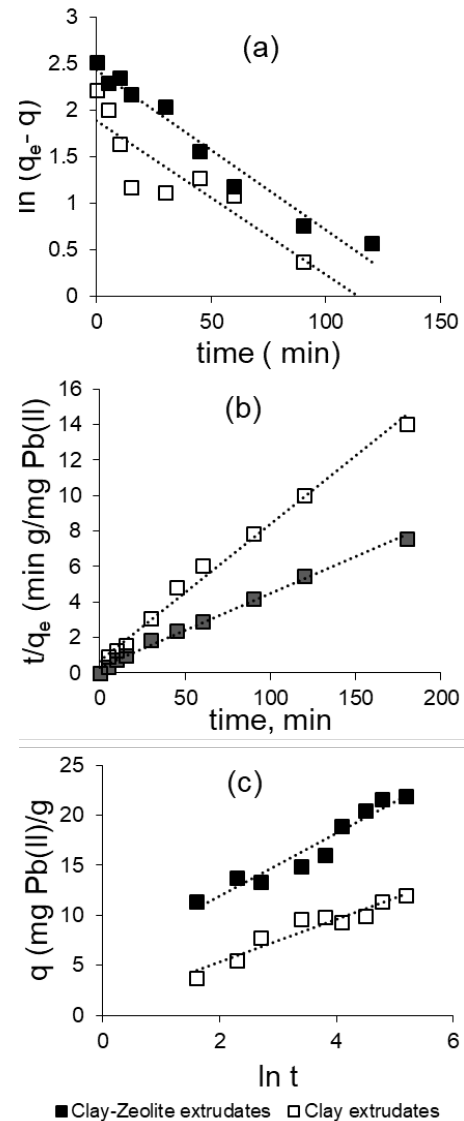


Figure 10. Kinetic plots for (a) Pseudo first order model, (b) Pseudo second order model and (c) Elovich model.

Source: Authors

extrudate maintains the crystalline structure and increases the specific surface area 10 times compared to the clay-only material, notably improving the adsorption capacity of Pb(II), which is favoured at pH = 5. The adsorption equilibrium isotherm (at 30 °C) was adjusted applying the Langmuir model, with a separation factor R_L indicating favorable adsorption. The maximum adsorption capacity Q_m was 132 mg Pb(II)/g, a comparable value and even higher than reported values for a variety of solid adsorbents. The adsorption kinetics were adjusted to the pseudo second order model with chemical adsorption controlling the process. The value of the kinetic constant is of the same order in the evaluated materials. However, in the combined material, the adsorption capacity q_e is almost double. The liquid film diffusion and intra-particle diffusion influence the kinetic mechanism.

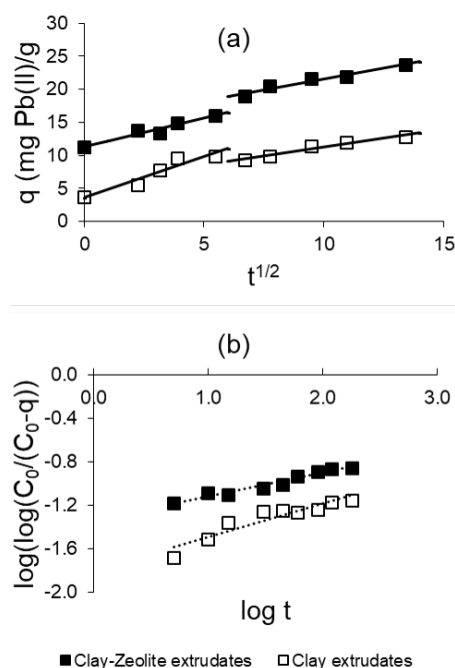


Figure 11. Kinetic plots for (a) Webber Morris model (b) Bangham model.

Source: Authors

Acknowledgements

The authors acknowledge the Master's degree program in Applied Chemistry of Universidad Técnica Particular de Loja for funding this research, as well as Dr. Paulina Aguirre and Mgtr. Diego Maza for their collaboration in the adsorption experiments.

References

- Ahrouch, M., Gatica, J., Draoui, K., Bellido, D., and Vidal, H. (2019). Lead removal from aqueous solution by means of natural clays honeycomb monoliths. *Journal of Hazardous Materials*, 365, 519-530. 10.1016/j.jhazmat.2018.11.037
- Akthar, F., Anderson, L., Ogunwumi, S., Hedin, N., and Bergström, L. (2014). Structuring adsorbents and catalyst by processing of porous powders. *Journal of the European Ceramic Society*, 34(7), 1643-1666. 10.1016/j.jeurceramsoc.2014.01.008
- Albis, A., Martínez, J., Severiche, M., and García, J. (2016). Removal of lead from aqueous solution using cassava peel modified with citric acid. *Avances: Investigación en Ingeniería*, 13(1), 1-11. 10.18041/1794-4953/avances.2.254
- Alsuhybani, M., Alshahrani, A., Algamdi, M., Al-Kahtani, A., and Alqadami, A. (2020). Highly efficient removal of Pb(II) from aqueous systems using a new nanocomposite: Adsorption, isotherm, kinetic and mechanism studies. *Journal of Molecular Liquids*, 301, 112393. 10.1016/j.molliq.2019.112393
- Gilson Co. (n.d.) *ASTM test sieves*. <https://www.globalgilson.com/astm-test-sieves>
- Ayele, L., Pérez-Pariente, J., Chebude, Y., and Díaz, I. (2016). Conventional versus alkaline fusion synthesis of zeolite A from low grade kaolin. *Applied Clay Science*, 132-133, 485-490. 10.1016/j.clay.2016.07.019
- Bai, S., Zha, L., Chang, Z., Zhang, Ch., and Chu, M. (2018). Synthesis of Na-X zeolite from Longkou oil shale ash by alkaline fusion hydrothermal method. *Carbon Resources Conversion*, 1(3), 245-250. 10.1016/j.crcon.2018.08.005
- Bai, Ch., Wang, L., and Zhu, Z. (2020). Adsorption of Cr(III) and Pb(II) by graphene oxide/alginate hydrogel membrane: Characterization, adsorption kinetics, isotherm and thermodynamics studies. *International Journal of Biological Macromolecules*, 147, 898-910. 10.1016/j.ijbiomac.2019.09.249
- Belova T., (2019). Adsorption of heavy metal ions (Cu+2, Ni+2, Co+2 and Fe+2) from aqueous solutions by natural zeolite. *Heliyon*, 5(9), e02320. 10.1016/j.heliyon.2019.e02320
- Bhatt, A., Sakaria, P., Vasudeven, M., Pawar, R., Sudheesh, N., Bajaj, H., and Mody, H. (2012). Adsorption of an anionic dye from aqueous medium by organoclays: equilibrium modeling, kinetic and thermodynamic exploration. *RSC Advances*, 2(23) 8663-8671. 10.1039/C2RA20347B
- Boskabady, M., Marefati, N., Farkhondeh, T., Shakeri, F., Farshbaf, A., and Boskabady, H. M. (2018). The effect of environmental lead exposure on human health and the contribution of inflammatory mechanisms, a review. *Environment International*, 120, 404-420. 10.1016/j.envint.2018.08.013
- Boycheva, S., Marinov, I., Miteva, S., and Zgureva, D. (2020). Conversion of coal fly ash into nanozeolite Na-X by applying ultrasound assisted hydrothermal alkaline activation. *Sustainable Chemistry and Pharmacy*, 15, 100217. 10.1016/j.scp.2020.100217
- Bustillo, M., Fort, R., and Bustillo, M. (1993). Specific surface area and ultramicroporosity in polymorphs of silica. *European Journal of Mineralogy*, 5(6) 1195-1204. 10.1127/ejm/5/6/1195
- Carolin, F. C., Kumar, S. P., Saravanan, A., Joshiba J. G., and Naushad, M. (2017). Efficient techniques for the removal of toxic heavy metals from aquatic environment: A review. *Journal of Environmental Chemical Engineering*, 5(3), 2782-2799. 10.1016/j.jece.2017.05.029
- Chu, Y., Khan, M., Wang, F., Xia, M., Lei, W., and Zhu, S. (2019). Kinetics and equilibrium isotherms of adsorption of Pb(II) and Cu(II) onto raw and arginine-modified montmorillonite. *Advance Powder Technology*, 30(5), 1067-1078. 10.1016/j.appt.2019.03.002
- Elwakeel, K., El-Bindary, E., Kouta, E., and Guibal, E. (2018). Functionalization of polyacrylonitrile/Na-Y-zeolite composite amidoxime groups for the sorption of Cu(II), Cd(II) and Pb(II) metal ions. *Chemical Engineering Journal*, 332, 727-736. 10.1016/j.cej.2017.09.091
- García, A., López, C. M., García, L., Casanova, J., and Goldwasser, M. (2016). Improvements in the synthesis with low Si/Al

- ratio from Venezuelan sodium silicate for an environmentally friendly process. *Ingeniería e Investigación*, 36(1), 62-69. 10.15446/ing.investig.v36n1.52855
- Giannetto, G., Montes, A., and Rodríguez, G. (2000). *Zeolitas: Características, propiedades y aplicaciones industriales*. Caracas, Venezuela: Innovación Tecnológica, Universidad Central de Venezuela.
- Inyibor, A., Adekola, F., and Olatunji, G. (2016). Kinetics, isotherms and thermodynamic of liquid phase adsorption of Rhodamine B dye onto *Raphia hookeri* fruit epicarp. *Water Resources and Industry*, 15, 14-27. 10.1016/j.wri.2016.06.001
- Jensen, P., Ottosen, L., and Pedersen, J. (2006). Speciation of Pb in industrially polluted soils. *Water, Air, and Soils Pollution*, 170, 359-382. 10.1007/s11270-005-9008-7
- Ke, G., Shen, H., and Yang, P. (2019). Synthesis of X-zeolite from waste basalt powder and its influencing factors and synthesis mechanism. *Materials*, 12(23), 3895. 10.3390/ma12233895
- Kobayashi, Y., Ogata, F., Nakamura, T., and Kawasaki, N. (2020). Synthesis of novel zeolites produced from fly ash by hydrothermal treatment in alkaline solution and its evaluation as an adsorbent for heavy metal removal. *Journal of Environmental Chemical Engineering*, 8(2), 103687. 10.1016/j.jece.2020.103687
- Kongnoo, A., Tontisirin, S., Worathanakul, P., and Phalakornkule, Ch. (2017). Surface characteristics and CO₂ adsorption capacities of acid-activated zeolite 13X prepared from palm oil mill fly ash. *Fuel*, 193, 385-394. 10.1016/j.fuel.2016.12.087
- Liu, X., Lai, D., and Wang, Y. (2019). Performance of Pb(II) removal by an activated carbon supported nanoscale zero-valent iron composite at ultralow iron content. *Journal of Hazardous Materials*, 361, 37-48. 10.1016/j.jhazmat.2018.08.082
- Luo, H., Lau, W., Wu, Y., Zhu, W., and Yang, E-H. (2018). Hydrothermal synthesis of needle-like nanocrystalline zeolites from metakaolin and their applications for efficient removal of organic pollutants and heavy metals. *Microporous Mesoporous Materials*, 272, 8-15. 10.1016/j.micromeso.2018.06.015
- Montalvo, S., Huiliñir, C., Borja, R., Sánchez, E., and Hermann, C. (2020). Applications of zeolites for biological treatment processes of solids wastes and wastewaters – A review. *Bioresource Technology*, 301, 122808. 10.1016/j.biortech.2020.122808
- Moussi, B., Hajjaji, W., Hachani, M., Hatira, N., Labruncha, J., Yans, J., and Jamoussi, F. (2020). Numidian clay deposits as raw material for ceramics tile manufacturing. *Journal of African Earth Science*, 164, 103775. 10.1016/j.jafrearsci.2020.103775
- Nasiri-Ardali, M., and Nezamzadeh-Ejhieh, A. (2020). A comprehensive study on the kinetics and thermodynamic aspects of batch and column removal of Pb(II) by the clinoptilolite-glycine adsorbent. *Materials Chemistry Physics*, 240, 122142. 10.1016/j.matchemphys.2019.122142
- Ohale, P., Onu, C., Ohale, N., and Oba, S. (2020). Adsorptive kinetics, isotherm and thermodynamic analysis of fishpond effluent coagulation using waste *Brachyura* shell. *Chemical Engineering Journal Advances*, 4, 100036. 10.1016/j.cej.2020.100036
- Pandey, P., Sharma, S. K., and Sambi, S. (2015). Removal of lead(II) from waste water on zeolite NaX. *Journal of Environmental Chemical Engineering*, 3(4), 2604-2610. 10.1016/j.jece.2015.09.008
- Poma, P. (2008). Intoxicación por plomo en humanos. *Anales de la Facultad de Medicina*, 69(2), 120-126.
- Puigdomenech, I. and Of, K. R. I. T. (2010). *MEDUSA, HYDRA and INPUT-SED-PREDOM*. <https://www.kth.se/che/medusa/>
- Ramola, S., Belwal, T., Li, C., Wang, Y., and Zhou, Ch. (2020). Improved lead removal from aqueous solution using novel porous bentonite and calcite biochar composite. *Science of the Total Environment*, 709, 136171. 10.1016/j.scitotenv.2019.136171
- Robati, D. (2013). Pseudo second order kinetic equations for modeling adsorption systems for removal of lead ions using multi walled carbon nanotube. *Journal of Nanostructure in Chemistry*, 3(1), 55. 10.1186/2193-8865-3-55
- Shariatina, Z. and Bagherpour, A. (2018). Synthesis of zeolite NaY and its nanocomposite with chitosan adsorbents for lead(II) removal from aqueous solution. *Powder Technology*, 338, 744-763. 10.1016/j.powtec.2018.07.082
- Shirzadi, H. and Nezamzadeh-Ejhieh, A. (2017). An efficient modified zeolite for simultaneous removal of Pb(II) and Hg(II) from aqueous solution. *Journal of Molecular Liquids*, 230, 221-229. 10.1016/j.molliq.2017.01.029
- Sulaiman, K., Sajid, M., and Alhooshani, K. (2020). Application of porous membrane bag enclosed alkaline treated Y-zeolite for removal of heavy metal ions from water. *Microchemical Journal*, 152, 104289. 10.1016/j.microc.2019.104289
- Tan, K. and Hameed, B. (2017). Insight into the adsorption kinetics models for the removal of contaminants from aqueous solutions. *Journal of the Taiwan Institute of Chemical Engineers*, 74, 25-48. 10.1016/j.jtice.2017.01.024
- Tracy, J. and Higgins, B. (2001). *Collection of Simulated XRD Powder Patterns for Zeolites*. Structure Commission of the International Zeolite Association.
- Uddin, K. M. (2017). A review on the adsorption of heavy metals by clay minerals, with special focus on the past decade. *Chemical Engineering Journal*, 308, 438-462. <https://doi.org/10.1016/j.cej.2016.09.029>
- Visa, M., (2016). Synthesis and characterization of new zeolites obtained from fly ash for heavy metals removal in advanced wastewater treatment. *Powder Technology*, 294, 338-347. 10.1016/j.powtec.2016.02.019
- Wajima, T. and Ikaezami, Y. (2009). Synthesis of crystalline zeolite 13X from waste porcelain using alkali fusion. *Ceramics International*, 35(7), 2983-2986. 10.1016/j.ceramint.2009.03.014

- Wang, H., Zhou, A., Peng, F., Yu, H., and Yang, J. (2007). Mechanism study on adsorption multiwalled carbon nanotubes. *Journal of Colloid Interface Science*, 316(2) 277-283. 10.1016/j.jcis.2007.07.075
- Wi, S., Yang, S., Park, J., Chang, S., and Kim, S. (2020). Climatic cycling assessment of red clay/perlite and vermiculite composite PCM for improving thermal inertia in building. *Building Environmental*, 167, 106464. 10.1016/j.buildenv.2019.106464
- Webb, P., Orr, C., Camp, R., Olivier, J., and Yunes, S. (1997). *Analytical methods in fine particle technology*. Norcross, GA: Micromeritics Instrument Corporation.
- Yuan, M., Xie, T., Yan, G., Chen, Q., and Wang, L. (2018). Effective removal of Pb+2 from aqueous solutions by magnetically modified zeolite. *Powder Technology*, 332, 234-241. 10.1016/j.powtec.2018.03.043
- Zafarzadeh, A., Sadeghi, M., Golbini-Mofrad, A., and Beirami, S. (2018). Removal of lead by activated carbon and citrus coal from drinking water. *Desalination Water Treatment*, 105, 282-286. 10.5004/dwt.2018.22024
- Zhou, L., Li, N., Jin, X., Owens, G., and Chen, Z. (2020). A new nFe@ZIF-8 for the removal of Pb(II) from wastewater by selective adsorption and reduction. *Journal of Colloid Interface Science*, 565, 167-176. 10.1016/j.jcis.2020.01.014

Comparative Study of Theoretical and Real Deflection of Simple and Reinforced Concrete Joists

Estudio comparativo de la deflexión teórica y real de viguetas de concreto simple y reforzado

Socrates P. Muñoz-Perez¹, Angel A. Ruiz-Pico², Juan M. Anton-Perez³, and Dandy B. Roca-Loayza⁴

ABSTRACT

The objective of this research is to determine the real deflection of a concrete joist and correlate the result with theoretical deflection, which is based on a stress vs. deformation model which was proposed by Mander *et al.* (1988) for monotonic loads of reinforced and non-reinforced concrete. The construction of a concrete joist does not result in a 100% homogenous, isotropic, and linearly elastic element, since its production depends on many conditions, such as aggregate selection, water, cement manufacturing, tests performed for mixture design, the operator in charge of the mixture, and the construction of the joist. Therefore, research was carried out on the variation of real reflection with respect to theoretical calculations. To this effect, 30 simple-concrete and 30 reinforced-concrete joists were elaborated. They were tested by measuring their maximum deflection and comparing it to its theoretical counterpart. To calculate the theoretical deflection, a curvature moment diagram was elaborated with the Rect_Mom software by Restrepo and Rodríguez (2012), which uses the model by Mander *et al.* (1988). Experimental results showed a greater deflection than the one reported by theoretical calculations.

Keywords: joist deflection, inelastic behavior, curvature moment

RESUMEN

Esta investigación tiene como objetivo determinar la deflexión real de una viga de concreto y correlacionar el resultado con la deflexión teórica, que está basada en el modelo esfuerzo vs. deformación propuesto por Mander *et al.* (1988) para cargas monótonas de concreto reforzado y no reforzado. La construcción de una viga de concreto no conforma un elemento 100% homogéneo, isotrópico y linealmente elástico, ya que su fabricación depende de muchas condiciones como la elección de los agregados, el agua, la fabricación del cemento, los ensayos realizados para el diseño de mezclas, el operario a cargo de la mezcla y la construcción de la viga. Por ello se investigó la variación de la deflexión real con respecto a los cálculos teóricos, para lo cual se fabricaron 30 viguetas de concreto simple y 30 viguetas de concreto armado, que se ensayaron midiendo la deflexión máxima y se comparándola con la teórica. Para el cálculo de la deflexión teórica se elaboró el diagrama de momentos de curvatura con el programa Rect_Mom de Restrepo y Rodríguez (2012), que utiliza el modelo de Mander *et al.* (1988). Los resultados experimentales mostraron una deflexión mayor que los cálculos teóricos.

Palabras clave: deflexión en viguetas, comportamiento inelástico, momento de curvatura

Received: April 28th, 2020

Accepted: February 12th, 2021

¹Civil Engineer, Pedro Ruiz Gallo National University, Master in Earth Sciences with a major in Geotechnics, National University of San Agustín. Affiliation: Faculty of Engineering, Architecture and Urbanism, Professional School of Civil Engineering of Lord of Sipan University. Email: pedro_munoz19@hotmail.com

²Geological Engineer, University of Granada, Doctor in Civil Engineering, Da Coruña University. Affiliation: Faculty of Engineering, Professional School of Environmental Civil Engineering of Santo Toribio de Mogrovejo University. Email: aaruzpico@gmail.com

³Graduate in Statistics, Pedro Ruiz Gallo National University, Master of Science, Mention in Applied Statistics, National University of Trujillo. Affiliation: Faculty of Physical and Mathematical Sciences of the Pedro Ruiz Gallo National University. Lambayeque, Perú. Email: janton@unprg.edu.pe

⁴Civil Engineer, Universidad Nacional San Luis Gonzaga, Master of Science with a major in Structural Engineering, National University of Engineering. Affiliation: Faculty of Engineering of the Autonomous University of Mexico. Email: dandyberlie@gmail.com

How to cite: Muñoz, S., Ruiz Pico, Á. A., Anton, J., and Roca, D. (2021). Comparative Study of Theoretical and Real Deflection of Simple and Reinforced Concrete Joists. *Ingeniería e Investigación*, 41(2), e86742. 10.15446/ing.investig.v41n2.86742



Attribution 4.0 International (CC BY 4.0) Share - Adapt

Introduction

The calculation of deformations or deflections in reinforced concrete elements subjected to bending is important because these elements must have an adequate rigidity to eliminate any deformation along a structure, which constitutes a risk for its resistance or operation under service conditions (Carrillo and Silva-Páramo, 2016; Carrillo, Cárdenas Pulido, and Aperador, 2017).

Likewise, reinforced concrete elements are used when there is a deficit in any of the properties of a structure due to a new state of charge during its useful life. These increased loads generally result from the state of service for which these deflections must be controlled (Falope, Lanzoni, and Tarantino, 2019)

It is important to know the responses and resistant mechanisms present in a reinforced concrete element when

subjected to different kinds of stress. These factors can be measured through experimental tests, which allows verifying the theories formulated by standards or studying other theories (Chiorean and Buru, 2017).

Carrying out this type of study is important because it will help us have a clearer perspective of real deflection (depending on compressive strength, applied load, reinforcement and geometry), which will allow adjusting the calculations. It is important to verify deformations in structural elements with little inertia to ensure the operation of the structure as a whole and not endanger human life (Hemn Qader, Dishad Kakasor, and Abdulkhaleq, 2020).

Regarding deflections and cracking, adequate service behavior can be achieved in beams with less than the maximum allowable by standard E 060 (L 300). For 200 x 300 mm beams with 290 cm of free length between supports and 30% of redistribution in negative steel, deformations of 7,90 mm of deflection and 0,35 mm of cracking were obtained (Ministerio de Vivienda, Construcción y Saneamiento, 2009).

For the comparison of both general models and simplified formulae, experimental data are required which adequately represent the magnitudes of the most significant variables of the structural elements with deformation problems, as well as sufficient complementary data to allow the theoretical analysis of the problem (Purushothama Raj and Ramasamy, 2012).

The only way to rationalize force and displacement factors is by quantifying the relationships of resistance and structural ductility through analytical studies and experimental tests, determining design forces and displacements in a more rational way (related theories) and contemporary trends in building code (Carrillo, Blandón Valencia, and Rubiano, 2013; Ismail *et al.*, 2018).

Materials and methods

This research was experimental. Several mixtures were designed, whose compressive strength varied from $f'c = 280$ kg/cm² up to 400 kg/cm². The aggregates were from the quarries of Tres Tomas, Pátapo, and Batangrande, which are located in the Lambayeque region, as well as from Talambo, near Chepén, which belongs to the region of La Libertad. Using type I cement, the physical properties of these mixtures were studied for the purpose of preparing concrete mixtures. Simple and reinforced concrete joists were manufactured with dimensions of 15 cm x 15 cm x 53,5 cm, which were flexurally tested at 7, 14, and 28 days. At the same time, specimens were produced to obtain compressive strength at the same ages as the joist. A mix was designed for each quarry, and 02 joists were tested for each break, with 10 joists at 7, 14, and 28 days for both simple and reinforced concrete. The flexion of a total of 60 joists was therefore tested (Alhajri, Tahir, Azimi, Mirza, and Ragaee, 2016).

Figure 2 shows the molds used to manufacture the joists, Figure 3 shows the specimens of the tested joists, Figure 4 shows the bending test of the joist, and Figure 5 shows the break of the joist after being tested.



Figure 1. Joist formwork.

Source: Authors



Figure 2. Joist reinforcement.

Source: Authors



Figure 3. Simple and reinforced joists.

Source: Authors



Figure 4. Beam flexure test.

Source: Authors



Figure 5. Joist fissure.

Source: Authors

The resistance design method, together with the use of higher resistance concrete and steels, has allowed the use of relatively slim elements. Consequently, deflections and deflection cracking have become more severe problems than they were a few decades ago (Hemn Qader, Dishad Kakasor, and Abdulkhaleq, 2020; Luo, *et al.*, 2019).

One of the best ways to reduce deflections is by increasing the cant of the members, but the designers are always under pressure to keep the members with the cant as low as possible. Another solution is improving the quality of the material's resistance to deformation, in other words, increasing the elasticity modulus of the material. For this reason, it is necessary to have an adequate calculation of deflections, so as not to affect the resistance or functionality of the analyzed structure. If the designer decides not to use the minimum thicknesses given in Table 1, then he or she will be forced to determine the actual deflections, which must not exceed the values in Table 2.

Table 1. Cant or minimum thickness of non-prestressed beams or reinforced slabs in one direction unless deflections are calculated

Elements	Minimum thickness or cant h			
	Simply supported	With a continuous end	Both ends continuous	Cantilever
Elements that do not support or are linked to divisions or other types of non-structural elements susceptible to damage due to large deflections				
Solid tiles in one direction	$\frac{\ell}{20}$	$\frac{\ell}{24}$	$\frac{\ell}{28}$	$\frac{\ell}{10}$
Beams or slabs ribbed in one direction	$\frac{\ell}{16}$	$\frac{\ell}{18.5}$	$\frac{\ell}{21}$	$\frac{\ell}{8}$

Source: Table 9.1 of Peruvian Building Standard E 060 (Ministerio de Vivienda, Construcción y Saneamiento, 2009).

Elastic methods are used to obtain and determine the equations to define the slope and elastic curve of a beam (Hamrat *et al.*, 2020).

The lateral part of the surface of a deformed beam is called the elastic, deformed, or elastic curve of the beam. It is the curve that forms the longitudinal axis, which at the beginning was straight. As shown in Figure 6, it is in this section that we can deduce the elastic curve, which also allows us to determine the deflection of any point based on its length or X coordinate.

The left end is the origin of the x axis, directed according to the initial direction of the beam without deforming, and the positive y axis upward. The deformations are so small

that it is not possible to distinguish between the initial length and the projection of its already deformed length. Therefore, the elastic curve is very flat and its slope at any point is also very small.

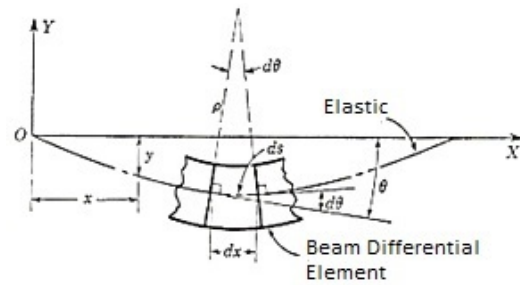


Figure 6. Elastic curve of a beam.

Source: Singer and Pytel (1994)

Table 2. Maximum allowable deflections

Item type	Considered deflection	Deflection limit
Flat roofs that do not support or are linked to non-structural elements susceptible to damage due to large deflections	Immediate deflection due to live load	$\ell/180^\circ$
Floors that do not support and are linked to non-structural elements susceptible to damage due to large deflections	Immediate deflection due to live load	$\ell/360^\circ$
Floors or ceilings that support and are linked to non-structural elements susceptible to damage due to large deflections	The part of the total deflection that occurs after the union of the non-structural elements (the sum of the long-term deflection due to all permanent loads, and that of immediate deflection due to any additional live load)	$\ell/480$
Floors or ceilings that support or are linked to non-structural elements not susceptible to damage due to large deflections.		$\ell/240$

Source: Table 9.2 of Peruvian Building Standard E 060 (Ministerio de Vivienda, Construcción y Saneamiento, 2009).

Some structural analysis problems can be solved using linear analysis, but the geometric nonlinearity, the nonlinearity due to the behavior of the material, and the nonlinearity due to the boundary conditions change when posing and solving non-linear problems (Beléndez, Neipp, and Beléndez, 2002; Ismail *et al.*, 2018).

Theoretical deflection

To make a prediction of the experimental displacement, the deflection was calculated from the analytical calculations described below.

The joists were modeled using the SAP2000 software with frame elements that can be used to model beams, columns,

braces, and trusses in planar and three-dimensional structures. Nonlinear material behavior is available through frame hinges and includes the effects of biaxial bending, torsion, axial deformation, and biaxial shear deformations.

A frame element is modeled as a straight line connecting two points, and each element has its own local coordinate system for defining section properties and loads, as well as for interpreting output, as shown in Figure 7.



Figure 7. Joist modeled with frame elements in the SAP2000 program.
Source: Authors

To consider inelastic behavior, a plastic hinge was located in the center of the span, which is the point where the greatest deformation occurs.

When nonlinear properties are present in the element, they only affect nonlinear analyses. Linear analyses starting from zero conditions (the unstressed state) behave as if the nonlinear properties were not present. Linear analyses using the stiffness from the end of a previous nonlinear analysis use the stiffness of the nonlinear property as it existed at the end of the nonlinear case (Alhajri *et al.*, 2016; Luo *et al.*, 2019)

Each hinge represents concentrated post-yield behavior in one or more degrees of freedom. Hinges only affect the behavior of the structure in nonlinear static and nonlinear time-history analyses.

Since the predominant behavior was bending, the M3 ball joint type was used, which was also in the program's library. Hinge properties can be computed automatically from the element material and section properties according to Federal Emergency Management Agency FEMA-356 or American Society of Civil Engineers ACSE 41-13 criteria (FEMA and ASCE, 2000). For our case, the properties were entered manually and obtained from the curvature moment diagram of the joist section.

To obtain the curvature moment diagram, the Rect_Mom software (Rodriguez and Restrepo, 2012) was used. This application uses the model proposed by Mander *et al.* (1988) shown in Figure 8 for concrete modelling. This behavior allows the effect of the interaction between concrete and reinforcement bars by introducing tension reinforcement into the softening side of the curve (Sinaei, Mohd Zamin, and Mahdi, 2011).

Likewise, for the reinforcing steel, the Mander model was used, which is shown in Figure 9. This model considers three zones: the elastic zone, the creep zone, and the strain hardening zone.

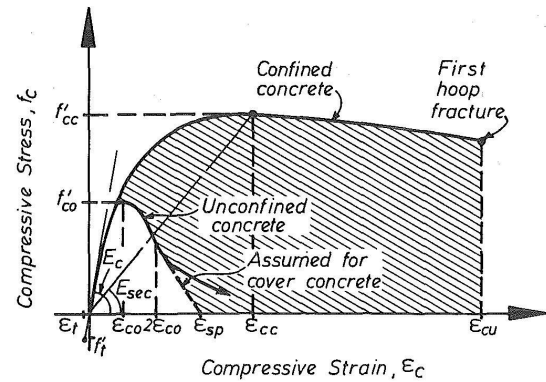


Figure 8. Stress-strain model proposed for monotonic loading of confined and unconfined.

Source: Mander *et al.* (1988)

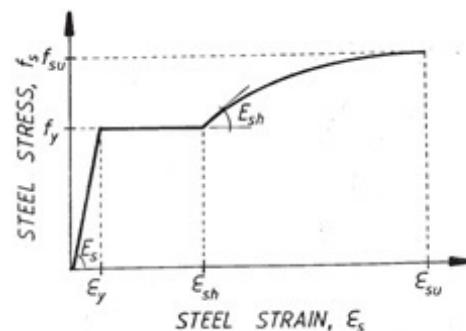


Figure 9. Monotonic stress-strain curve typical of a rebar.

Source: Mander *et al.* (1983)

Real Deflection

For the experimental deflection, the Peruvian Technical Standard NTP 339.079 testing method was applied to determine the flexural strength of concrete in simply supported beams with loads in the center of the span (Comisión de Normalización y Fiscalización de Barreras Comerciales no Arancelarias - INDECOPI, 2012).

The equipment to perform the test had to comply with the requirements of the sections based on the verifications, corrections, and the time interval between verifications. The mechanism by which loads are applied to the specimen employed one load application block and two specimen support blocks. The load was to be applied perpendicularly to the upper face of the beam, in such a way that eccentricities could be avoided (Comisión de Normalización y Fiscalización de Barreras Comerciales no Arancelarias - INDECOPI, 2012).

The specimens on which the tests were carried out had to be prepared according to the test method indicated above to meet the required compressive strength. The beam had a free span between supports approximately three times its height, with a tolerance of 2%. The lateral faces of the beam formed right angles with the upper and lower face. All surfaces were smooth and free of any porosity, according to Figure 10 (Comisión de Normalización y Fiscalización de Barreras Comerciales no Arancelarias - INDECOPI, 2012).

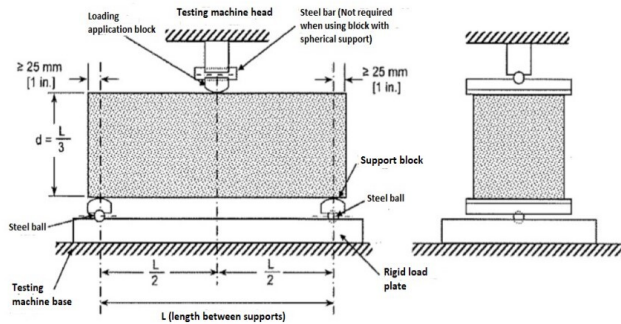


Figure 10. Diagram of a suitable device for concrete flexural testing by the mid-point load method and the application of the double integration method in a simply supported beam.

Source: Comisión de Normalización y Fiscalización de Barreras Comerciales no Arancelarias - INDECOPI, 2012.

During the test, the beam had to be loaded continuously and without impacts. The load must be applied at a constant speed until breakage is reached (Comisión de Normalización y Fiscalización de Barreras Comerciales no Arancelarias - INDECOPI, 2012).

Justification of the investigation

The calculation of the deflections of a beam is carried out according to the theory of elasticity, considering concrete as a linearly elastic material, even though the deflections of the beam are actually due to the nonlinearity of the material, which is the result of external factors such as its composition (cement, aggregates, water), the preparation of the concrete mixture, and the construction of the beam. To date, these conditions cannot be mathematically modeled and are part of the calculation of the theoretical deflection.

Results

This section presents the results of the analysis performed in the laboratory and the correlation between theoretical and real deflection, as shown in Tables 3, 4, and 5. The test was performed for 3 different cure times: 7, 14, and 28 days. The elasticity modulus was calculated, as indicated by the Peruvian building standard E 060 and the inertia of the cross section (Ministerio de Vivienda, Construcción y Sanearamiento, 2009). Likewise, with the load resulting from the test, the theoretical deflection was calculated. After reviewing the results of the theoretical and actual deflection, we concluded that there is a very wide difference between the two values. We verify that the theoretical calculations do not reflect the actual deformation of the element, which is due to the nonlinearity of concrete.

The obtained moment curvature diagram shown in Figure 11 is simplified by using bilinear approximation in the SAP2000 program; the abscissa is multiplied by the plastic length to express it as a function of rotation and reduced only to the part plastic diagram.

Table 3. Results of compressive strength, elasticity modulus at 7, 14 and 28 days of the tested concrete and cross section of the joist (area = 176,7 cm², joist cross-section = 225 cm², and length between supports = 45 cm)

Quarries name	Time (days)	Applied load (kg)	Compressive strength f'_c (kg/cm ²)	Elasticity Module $15000 \sqrt{f'_c}$ (kg/cm ²)
Olmos	7	35 289	199,71	211 978,91
	14	42 309	239	231 894,37
	28	51 685	292	256 320,11
Talambo Chepen	7	43 466	246	235 265,81
	14	46 738	264	243 721,15
	28	50 899	288	254 558,44
Tres Tomas	7	32 924	181	201 804,36
	14	44 762	250	237 170,82
	28	49 585	281	251 445,82
Patapo	7	38 612	218	221 472,35
	14	46 122	261	242 332,42
	28	61 408	347	279 419,04
Batan Grande	7	40 290	228	226 495,03
	14	57 432	325	270 416,35
	28	71 216	403	301 122,90

Source: Authors

Table 4. Inertia, length between supports, applied point load, theoretical and real deflection of the simple concrete joist (inertia = 4218,75 cm⁴, length between supports = 45 cm)

Quarries name	Punctual face (kg)	Elasticity Module $5000 \sqrt{f'_c}$ (kg/cm ²)	Theoretical deflection (mm)	Real deflection (mm)
Olmos	2 200	211 978,91	1,8577	2,300
	2 940	231 894,37	4,5484	5,200
	3 450	256 320,11	6,2003	6,400
Talambo Chepén	3 375	235 265,81	1,9251	1,800
	3 883	243 721,15	2,5851	2,900
	4 180	254 558,44	4,4996	3,700
Tres Tomas	1 150	201 804,36	2,2711	1,900
	1 370	237 170,82	3,2399	3,800
	1 550	251 445,82	7,3146	6,400
Pátapo	3 220	221 472,35	2,8526	3,150
	3 850	242 332,42	5,3213	4,950
	4 550	279 419,04	5,1367	5,780
Batangrande	2 180	226 495,03	1,5802	1,300
	2 986	270 416,35	4,3729	3,600
	3 504	301 122,90	6,5544	5,500

Source: Authors

Once the plastic hinge was defined and assigned, a point load was applied which was gradually increased according to the laboratory test until the failure of the section was reached. The values obtained are shown in Tables 4 and 5.

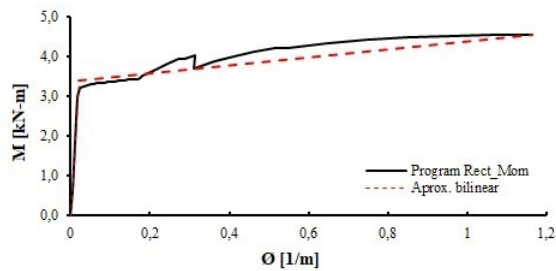


Figure 11. Moment-Curvature diagram for joist section.

Source: Authors

Table 5. Inertia, length between supports, applied point load, theoretical and real deflection of the reinforced concrete beam (inertia = 4218,75 cm⁴, length between supports = 45cm)

Quarries name	Punctual face (kg)	Elasticity Module 15 000 $\sqrt{f'_c}$ (kg/cm ²)	Theoretical deflection (mm)	Real deflection (mm)
Olmos	6 874	211 978,91	2,8900	2,500
	7 997	231 894,37	4,1607	4,300
	10 450	256 320,11	9,7037	8,400
Talambo Chepen	6829	235 265,81	4,2158	3,680
	8 354	243 721,15	11,3128	10,320
Tres Tomas	9 359	254 558,44	13,2863	15,460
	2980	201 804,36	5,7345	4,875
	3 780	237 170,82	5,1149	5,535
Patapo	4 150	251 445,82	7,4091	6,485
	7 650	221 472,35	7,2040	7,900
	8 985	242 332,42	10,6756	10,120
Batan Grande	10 658	279 419,04	11,4471	12,390
	3 150	226 495,03	7,8125	7,560
	3 390	270 416,35	5,7550	5,675
	3 431	301 122,8985	3,9517	4,875

Source: Authors

Figure 12 shows the diagram of the theoretical and real deformation of a simple concrete beam per quarry, where non-linear trends are observed between the theoretical and real deformation.

The correlation of the theoretical and real deflection of a simple concrete joist is shown in Figure 13, obtaining an Equation (1) of degree 4: $y = (-0,33764)x^4 + (0,01252)x^3 + (-0,71775)x^2 + (6,05057)x + 3,91200$, which was a good model of adjustment because it had an acceptable coefficient of determination ($R^2 = 0,9123$), because the 99% confidence interval included all the pairs of observed values, and because the result of the analysis of variance indicated that at least one coefficient of the polynomial model is significantly different from zero ($p\text{-value} = 1,788e^{-07}$).

A very good positive correlation was found between the theoretical and actual deformation of a simple concrete beam ($R = 0,9551$).

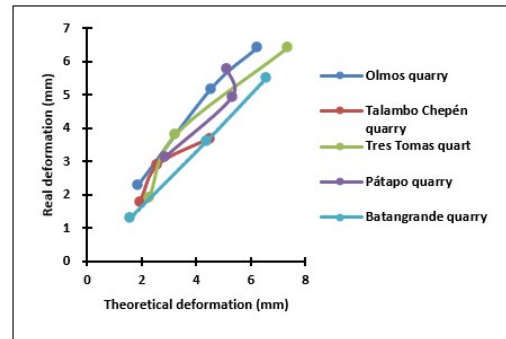


Figure 12. Diagram of the theoretical and real deformation of the simple concrete joist by quarry.

Source: Authors

According to the Shapiro Wilk test, residues originating from the order 4 polynomial model presented a normal distribution ($p\text{-value} = 0,3857$).

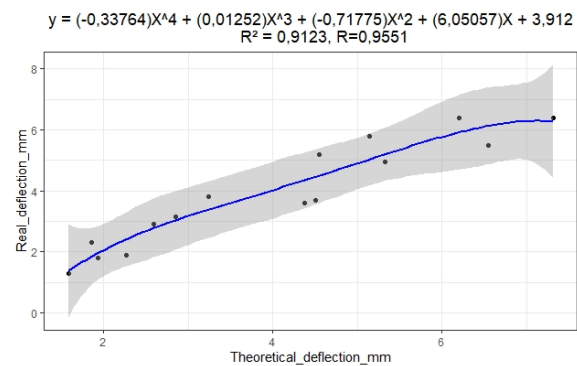


Figure 13. Correlation of theoretical and real deformation of a simple joist.

Source: Authors

Figure 14 shows the diagram of the theoretical and real deformation of a quarry-reinforced concrete beam, where non-linear trends are observed between the theoretical and real deformation, but these together will give rise to figure 15.

The correlation of the theoretical and real deflection of the reinforced concrete joist is shown in figure 15, obtaining an Equation (II) of degree 4: $y = (-0,0652)x^4 + (1,7485)x^3 + (1,7920)x^2 + (12,7575)x + 7,3383$, which was a good model of adjustment, because it had an acceptable coefficient of determination ($R^2 = 0,9686$), because the 99% confidence interval included all the pairs of observed values, and because the result of the analysis of variance indicates that at least one coefficient of the polynomial model is significantly different from zero ($p\text{-value} = 1,788e^{-07}$).

A very good positive correlation was found between the theoretical and actual deformation of the reinforced concrete beam ($R = 0,9842$).

According to the Shapiro Wilk test, the residuals originating from the order 4 polynomial model were adjusted for the normal distribution ($p\text{-value} = 0,2811$).

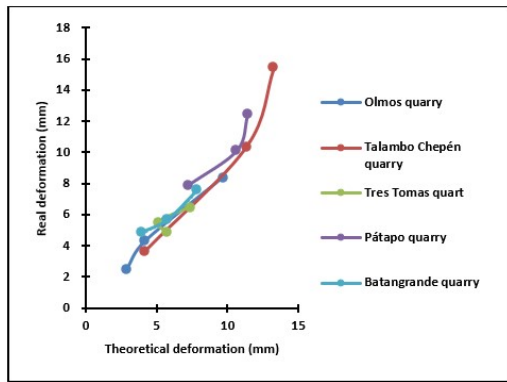


Figure 14. Diagram of the theoretical and actual deformation of a reinforced concrete joist by quarry.

Source: Authors

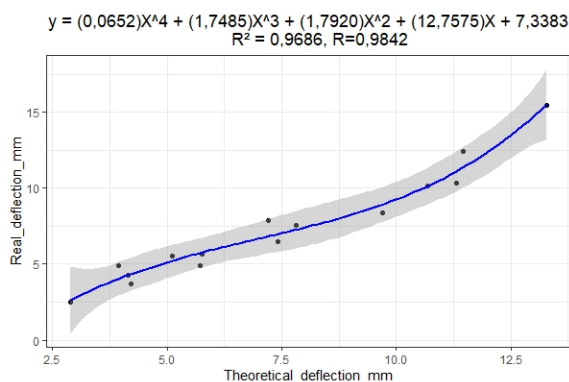


Figure 15. Correlation of theoretical and real deformation of a reinforced concrete joist.

Source: Authors

Conclusions

Based on the results obtained regarding the correlation of theoretical and practical deflection, we reached the following conclusions:

1. A very good positive non-linear correlation was found between the theoretical and actual deformation of both the simple and reinforced concrete beams.
2. The actual deflections for both the simple beam and the reinforced beam are greater than those calculated by the model proposed by Mander *et al.* (1988).
3. The evaluated analysis of the experimental results and the parameters calculated using the developed methodology is not within the expected ranges reported by the literature.
4. For subsequent work, it is recommended to make the stress-strain diagram of the joist to make a more detailed comparison of how it varies and where the divergence between the theoretical and actual deformation lies.

5. It was also concluded that the days of concrete curing influence the deflection of the joists, obtaining less resistance to deflection during the first weeks.

Acknowledgements

We thank the students of the Resistance of Materials course for the 2020-0 semester of the Professional School of Civil Engineering at the Señor de Siapan University, who collaborated in the experiments and search for information in this research.

References

- Alhajri, T., Tahir, M., Azimi, M., Mirza, J., and Ragaee, M. (2016). Behavior of precast U-shaped composite beam integrating cold formed steel with ferro cement slab. *Thin Walled Structures*, 102, 18-29. 10.1016/j.tws.2016.01.014
- Arabnejad Khanouki, M., Ramli Sulong, N., Mahdi Shariati, and Tahir, M. (2016). Investigation of through beam connection to concrete filled circular steel tube (CFCST) column. *Journal of Constructional Steel Research*, 121, 144-162. 10.1016/j.jcsr.2016.01.002
- Belendez, T., Neipp, C., and Belendez, A. (2002). Estudio de la Flexión de una Viga de Material Elástico no Lineal. *Revista Brasileira de Ensino de Física*, 24(4). <https://www.scielo.br/scielo.php>
- Carrillo, J. and Silva-Páramo, D. (2016). Flexural Tests of Concrete Slabs-on-Ground Reinforced with Steel Fibers. *Ingeniería Investigación y Tecnología*, 17(3), 317-330. 10.1016/j.riit.2016.07.003
- Carrillo, J., Blandón Valencia, J., and Rubiano, A. (2013). A review of conceptual transparency in US and Colombian seismic design building codes. *Ingeniería e Investigación*, 33(2), 24-29. 10.15446/ing.investig.v33n2.39506
- Carrillo, J., Cárdenas Pulido, J., and Aperador, W. (2017). Flexural mechanical properties os steel fiber reinforced concrete under corosive environments. *Revista Ingeniería de Construcción RIC*, 32(2), 59-72. <https://www.ricuc.cl/index.php/ric/article/view/582>
- Comisión de Normalización y Fiscalización de Barreras Comerciales no Arancelarias - INDECOPI. (2012). Norma Técnica Peruana N.T.P. 339.079 2012. Concreto. Método de Ensayo para determinar la resistencia a la flexión del concreto en vigas simplemente apoyadas con cargas en el centro del tramo, Tercera Edición. Lima, San Borja, Peru: R.0092-2012/CNB - INDECOPI.
- Falope, F., Lanzoni, L., and Tarantino, A. (2019). The bending of fully nonlinear beams. Theoretical, numerical and experimental analyses. *International Journal of Engineering Science*, 145. 10.1016/j.ijengsci.2019.103167
- FEMA and ASCE. (2000). Prestandard And Commentary for the seismic rehabilitation of buildings. *FEMA 356*. <https://www.conservantech.com/FEMA-publications/FEMA356-2000.pdf>

- G. Chiorean, C., and M. Buru, S. (2017). Practical non-linear inelastic analysis method of composite steel concrete beams with partial composite action. *Engineering Structures*, 134, 74-106. 10.1016/j.engstruct.2016.12.017
- Hamrat, M., Bouziadi, F., Boulekbache, B., Daouadji, H., Chegui, S., Labed, A., and Amziane, S. (2020). Experimental and numerical investigation on the deflection behavior of precracked and repaired reinforced concrete beams with fiber-reinforced polymer. *Construction and Building Materials*, 249. 10.1016/j.conbuildmat.2020.118745
- Hemn Qader, A., Dishad Kakasor, J., and Abdulkhaleq, Y. (2020). Flexural capacity and behaviour of geopolymer concrete beams reinforced with glass fibre reinforced polymer bars. *International Journal of Concrete*, 14(4), 1-16. 10.1186/s40069-019-0389-1
- Ismail, M., Shariati, M., Abdul Awal, A., Chiong, C., Chahnasir, E., Porbar, A., Heydari, A., and Khorami, M. (2018). Strengthening of bolted shear joints in industrialized ferrocement construction. *Steel and Composite Structures*, 28(6), 681-690. 10.12989/scs.2018.28.6.681
- Luo, Z., Sinaei, H., Ibrahim, Z., Shariatit, M., Jumaat, Z., Wakil, K., Pham, B. T., Mohamad, E. T., and Khorami, M. (2019). Computational and experimental analysis of beam to column joints reinforced with CFRP plates. *Steel and Composite Structures*, 30(3), 271-280. 10.12989/scs.2019.30.3.271
- Mander, B., Priestley, M., Park, R., Fellow, and ASCE. (1988). Theoretical Stress-Strain Model for confined concrete. *Journal of Structural Engineering*, 114(8), 1804-1826. 10.1061/(ASCE)0733-9445(1988)114:8(1804)
- Mander, J. (1983). Seismic Design of Bridge Piers. (Doctoral thesis, University of Canterbury, Christchurch, Australia) 10.26021/3134
- Ministerio de Vivienda, Construcción y Saneamiento. (2009). Norma E 060 Concreto Armado - Reglamento Nacional de Edificaciones. Servicio Nacional de Capacitación para la Industria de la Construcción – SENCICO.
- Purushothama Raj, P., and Ramasamy, V. (2012). Strength of Materials. Chennai, India: Pearson India.
- Rodriguez, M., and Restrepo, J. (2012). Práctica y diseño sísmico de edificios en México - cambios necesarios. *Revista de Ingeniería Sísmica*, 86, 89-118. 10.18867/ris.86.154
- Sahmani, S., and Safaei, B. (2020). Influence of homogenization models on size dependent nonlinear bending and post-buckling of bidirectional functionally graded micro/nano beams. *Applied Mathematical Modelling*, 82, 336-358. 10.1016/j.apm.2020.01.051
- Sinaei, H., Mohd Zamin, J., and Mahdi, S. (2011). Numerical investigation on exterior reinforced concrete Beam-Column joint strengthened by composite fiber reinforced polymer (CFRP). *International Journal of the Physical Sciences*, 6(28), 6572-6579. 10.5897/IJPS11.1225

A Novel Dynamic and Fuzzy Value Stream Mapping (DFVSM): System Dynamics and Fuzzy Logic Integration

Un novedoso *Value Stream Mapping* dinámico y difuso (DFVSM): integración de dinámica de sistemas y lógica difusa

Roberto Baeza-Serrato ¹

ABSTRACT

Value stream mapping (VSM) is a method to identify waste and activities that do not add value. One of its main disadvantages is that the parameters used in the process and material flows are deterministic. The motivation of this research is to improve the reliability of the estimation of the lead time in VSM, transitioning from a static model to a dynamic model that incorporates uncertainty and imprecision in the data, as well as to develop a novel dynamic and fuzzy value stream mapping (DFVSM) based on integrating system dynamics and fuzzy logic. One of the main contributions of this research is to develop a fuzzy system in the same system dynamics interface that incorporates uncertainty and vagueness to the efficiency and effectiveness percentage variable (OEE%) to increase the reliability of the delivery time planning. The stages of DFVSM are explicitly described and applied to real data for a textile company in southern Guanajuato. A sensitivity analysis of the proposed model was integrated which identifies the critical factors for the delivery of the order, and achievable times were proposed for the delivery times of the supplier and the client, thus reducing the expected delivery time by 28%. One of the relevant conclusions of this work is that, to plan the lead time of an order, the uncertainty of the main parameters such as supplier and customer shipping times be considered to satisfy the customer.

Keywords: value stream mapping, system dynamic, fuzzy system, normal probability density

RESUMEN

El mapeo de flujo de valor (MFV) es un método para identificar desperdicios y actividades que no agregan valor. Una de sus principales desventajas es que los parámetros utilizados en el proceso y los flujos de material son deterministas. La motivación de esta investigación es mejorar la confiabilidad de la estimación del tiempo de entrega en un MFV, transicionando de un modelo estático a un modelo dinámico que incorpora la incertidumbre e imprecisión de los datos; así como desarrollar un nuevo mapeo dinámico y difuso de flujo de valor (DFSVSM) basado en la integración de la dinámica de sistemas y la lógica difusa. Una de las principales contribuciones de esta investigación es desarrollar un sistema difuso en la misma interfaz de dinámica de sistemas que incorpore incertidumbre y vaguedad en la variable porcentaje de eficiencia y eficacia (OEE %) para aumentar la confiabilidad de la planificación del tiempo de entrega. Este sistema se describe explícitamente y se aplica a datos reales para una empresa textil del sur de Guanajuato. Se integró un análisis de sensibilidad identificando los factores críticos para la entrega del pedido y se propusieron tiempos de entrega alcanzables para el proveedor y el cliente, reduciendo el tiempo esperado en un 28 %. Una de las conclusiones relevantes de este trabajo es que, para planificar el tiempo de entrega de un pedido, se debe considerar la incertidumbre de parámetros como los tiempos de envío del proveedor y al cliente para poder satisfacer al cliente.

Palabras clave: mapeo de flujo de valor, dinámica de sistemas, sistema difuso, densidad de probabilidad normal

Received: January 13th, 2020

Accepted: February 22nd, 2021

Introduction

Lean Manufacturing (LM) has traditionally helped industries in removing the non-value-added (NVA) processes to achieve operational excellence (Sadiq *et al.*, 2021). Wastes are mainly explored by drawing a value stream map of as-is state using the Gemba walk. This "as-is" map aids in capturing the snapshots of how things are currently done and areas of potential improvements (Tyagi, Choudhary, Cai, and Yang, 2015). Lean Thinking thus emerged as an effective way to continuously decrease costs and improve profits by utilizing the minimum required level of essential attributes such as time, space, machine, equipment, and energy to produce a product or provide a service. Liu and Yang (2020) claim that value stream mapping (VSM) is one of the primary analytical

tools for identifying waste and optimizing a production line. The value of a product also increases when wastes from transportation, inventory, waiting, over-production, over-processing, defects, and rework are eliminated or reduced (Sullivan, McDonald, and Aken, 2002). The method is based on the Toyota Production System (TPS) and consists of two main phases: value stream analysis, in which the current

¹Ph.D. in Industrial Engineering, CIATEC, México. Affiliation: Associate Professor, Universidad de Guanajuato, Sede Yuriria, México. E-mail: r.baeza@ugto.mx

How to cite: Baeza-Serrato, Roberto (2021). A Novel Dynamic and Fuzzy Value Stream Mapping (DFVSM): System Dynamics and Fuzzy Logic Integration. *Ingeniería e Investigación*, 41(2), e84539. 10.15446/ing.investig.v41n2.84539



Attribution 4.0 International (CC BY 4.0) Share - Adapt

value stream is visualized; and value stream design, in which sources of waste within the production process are uncovered and reduced (Ono, 1988). VSM is a static lean manufacturing tool that is becoming popular in identifying activities that add and do not add value in production sectors. Through this kind of identification, it is possible to achieve significant performance improvement in the industry. However, VSM has some disadvantages, since each job order must be mapped, and the parameters used in the process and material flows are deterministic. Preuss, Luz, Narayanamurthy, Gaiardelli, and Sawhney (2021) argue that traditional value stream mapping fails in considering the inherent variability of processes, hence reinforcing improvements that might not lead to significant results. Balaji, Venkumar, Sabitha, and Amuthaguka (2020) mentioned that VSM tends to be static and skill dependent. A single calculation is made to estimate the lead time without considering uncertainty in the parameters, as well as the variability in cycle times due to common factors such as manpower, machines, measurement, material, methods, and environment. This paper aims to study the effectiveness of developing a dynamic and fuzzy VSM model to understand the behaviour of its variables at multiple simulations considering the imprecision and variability of the data. Lead time in a VSM consists of identifying and determining the activities that add value (AV) and those that do not add value (NVA). AV activities are the cycle times (CT) of each operation in the process, whereas NVA activities in each operation of the process are related to size order (SO), available time (AT), number of machines (NM), and percentage of efficiency and effectiveness (OEE). The most critical parameter to identify NVA activities is OEE, which frequently presents imprecision in the data. This parameter is based on the following attributes: availability (Ava), quality (Q), and performance (P), which will be used as linguistic variables in DFVSM. The novelty of this study lies in two points: the first one is an integration of Fuzzy Inference Systems Theory (FIS) with the Theory of System Dynamics (SD) in the same interface to identify the variables that are relevant to enhancing lead time behavior; and the second one is the employment of an SD approach, which is not currently used, to present VSM approaches. Through SD, systems thinking provides methods and techniques for viewing problems and human action as interconnected wholes, as well as for understanding the often lagged feedback loops that may make complexity very difficult to address through traditional linear modeling processes (Ricciardi, De Bernardi, and Cantino, 2020).

Literature review

Value stream mapping, dynamic systems and fuzzy logic systems have had applications in various productive sectors with successful results.

Salvador *et al.* (2021) proposed a model based on the integration of Life Cycle Assessment (LCA) and VSM to improve the environmental and manufacturing aspects of organizations. Wang, Wu, Chi, and Li (2020) did research on the way VSM can be applied as a lean tool

to help improve operation training performance through an immersive personalized training program based on virtual reality (VR). Sposito and Santos (2020) proposed an integration of lean manufacturing tools and 4.0 technologies considering the perspectives of the industrial field in the digital era. From interactions, multi-level circular diagrams pointed out the main contributions of Just in Time 4.0 (JIT 4.0), Kaizen 4.0, Kanban 4.0, Poka-Yoke 4.0, Value Stream Mapping 4.0 (VSM 4.0), and Total Productive Maintenance 4.0 (TPM 4.0). Rodríguez, Cervera, López, and Pérez-Fernández (2020) used VSM to identify empty transport and unnecessary CO₂ emissions. Their study analyzes VSM as a tool that can enable the objectives of the different Alliance for Logistics Innovation through Collaboration (ALICE) roadmaps for logistics innovation to be achieved, as well as allowing Physical Internet principles to be reached on the established dates. VSM processes enabled the identification of non-value-added activities that threatened the integrity of the process. Standardizing the medication administration process and creating a safe space to facilitate the process successfully reduced interruptions and distractions from all sources (Kavanagh and Donnelly, 2020). A VSM application was proposed by Bin, Petersen, and Schneider (2016), where the combination of VSM and FLOW was evaluated to identify and alleviate information and communication related to challenges in large-scale software development. Baeza-Serrato (2016) proposed an approach called REDUTEX, which is based on theoretical concepts of lean and synchronous manufacturing to help to understand the behaviour of SMEs and to improve the manufacturing process by reducing customer lead times. Each of these studies used VSM to identify and eliminate activities that do not add value to the process integrating industry 4.0 tools. None of them used a dynamic approach to the development of VSM. The proposed approach has used a system dynamics approach to understand the behavior of lead time through VSM integrating a fuzzy system inference in the dynamic model.

Lagos, Mancilla, Leal, and Fox (2019) assessed the performance of a solution to the problem of assigning service squads by incorporating the variability of service times. Cardiel, Baeza-Serrato, and Lizárraga (2017) proposed a dynamic model to analyze the complexity associated with manufacturing systems and improve the performance of the process through the Six Sigma philosophy. Langroodi and Amiri (2016) used a system dynamics approach to design a five-level supply chain consisting of retailer, final product distributor, manufacturer, material distributor, and supplier in four different regions. Babader, Ren, Jones, and Wang (2016) studied the effectiveness of improving the social aspects of reuse behavior and investigated the variables that lead to increased reuse behavior within a short period. This paper selected a quantitative approach, the SD method, which offers a means to highlighting the dynamics and interrelationships between the different social aspects in reuse behavior. Pasaoglu *et al.* (2016) presented an extensive SD simulation model running up to 2050 and employing an agent-based approach, as well as incorporating major factors that influence the technology transition in the EU light-duty vehicle

road transport sector. Gao, Hong, Swaney, Howarth, and Guo (2016) developed and presented a system dynamics model simulating regional N inputs (NANI-SD) based on the concept of net anthropogenic N inputs (NANI), a quasi-mass balance method. Each of these recent studies presents complex dynamic models in which there are multiple interactions and feedback, which enable better decision making as a base reference for the approach proposed in this research.

Keykavoussi and Ebrahimi (2020) developed a new fuzzy approach of cost-time profile (CTP) that has been considered and compared to draw future VSM. Liu and Yang (2020) proposed a fuzzy VSM to consider the variability in manufacturing environments. They used two alternative forms of fuzzy number: triangular fuzzy numbers (TFNs) and normal fuzzy numbers (NFNs). These were applied to depict time intervals, inventories, and other operating variables in VSM. Darvish (2020) designed a robust and intelligent controller that can effectively augment the operational function of the AGC system with a type-2 Fuzzy Logic Controller together with the Fractional Order Proportional Integral Derivative to more abate low-frequency oscillations. Bocklisch and Hausmann (2018) proposed a modelling method using multidimensional fuzzy patterns based on parametric membership functions of the potential type. Baeza-Serrato (2018) proposed a novel multidimensional stochastic Fuzzy Logic System (msFLS) approach to execute a plan with stochastic behavior in knitting SMEs and their evaluation. Fu and Chen (2017) applied the fuzzy theory to study the supply chain partner selection and the task coarse allocation problem under multi-attribute fuzzy comprehensive decision-making and fuzzy constraints. Arsenyan and Büyükožkan (2016) offered an integrated IT planning methodology combining fuzzy quality function deployment, fuzzy axiomatic design, and fuzzy rule-based systems. Each of the references cited above developed Mamdani fuzzy systems integrating conditions of uncertainty in input variables, as well as expert models based on a set of fuzzy rules.

The following limitations or gaps were detected after the literature review:

- VSM is a static lean manufacturing tool.
- For each job order, it is mandatory to draw a value stream map.
- The parameters used in the process and material flows are deterministic.
- None of them uses systems dynamics and fuzzy logic integration in the same interface.

This research proposes an system dynamics approach and fuzzy logic integration in the same interface. The proposal allows eliminating the need to carry out advanced programming code in any of the languages available for other platforms, as well as creating links to export and import data. Such an interface can be used as a basis for any dynamic model and can integrate a fuzzy assessment for any qualitative variables or uncertainty in any parameters.

Methodology

The DFVSM methodology consists of three stages: theoretical conceptualization, problem articulation, and development of a dynamic and fuzzy value stream mapping (Figure 1).

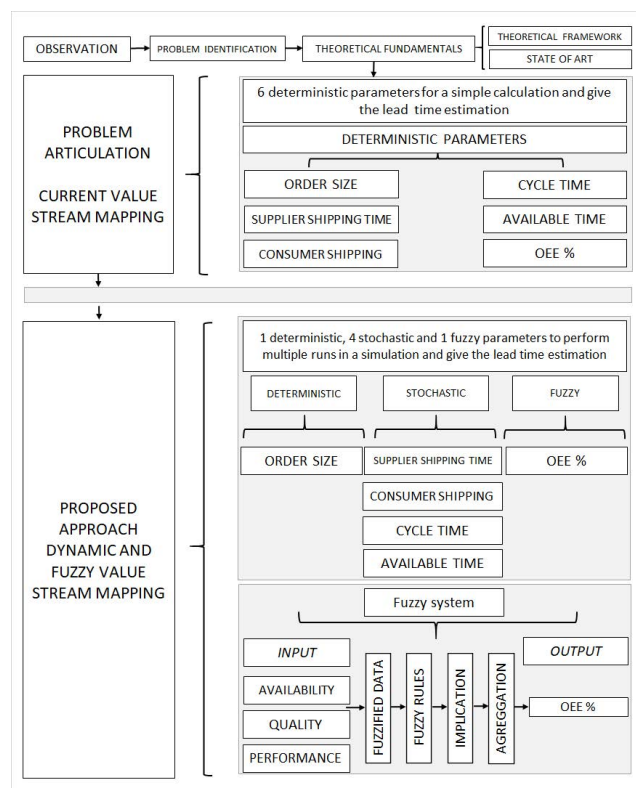


Figure 1. Research methodology.

Source: Authors

The first stage of this research was the conceptualization of the problem of establishing deterministic planning and stochastic execution of plans for each company, supported by an exhaustive review of the literature on system dynamics, fuzzy logic, and normal probability distribution. Administrators are not aware that, when carrying out deterministic planning of delivery time, variability is integrated in each one of the process operations, which causes non-compliance

In the second stage, current VSM of the cutting process in a textile company was developed using six deterministic parameters, which validated the conceptualization of the problem of establishing a deterministic planning that will contrast with the stochastic execution of daily activities in each of the operations of the process. In the lean manufacturing approach, the cycle times of each operation are the only AV activities. To determine the NVA activities in each operation, the parameters involved are the size of the order, the available time, the percentage of efficiency and effectiveness, and the number of machines.

The main contribution of this research is in the third stage. Fuzzy and stochastic behavior were integrated to consider uncertainty and variability on process efficiency within the dynamic model, which allows companies to establish fuzzy and stochastic planning to compete with other large-scale

companies in meeting their deliveries. Supplier shipping time, cycle times, available time and, customer shipping time are determined through the normal probability distribution function. For the critical OEE parameter that presents imprecision and vagueness in the data, a fuzzy system was constructed with its availability, performance, and quality attributes as input variables. The research was validated with real data in the southern region of the state of Guanajuato, Mexico, where there are dozens of knitting SMEs. The proposed approach was simulated using the Stella software.

This article aims to provide an approach to developing a novel dynamic and fuzzy value stream mapping. DFVSM proposes the integration of a fuzzy system to determine OEE at each stage of the process as an output variable. The variables involved in the calculation are imprecise in the collection of records, such as Ava, P, and Q, which represent the input variables of the fuzzy system. This is the reason why this integration is proposed. Another contribution is to validate whether each variable in the study has a normal probability distribution. Otherwise, we use the transformations of the central limit theorem and the Johnson families as mechanisms to obtain a normal probability distribution and a DFVSM.

Results

Problem articulation

The development of a current VSM consists of three classes of flow: process flow, material flow, and information flow (Figure 2).

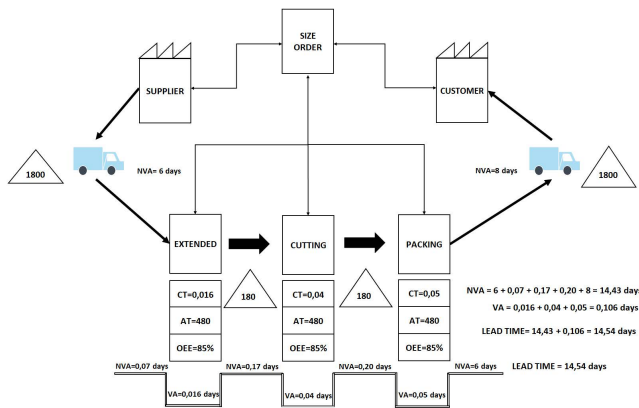


Figure 2. Current value stream mapping.

Source: Authors

Key variables

The parameters used in each of the flows are deterministic and fixed: CT, AT, SST, CST, OS, NM, OEE (Figure 2).

Horizon time

The lead time is calculated by identifying AV and NVA activities. A single calculation is made to estimate the corresponding lead time.

$$\text{Lead time} = \text{Total AV} + \text{Total NVA} \quad (1)$$

$$\text{Total AV} = \sum_{i=1}^n \text{AV}_i \quad (2)$$

Where AV_i are the cycle times of each operation.

$$\text{Total NVA} = \text{SST} + \text{CST} + \sum_{i=1}^n \text{NVA}_i \quad (3)$$

Where NVA_i are the NVA of each operation.

$$\text{NVA}_i = \frac{\text{CT}_i * \text{OS}}{\text{AT}_i + \text{NM}_i + \text{OEE}_i} \quad (4)$$

where $I = 1, 2, 3$.

$\text{SST} = 6$ days, $\text{CST} = 8$ days, $\text{NVA}_1 = 0,07$ days, $\text{NVA}_2 = 0,17$ days, $\text{NVA}_3 = 0,20$ days

$$\text{Total NVA} = 6 + 8 + 0,07 + 0,17 + 0,20 = 14,43 \text{ days} \quad (5)$$

$$\text{Total AV} = 0,016 + 0,04 + 0,05 = 0,106 \text{ days} \quad (6)$$

$$\text{Lead time} = 14,43 + 0,106 = 14,54 \text{ days} \quad (7)$$

Proposed approach

The perception of the level of efficiency and effectiveness (OEE) generally shows imprecision and vagueness in the data, so a fuzzy system was developed to evaluate the variable, which is a function of three attributes: availability, quality, and performance. The evaluation of a percentage in decimal form has a gradually incremental behavior ranging from 0 to 1. The sigmoidal membership function had a similar incremental behavior in the range from 0 to 1, so the data was fuzzified in the system. For this proposal, the percentage of efficiency and effectiveness was used as a linguistic variable, and a diffuse system was developed in the VSM's dynamic model, where the 3 attributes were used as input linguistic variables and the efficiency percentage and efficiency as an output variable. Each of the variables of the fuzzy system consisted of two linguistic labels: regular and good. The sigmoidal type membership function was used for fuzzification. 3 variables and 2 linguistic labels formed the basis of knowledge of the diffuse system, thus creating 8 fuzzy rules. The maximum fuzzy operator was used in the stages of implication and aggregation. For this model, the defuzzification phase was not implemented, given the similarity of the fuzzified data and the percentage expressed in decimals from 0 to 1, which were used as input values in the simulation of the model. Another modification to the traditional VSM is that the variables of the cycle time, available time were used through a normal probability distribution to add the uncertainty factor in the fulfilment of the activities carried out by the operators.

Input linguistic variables are explained below:

Availability: the proportion of run time (B) between total operative mode time (A).

$$Availability = \frac{B}{A} \quad (8)$$

Performance: the proportion of actual speed (D) versus normal speed (C).

$$Performance = \frac{D}{C} \quad (9)$$

Quality: the proportion of actual good products (F) versus product output (E).

$$Quality = \frac{F}{E} \quad (10)$$

$$OEE\% = \frac{B}{A} \times \frac{D}{C} \times \frac{F}{E} \quad (11)$$

Sigmoidal membership function

$$\mu_A(x) = \begin{cases} 0 & \text{if } x \leq a \\ 2 \left[\frac{x-a}{b-a} \right]^2 & \text{if } a < x \leq m \\ 1 - 2 \left[\frac{x-b}{b-a} \right]^2 & \text{if } m < x < b \\ 1 & \text{if } x \geq b \end{cases} \quad (12)$$

Table 1. Fuzzy system parameters

Linguistic variables	Sigmoidal membership function. Regular label			Sigmoidal membership function. Good label		
	a	m	b	a	m	b
Availability	0,2	0,4	0,6	0,4	0,6	0,8
Performance	0,2	0,5	0,8	0,4	0,7	1,0
Quality	0,5	0,6	0,7	0,7	0,8	0,9
OEE	0	0,4	0,7	0,6	0,8	1,0

Source: Authors

Table 1 shows the ranges of the sigmoidal membership function for the linguistic labels (regular and good) by the three input variables (availability, performance, quality) and one output variable (OEE). Figure 3 shows the development of the fuzzification stage, using only auxiliary variables in the dynamic model. The parameters for each linguistic label a , m , and b were determined for the regular and good labels. The linguistic input variables consider each of the 3 processes of the manufacturing system, and their values can be seen in the indicators.

We defined a total of 8 fuzzy rules as the basis of knowledge of the Mamdani fuzzy system integrated into the same dynamic systems interface (Figure 4).

Figure 4 shows the 8 fuzzy rules for each process operation. For the OEE auxiliary variables, the implication stage was

carried out, introducing a logical function with the minimum fuzzy operator to related variables. Finally, the aggregation stage of the fuzzy system was performed with the maximum fuzzy operator for the fuzzy OEE variable. These values were used to determine the times of NVA activities in each process operation on the VSM.

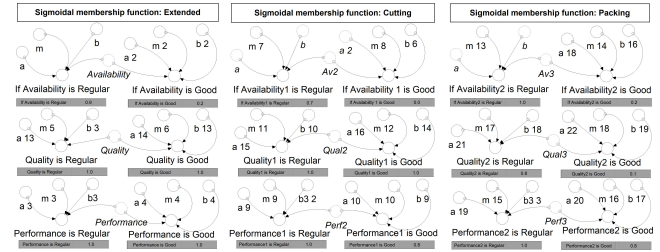


Figure 3. Sigmoidal membership functions.

Source: Authors

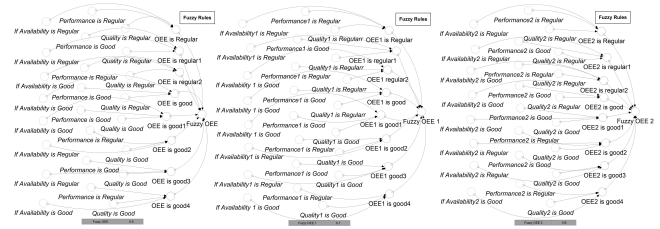


Figure 4. Fuzzy rules.

Source: Authors

Fuzzy rules in each operation process:

- IF availability is regular AND performance is regular AND quality is regular THEN OEE is regular.
- IF availability is regular AND performance is good AND quality is regular THEN OEE is regular.
- IF availability is good AND performance is regular AND quality is regular THEN OEE is regular.
- IF availability is good AND performance is good AND quality is good THEN OEE is good.
- IF availability is good AND performance is regular AND quality is good THEN OEE is good.
- IF availability is good AND performance is good AND quality is regular THEN OEE is good.
- IF availability is regular AND performance is good AND quality is good THEN OEE is good.
- IF availability is regular AND performance is regular AND quality is good THEN OEE is good.

Implication

Minimum fuzzy operator

Aggregation

Maximum fuzzy operator

The parameters used by the membership functions of the sigmoidal type, as well as their function and the fuzzy rules, were integrated into the dynamic model as auxiliary variables.

Forrest diagram

Figure 5 shows the DFVSM design, where process and material flows are displayed. In the final part of the Figure, the timeline that determines the lead time of the product order is observed. AV activities are only the cycle times, and NVA activities are related to waiting times for SST and CST, as well as waiting times in each operation. The parameters used for its determination are, cycle time (CT), order size (OS), available time (AT), machine number (MN), and OEE. They were determined with the following function:

$$NVA = \frac{CT * OS}{AT * MN * OEE} \quad (13)$$

For each operation, a balancing loop was developed to fulfill the specific goal or order size. The contribution of this dynamic model is the integration of a fuzzy system for the OEE% variable, since the evaluation of the availability, quality, and performance attributes are subjective and imprecise, and an uncertainty approach is also integrated into the model when using normal distribution functions for variables such as cycle time, available time, supplier time, and delivery time. A fuzzy system was developed for each operation of the textile cutting process. Parameters for the sigmoidal membership function were defined through auxiliary variables. Eight fuzzy rules were defined. The stage of implication and aggregation was performed through a maximum fuzzy operator. In this way, it contributes to the modelling of systems dynamics for variables that are imprecise or qualitative variables for any case.

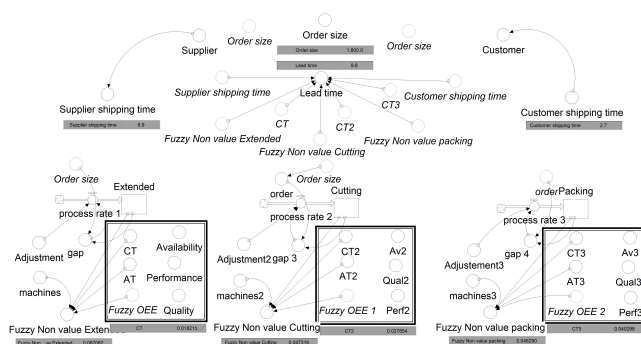


Figure 5. Forrester diagram.

Source: Authors

120 simulations were performed to be able to explain the process behavior of an order size of 1800 products. The lead time oscillated between 6 and 24 days. The expected lead time after 120 runs was 15,05 days (Figure 6).

The central limit theorem describes the distribution of the mean of a random sample from a population with finite variance. When the sample size is large enough, the distribution of

means flows approximately normal. The proposed approach uses a sample of 120 simulations, large enough to estimate the expected value of reliable lead time. Table 2 shows the results of 120 runs in a simulation of the proposed approach DFVSM, support to give the estimate of the expected delivery time of 15,05 days.

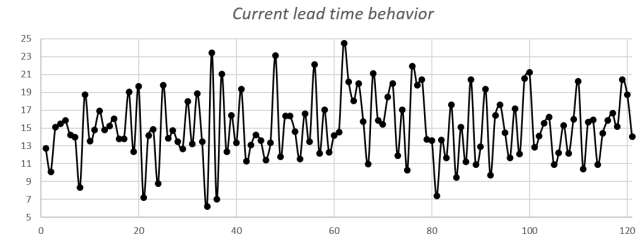


Figure 6. 120 simulations of current lead time behavior for a size order of 1800 products.

Source: Authors

Table 2. 120 runs in dynamic simulation

Simulations of lead time					
12,69	7,21	19,34	14,54	7,41	12,81
10,09	14,18	11,29	24,51	13,65	14,07
15,09	14,86	13,11	20,16	11,68	15,54
15,44	8,77	14,23	18,02	17,57	16,22
15,87	19,82	13,58	20	9,47	10,89
14,24	13,83	11,4	15,74	15,1	12,2
13,95	14,73	13,33	10,97	11,21	15,3
8,34	13,48	23,09	21,09	20,39	12,13
18,7	12,68	11,75	15,83	10,91	15,99
13,5	17,97	16,35	15,4	12,89	20,22
14,81	13,2	16,34	18,49	19,34	10,41
16,93	18,88	14,62	19,95	9,69	15,68
14,81	13,48	11,52	11,92	16,43	15,91
15,24	6,23	16,58	17,04	17,61	10,87
16,06	23,43	13,47	10,26	14,45	14,41
13,78	7,01	22,09	21,94	11,66	15,86
13,78	21,04	12,14	19,81	17,16	16,63
19,03	12,31	17,04	20,42	12,11	15,17
12,31	16,42	12,3	13,69	20,55	20,4
19,66	13,34	14,15	13,58	21,22	18,75

Source: Authors

Minimum: 6,23 days

Maximum: 24,51 days

Expected lead time: 15,05 days

The results of the DFVSM simulations show significant variability in lead times, based on the vagueness and stochastic uncertainty when using probability distribution functions. The estimate of the expected time is based on the average of the 120 simulations, thus providing greater reliability to the fulfillment of orders, in comparison with deterministic calculation of conventional VSM.

Conventional VSM through a simple calculation:

$$NVA = 6 + 0,07 + 0,17 + 0,20 + 8 = 14,43 \text{ days} \quad (14)$$

$$AV = 0,016 + 0,04 + 0,05 = 0,106 \text{ days} \quad (15)$$

$$\text{Lead time} = 14,43 + 0,106 = 14,54 \text{ days} \quad (16)$$

Sensitivity analysis

When analyzing the behavior of the dynamic model, the 2 critical activities in the delivery of an order of 1800 products were identified, which are the supplier shipping time (SST) and customer shipping time (CST). A tangible scenario was proposed by asking the supplier for a guarantee of improving their delivery times, as well as guaranteeing a reduction in delivery time to the customer.

Current times:

SST = normal (8,2), mean time = 8, and standard deviation = 2

CST = normal (6,3), mean time = 6, and standard deviation = 3

Improved times:

SST = (6,1), mean time = 6, and standard deviation = 1

CST = (4,1), mean time = 4, and standard deviation = 1

Figure 7 shows the behavior of 120 runs with improved times, significantly reducing by 28% the estimate of the expected delivery time to the end customer and significantly reducing the dispersion of results.



Figure 7. 120 simulations of improved lead time behavior for a size order of 1800 products.

Source: Authors

Table 3 shows the results of 120 runs in a simulation of the proposed approach with improved times for SST and CST, which aids in estimating the expected delivery time of 10,89 days.

Minimum: 7,1 days

Maximum: 14,71 days

Expected lead time: 10,89 days

Conclusions

The use of deterministic plans and stochastic execution theory for structuring and deepening the research has proved useful by

Table 3. 120 runs in dynamic simulation with improved times

Simulations of lead time					
10,34	12,34	12,89	11,89	11,53	11,22
9,46	12,78	11,17	10,54	7,87	10,28
10,52	10,97	12,78	11,37	11,05	11,01
10,45	10,39	10,22	8,9	10,98	11,8
10,23	8,8	10,95	11,12	11,52	10,24
10,1	11,5	10,57	12,12	11,49	11,04
9,86	11,68	11,71	12,88	8,27	11,85
11,82	12,14	8,58	9,06	10,84	8,89
12,21	10,37	9,15	9,56	13,27	13,4
10,29	11,98	12,23	11,64	10,39	12,52
10,99	10,68	12,71	11,74	11,97	10,39
13,22	10,1	12,26	10,23	12,83	10,45
9,69	9,46	10,38	10,27	12,74	10,57
12,66	10,51	12,25	10,74	9,79	9,7
10,26	14,71	9,02	13,17	7,87	12,91
11,17	11,31	9,68	9,31	9,65	7,1
12,73	11,19	10,66	11,75	11,21	8,21
11,52	12,88	9,75	9,89	13,53	8,7
13,92	7,81	9,53	10,68	9,54	10,13
9,75	10,6	11,75	11,22	10,22	10,21

Source: Authors

conceptualizing the DFVSM approach as new knowledge being incorporated to a process in the form of a fuzzy and stochastic planning tool. This article presents a dynamic and fuzzy value stream mapping validated in a cutting production system of a knitting company. The model consists of 3 balanced loops where different order sizes from each of the departments are visualized. A normality test was performed on the variables of the main operations of the process. The cycle times were used through the normal distribution function to generate random numbers in each of the simulation iterations, integrating the inherent statistical variability of the process. One of the main contributions of the research was to develop a fuzzy system in the same system dynamics interface for the variable percentage of efficiency and efficacy that presents imprecision and vagueness in the data as the output variable. This fuzzy system was deployed in three linguistic input variables for their respective calculation: availability, performance, and quality. Each of them was categorized with two linguistic labels (regular and good). Sigmoidal membership function was used to fuzzify data. The implication and aggregation stages were developed. The proposed approach allows estimating the expected lead time from multiples runs in a dynamic simulation integrating conditions of variability and imprecision. The results of the simulation show a significant dispersion in the delivery times of an order of 1800 products, due to the variability in the parameters, which resembles reality. It should be noted that the desired number of runs in the model can be modified to make the estimate more accurate. A 120-run simulation was performed to calculate the corresponding reliable delivery time in order to make improve decision making, in comparison with the simple calculation of the conventional value stream mapping

used in recent investigations of VSM applications. A sensitivity analysis of the proposed model was integrated, which identified the critical factors for the delivery of the order, and achievable times were proposed for the delivery times of the supplier and the client, reducing the expected delivery time by 28%. This research contributes to the dynamic systems theory to integrate fuzzy systems for inaccurate variables or qualitative variables in the study.

The proposed approach was implemented and validated with real data of three knitting enterprises of the southern region of the Guanajuato state in Mexico, achieving an estimation of a stochastic lead time execution. The companies provided the records of the parameters of each operation of the process and participated in the development of fuzzy rules and the analysis of the results of the proposed DFVSM, thus validating the reliability of its execution in the field. From the implementations, it could be learned that commitment and employee involvement is fundamental for the proper stochastic execution of the deterministic plans. A proposal for future work would be to design a factory evaluation system for supply chain management with a genetic-neuro-fuzzy approach.


References

- Arsenyan, J. and Büyükoçkan G. (2016). An integrated fuzzy approach for information technology planning in collaborative product development. *International Journal of Production Research*, 54(11), 3149-3169. 10.1080/00207543.2015.1043032
- Babader, A., Ren, J., Jones, K., and Wang, J. (2016). A system dynamics approach for enhancing social behaviours regarding their use of packaging. *Expert Systems with Applications*, 46, 417-425. 10.1016/j.eswa.2015.10.025
- Baeza-Serrato, R. (2016). REDUTEX: a hybrid push-pull production system approach for reliable delivery time in knitting SMEs. *Production Planning and Control*, 27(4), 263-279. 10.1080/09537287.2015.1120362
- Baeza-Serrato, R. (2018). Stochastic plans in SMEs: A novel multidimensional fuzzy logic system (mFLS) approach. *Ingeniería e Investigación*, 38(2), 70-78. 10.15446/ing.investig.v38n2.65357
- Balaji, V., Venkumar, P., Sabitha, M. S., and Amuthaguka, D. (2020). DVSMs: dynamic value stream mapping solution by applying IIoT. *Sadhana*, 45(38), 263-279. 10.1007/s12046-019-1251-5
- Bin, N., Petersen, K., and Schneider, K. (2016). FLOW-assisted value stream mapping in the early phases of large-scale software development. *The Journal of Systems and Software*, 111, 213-227. 10.1016/j.jss.2015.10.013
- Bocklisch, F. and Hausmann, D. (2018). Multidimensional fuzzy pattern classifier sequences for medical diagnostic reasoning. *Applied Soft Computing*, 66, 297-310. 10.1016/j.asoc.2018.02.041
- Cardiel, J., Baeza-Serrato, R., and Lizárraga, R. (2017). Development of a system dynamics model based on six sigma methodology. *Ingeniería e Investigación*, 37(1), 80-90. 10.15446/ing.investig.v37n1.62270
- Darvish Falehi, A. (2020) Robust and Intelligent Type-2 Fuzzy Fractional-Order Controller-Based Automatic Generation Control to Enhance the Damping Performance of Multi-Machine Power Systems, *IETE Journal of Research*. 10.1080/03772063.2020.1719908
- Gao, W., Hong, B., Swaney, D. P., Howarth, R. W., and Guo, H. (2016). A system dynamics model for managing regional N inputs from human activities. *Ecological Modelling*, 322, 82-91. 10.1016/j.ecolmodel.2015.12.001
- Fu, X. and Chen, T. (2017). Research on supply chain partner selection and task allocation based on fuzzy theory under an uncertain environment. *Ingeniería e Investigación*, 38(1), 83-95. 10.15446/ing.investig.v38n1.64675
- Kavanagh, A. and Donnelly, J. (2020). A Lean approach to improve medication administration safety by reducing distractions and interruptions *Journal of Nursing Care Quality*, 35(4), E58-E62. 10.1097/NCQ.0000000000000473
- Keykavoussi, A. and Ebrahimi, A. (2020). Using fuzzy cost-time profile for effective implementation of lean programmes; SAIPA automotive manufacturer, case study. *Total Quality Management and Business Excellence*, 31(13-14), 1519-1543. 10.1080/14783363.2018.1490639
- Lagos, D., Mancilla, R., Leal, P., and Fox, F. (2019). Performance measurement of a solution for the travelling salesman problem for routing through the incorporation of service time variability. *Ingeniería e Investigación*, 39(3), 44-49. 10.15446/ing.investig.v39n3.81161
- Langroodi, R. R. P. and Amiri, M. (2016). A system dynamics modeling approach for a multi-level, multi-product, multi-region supply chain under demand uncertainty. *Expert Systems With Applications*, 51, 231-244. 10.1016/j.eswa.2015.12.043
- Liu, Q. and Yang, H. (2020). Incorporating Variability in Lean Manufacturing: A Fuzzy Value Stream Mapping Approach. *Mathematical Problems in Engineering*, 2020, 1347054. 10.1155/2020/1347054
- Ono, T. (1988). *Toyota Production System: Beyond Large-Scale Production*. New York, NY: Productivity Press.
- Pasaoglu, G., Harrison, G., Jones, L., Hill, A., Beaudet, A., and Thiel, C. (2016). A system dynamics based market agent model simulating future powertrain technology transition: Scenarios in the EU light duty vehicle road transport sector. *Technological Forecasting and Social Change*, 104, 133-146. 10.1016/j.techfore.2015.11.028
- Preuss, L., G., Luz T., G., Narayanamurthy, G., Giardelli, P., and Sawhney, R. (2021). A systematic literature review on the stochastic analysis of value streams, *Production Planning and Control*, 32(2), 121-131. 10.1080/09537287.2020.1713414
- Ricciardi, F., De Bernardi, P., and Cantino, V. (2020). System dynamics modelling as a circular process: The smart commons approach to impact management, *Technological Forecasting and Social Change*, 151, 119799. 10.1016/j.techfore.2019.119799

- Rodríguez, V., Cervera, A., López, L., and Pérez-Fernández, V. (2020). Lean thinking to foster the transition from traditional logistics to the physical internet, *Sustainability*, 12(15), 6053. 10.3390/su12156053
- Sadiq, S., Saad, M., Zeeshan, M., Hussain, S., Yasmeen, U., and Aámir, M. (2021). An integrated framework for lean manufacturing in relation with blue ocean manufacturing – A case study, *Journal of Cleaner Production*, 279, 123790. 10.1016/j.jclepro.2020.123790
- Salvador, R., Vetroni, M., Tagliaferro dos Santos, G., Godoi, K., Moro, C., and de Francisco, A. C. (2020). Towards a green and fast production system: integrating life cycle assessment and value stream mapping for decision making, *Environmental Impact Assessment Review*, 87, 106519. 10.1016/j.eiar.2020.106519
- Sposito, L. and Santos, A. C. (2020). Lean 4.0: A new holistic approach for the integration of lean manufacturing tools and digital technologies. *International Journal of Mathematical, Engineering and Management Sciences*, 5(5), 851-868, 10.33889/IJMEMS.2020.5.5.066
- Sullivan, W. G., McDonald, T. N., and Aken, E. M. (2002). Equipment replacement decisions and lean manufacturing. *Robotics and Computer-Integrated Manufacturing*, 18(3-4), 255-265. 10.1016/S0736-5845(02)00016-9
- Tyagi, S., Choudhary, A., Cai, X., and Yang, K. (2015). Value stream mapping to reduce the lead-time of a product development process. *International Journal of Production Economics*, 160, 202-212. 10.1016/j.ijpe.2014.11.002
- Wang, P., Wu, P., Chi, H-L., and Li, X. (2020). Adopting lean thinking in virtual reality based personalized operation training using value stream mapping. *Automation in Construction*, 119, 103355. 10.1016/j.autcon.2020.103355

Selection Criteria for Sustainable Suppliers in the Supply Chain of Copper Mining in Chile

Criterios de selección de proveedores sostenibles en la cadena de suministro de la minería del cobre en Chile

Orlando Gahona-Flores ¹

ABSTRACT

The objective of this research is to identify the criteria for the selection of sustainable suppliers in the supply chain of copper mining located in the Antofagasta region in Chile, through the information obtained from the application of a survey to executives of all mining companies in the Antofagasta region in 2018. The research results show that mining companies use economic, environmental and social criteria in the selection of sustainable suppliers, which are consistent with the research carried out by Dickson (1966) and Zimmer, Frohling and Schultmann (2016). However, the group of mining companies represented in this study differ from others regarding the criteria applied to suppliers of goods compare to service providers. In the case of suppliers of goods, economic criteria are valued more preferably, such as: quality, delivery on time, price, historical performance and previous sales. On the other hand, when it comes to service providers, environmental and social criteria, such as: occupational health and safety management and environmental management, are valued with greater importance.

Keywords: supply chain, selection criteria, sustainable suppliers, mining, copper, Chile

RESUMEN

El objetivo de esta investigación es identificar los criterios de selección de proveedores sostenibles en la cadena de suministro de la minería del Cobre localizada en la región de Antofagasta en Chile, a través de la información obtenida en la aplicación de una encuesta a directivos de todas las compañías mineras de la región de Antofagasta en el año 2018. Los resultados de la investigación evidencian que las mineras utilizan los criterios económicos, ambientales y sociales en la selección de proveedores sostenibles, los cuales son consistentes con las investigaciones realizadas por Dickson (1966) y Zimmer, Frohling y Schultmann (2016). No obstante, se destaca como un hallazgo importante la diferenciación que hacen las mineras en la valoración de los criterios cuando se trata de proveedores de bienes o proveedores de servicios. En el caso de proveedores de bienes se valoran con mayor preferencia los criterios económicos, tales como: calidad, entrega a tiempo, precio, desempeño histórico y ventas anteriores. En cambio, cuando se trata de proveedores de servicios se valoran con mayor importancia los criterios ambientales y sociales, tales como: gestión en seguridad y salud ocupacional, y gestión medioambiental.

Palabras clave: cadena de suministro, criterios de selección, proveedores sostenibles, minería, cobre, Chile

Received: August 1st, 2020

Accepted: January 21st, 2021

Introduction

The copper mining is the most relevant economic activity for Chile. Directly, it represents more than 10% of GDP, more than 50% of exports, and it is the main recipient of foreign direct investment, representing one of every three dollars that enters the country (Bustos-Gallardo and Prieto, 2019). The presence of new foreign capital has strongly boosted the development of the mining industry, transforming the Antofagasta region into the world capital of copper mining (Bustos-Gallardo and Prieto, 2019). Therefore, it is not surprising the incidence that this activity has on all the activities of this area. According to Bustos-Gallardo and Prieto (2019), the region contributed about 3.2 million tons of copper to national production, that is, about 57%. Currently, supply chain management has become an aspect that contributes to productivity and competitiveness in different mining industries, such as in the case of copper, gold, coal, nickel, among others; Because

logistics manages the flows of information, materials, minerals and money from the supply of inputs and supplies, through storage, use in exploration, exploitation and benefit activities, to transportation in order to meet the customer requirements (Pedrosa, Blazevec and Jasmand, 2015). Vendor selection is one of the critical decisions for any organization, due to its direct impact on profitability and maintaining the company's competitive position. Historically, sourcing decisions were made based on economic aspects. However, due to the growing trends in outsourcing of services, the increasingly

¹Commercial Engineer, Universidad Católica del Norte, Chile. Affiliation: Associate Professor, Universidad de Antofagasta, Chile. E-mail: orlando.gahona@uantof.cl

How to cite: Gahona, O. (2021). Selection Criteria for Sustainable Suppliers in the Supply Chain of Copper Mining in Chile. *Ingeniería e Investigación*, 41(2), e89641. [10.15446/ing.investig.v41n2.89641](https://doi.org/10.15446/ing.investig.v41n2.89641)



Attribution 4.0 International (CC BY 4.0) Share - Adapt

demanding environmental policies and the social demands of the territories where they carry out their operations are forcing companies to integrate the triple bottom line criteria, which are economic criteria. environmental and social issues in their supply chain activities (Ghayebloo, Tarokh, Venkatadri, Diallo, 2015). Sustainable supplier selection is a complicated decision, due to the permanent conflict between the regulation and legal regulation of sustainability and the organizational objectives of companies (Zimmer, Frohling and Schultmann, 2016).

The objective of this research is to generate knowledge on the selection criteria of suppliers in the supply chain of copper mining

located in the Antofagasta region in Chile, through the information obtained from the application of a survey to managers of the mining companies in 2018 and deliver recommendations that allow obtaining higher levels of productivity and efficiency in that industry. The research results show that mining companies use economic, environmental and social criteria in the pre-selection and selection processes of sustainable suppliers, which are consistent with the research carried out by Dickson (1966) and Zimmer, Frohling and Schultmann (2016). Notwithstanding the foregoing, the differentiation that mining companies make in evaluating criteria when it comes to suppliers of goods or service providers stands out as an important finding since they differ. In the case of suppliers of goods, economic criteria are valued more preferably, such as: quality, delivery on time, price, historical performance and previous sales. On the other hand, when it comes to service providers, environmental and social criteria, such as: occupational health and safety management and environmental management, are valued with greater importance.

Currently, to the best of my knowledge, there are no scientific studies or research on the criteria for selecting sustainable suppliers in the mining supply chain, and especially in the copper mining industry of the Antofagasta region in Chile.

The study is organized into four sections: the first section presents the importance of this research in the context of the existing literature. After that it is presented the methodology that is supported as a case study. In the third section the results obtained and their discussion are shown. The last section presents the conclusions which include recommendations and limitations of this study.

Literature review

The supply chain is "a set of three or more entities that directly participate in the flow of products, services, finances and/or information from a source to a customer" (Mentzer, Dewitt, Keebler and Zacharia, 2016). According to Marques, Paiva, Beheregarai and Teixeira (2012), the supply chain is a phenomenon that always occurs when companies establish relationships, regardless of the level of existing management. The supply chain concept is applicable to mining because it is made up of a group of companies that have facilities,

functional activities and distribution systems that seek to deliver minerals to different customers. Additionally, it should be pointed out that in the Chilean case, the production chains resemble the concept of the supply chain because they are made up of supply, exploration, exploitation, profit, marketing and consumer companies, which generate different relationships between them, such as: productive chains or agglomerations of companies among others, which focus on increasing productivity and the use of mineral resources (Arias, Atienza and Cademartori, 2014). The Copper mining is the most relevant economic activity for Chile since it represents more than 10% of GDP, more than 50% of exports, it is the main recipient of direct foreign investment, with 30% of total production and it maintains a third of the known reserves, the largest globally (Bustos-Gallardo and Prieto, 2019). In the case of Chilean mining, the importance of the supply chain is crucial, since mining companies have outsourced a large number of functions to their suppliers, concentrating their efforts on the core of the business, that is; the ownership, operation and management of the deposits. Therefore, an important part of the past and future success of Chilean mining depends directly on the productivity and competitiveness of suppliers (Korinek, 2013). The Antofagasta region is closely linked to the history and development of Chile's copper mining. Therefore, it is not surprising the incidence that this activity has on all the activities of this area. According to Bustos-Gallardo and Prieto (2019), this region contributed 3.2 million tons of copper to national production, that is, about 57%. Purchases play a strategic role and require adequate management in organizations, since they can represent between 40% and 60% of final product sales, and for these reasons, a small reduction in these costs can lead to an increase in the efficiency and profitability of the company (Grzybowska and Gajdzik, 2014). For this reason, identifying the relevant supplier selection criteria is a key activity in the management of the supply chain, which guarantees having reliable and competent suppliers that provide inputs, cost and adequate quality (Hanlin and Hanlin, 2012). Dickson (1966) was a pioneer in investigating the relevant criteria in the supplier selection process. This author identified and analyzed 23 criteria and concluded that quality was the highest priority criterion, followed by on-time deliveries and the good historical performance of the organization (Table 1).

The vendor selection is one of the critical decisions for any organization due to its direct impact on profitability and maintaining the organization's competitive position. Historically, sourcing decisions were made based on economic aspects. However, growing service outsourcing trends, environmental policies and social concerns are now forcing companies to integrate triple bottom line criteria, which encompass economic, environmental and social criteria in their supply chain activities (Ghayebloo, Tarokh, Venkatadri, Diallo, 2015). Sustainable supplier selection is a complicated decision, due to the permanent conflict between the regulation and legal regulation of sustainability and the organizational objectives of companies (Zimmer, Frohling and Schultmann, 2016). Consequently, the problem of selecting sustainable suppliers is commonly considered

Table 1. Supplier selection criteria

Selection criteria	Dickson research
Quality	1
Delivery	2
Performance history	3
Warranties and claims	4
Production facilities and capacity	5
Price	6
Technical capacity	7
Financial position	8
Conflict resolution	9
Communication system	10
Reputation and position in industry	11
Relationship closeness	12
Management and organisation	13
Operational controls	14
After sales services	15
Attitude	16
Impression	17
Packaging ability	18
Labour relations	19
Geographical location	20
Amount of past business	21
Training aids	22
Reciprocal arrangements	23

Source: Dickson (1966)

as a multi-criteria decision-making problem. There is a comprehensive systematic review dedicated to different criteria of environmental sustainability in the area of selection of sustainable and ecological suppliers (Govindan, Rajendram, Sarkis, Murugesan, 2015); (Zimmer, Frohling, Schultmann, 2016); (Awashi, Chauhan, Gokal, 2010). Recently, Zimmer, Frohling, and Schultmann (2016) examined 143 articles published between 1997 and 2014, and based on their research results, the top 10 economic, environmental, and social criteria are listed below in Table 2.

Among the environmental sustainability criteria are subcriteria:

- a) Environmental efficiency: it shows the way in which a supplier is carrying out external environmental policies together with internal policies (Govindan, Rajendram, Sarkis, Murugesan, 2015); (Amindoust, Ahmed, Saghafeinia, Bahrainijad, 2012); (Bai and Sarkis, 2010). It includes ecological process planning, environmental protection, regulatory compliance and continuous monitoring, the internal control process, environmental protection policies and certifications related to the environment, such as ISO 14001. Shen, Olfat, Govindan, Khodaverdi, Diabat (2013) highlighted the increasing attention of consumers regarding the economy and the environment. They also noted the critical role associated with environmental management systems, as well as environmental protection policies.

Table 2. Sustainable supplier selection criteria

Economic criteria	Environmental criteria	Social criteria
Quality	Environmental management system	Stakeholder engagement
Flexibility	Resource consumption	Staff training
Price	Ecological design	Commitment in social management
Delivery term	Recycling	Commitment to health and safety management
Relationship	Ecological impact control	Stakeholder relations
Cost	Sewage water	Code of social conduct
Technical capacity	Energy consumption	Donations for sustainable projects
Logistical costs	Reuse	Rights of interested parties
Reverse logistics	Air emissions	Safety practices
Rejection rate	Environmental code of conduct	Annual number of accidents

Source: Zimmer, Frohling and Schultmann (2016)

- b) Green image: try to establish a supplier image in the market as a green company that is capable of producing green items. The green image consists of market reputation, customer retention, stakeholder relationships, environmental staff training, and market share (Awashi, Chauhan, and Gokal, 2010); (Mafakheri, Breton and Ghoniem, 2011); (Kannan, Govindan and Rajendran, 2015).
- c) Pollution reduction: this is related to reducing the amount of greenhouse gas emissions from a supplier to be in line with regional and international green policies subject to the type of business. The subcriteria included in the reduction of pollution are the consumption of resources, wastewater, emissions to the atmosphere, the carbon footprint, solid waste and the use of harmful materials (Bai and Sarkis, 2010); (Cifci and Buyukozkan, 2011); (Dou, Zhu and Sarkis, 2014).
- d) Green competencies: measures suppliers' ability to reduce environmental influences from their operations through the use of different green technologies, for example, green recycling and packaging, recycling capacity, use of green materials, flexibility and green technology, and the capacity of response are the subcriteria associated with green skills (Mafakheri, Breton and Ghoniem, 2011); (Cifci and Buyukozkan, 2011); (Ghadimi, Dargi and Heavey, 2017); (Azimifard, Moosavirad and Ariaifar, 2018).

Among social sustainability criteria are subcriteria:

- a) Safety and health: describes the potential of a provider with respect to the offer of programs to protect its personnel, prevent occupational accidents that affect the health and safety of workers, OHSAS 18001 certification that allows standardized conditions and

health and safety practices (Govindan, Rajendram, Sarkis and Murugesan, 2015); (Bai and Sarkis, 2010); (Ghadimi, Dargi and Heavey, 2017); (Wittstruck and Teuteberg, 2012); (Vahidi, Torabi, and Ramezankhani, 2018).

- b) Employment practices: ensures that the current and future needs of company employees are met. This criteria includes subcriteria such as disciplinary and safety practices, employee contracts, discrimination, child labor, job opportunities, fair job sources, flexible work arrangements, professional development, workers compensation, research and development, employee interests and rights, employee well-being and diversity (Govindan, Rajendram, Sarkis and Murugesan, 2015); (Buyukozhan, 2012); (Thornton, Autry, Gligor and Brik, 2013).

According to Zimmer, Frohling, and Schultmann (2016), the buyer's price, delivery, and quality goals, along with the vendors' capabilities to meet all of those goals, are generally selected as important criteria. It should be noted that, in practice, the criteria for the selection of suppliers can be chosen in relation to the configuration of the company. There is also evidence from a study by Amindoust, Ahmed, Saghafeinia, Bahraini, and Bahraini (2012) that showed that the decision on the indicators for the selection of suppliers depends on the conditions of the organization and each company can think further about their own criteria for choosing the best providers. Due to the above presentation of the literature in this area, the motivations to develop this research are mainly two:

- Determine if the findings provided by Dickson (1966) and Zimmer, Frohling and Schultmann (2016), hold in the case of copper mining producers in Antofagasta, most important mining region in Chile.
- Identify the criteria for selecting sustainable suppliers in the copper mining supply chain located in the Antofagasta region of Chile. This is done for goods and services.

Materials and methods

The research was carried out in the Antofagasta region in Chile, where the main mining districts that concentrate about 57% of copper production in Chile are located (Bustos-Gallardo and Prieto, 2019). The approach is supported as a case study, which is framed as a descriptive investigation, based on the search for information, with the purpose of identifying the criteria for the selection of suppliers in the supply chain of copper mining in Chile and It was carried out during 2018. For this purpose, a survey was prepared that was applied to 41 managers of all the copper-producing mining companies in the Antofagasta region, according to the database provided by the Chilean Copper Corporation (COCHILCO). A questionnaire with semi-structured questions was developed, based on the

supplier selection criteria obtained by Dickson (1966) and Zimmer, Frohling and Schultmann (2016). The questionnaire is organized into four sections: the first section is about the location of the mining companies and the objective is to know their geographical location in the Antofagasta region. The second section is about the characterization of the managers who answered the survey with the aim of knowing which organizational area they belong to, seniority in the company and in their managerial position. The third section aims to know whether mining companies apply asynchronous and synchronous preselection methods, and what criteria they consider at each stage. The fourth and last section aim to know what are the criteria that mining companies apply to select suppliers of goods and service providers.

Results and discussion

Location of mining companies.

The mining companies in the Antofagasta region are 83% concentrated in the municipalities of Calama, Antofagasta and Sierra Gorda (Table 3). This is because the largest copper ore deposits are concentrated in these territories, and these communes are known as mining districts.

Table 3. Location of mining companies

Antofagasta	Mejillones	Sierra Gorda	Taltal	Calama	Tocopilla
24%	6%	24%	6%	35%	6%

Source: Author

Characterization of the managers of the mining companies that answered the survey.

This information was very relevant, since it allowed us to conclude that those who answered the survey know well how the internal organization of the mining company works, possess the necessary knowledge and have sufficient experience both in the company and in the position, to be considered as informants. valid in quality, relevance and relevance (Table 4).

Table 4. Characterization of managers

How long have you worked in the Company?			
1-3 years	4-5 years	6-10 years	Over 10 years
7%	27%	27%	39%
To which organizational area does your position belong?			
Supply and contracts	Human Resources	Safety and environment	Operations and maintenance
51%	3%	7%	39%
What is your position?			
Superintendent	Department head	Engineer and Analyst	Other
46%	27%	27%	0%
How long are you in that position?			
1-3 years	4-5 years	6-10 years	Over 10 years
19%	54%	27%	0%

Source: Author

Supplier pre-selection criteria

The pre-selection is the process of selecting candidates to participate in the formal purchase process, which is generally associated with new purchases or modified repurchases of services. They are based on the information that mining companies have, especially at the user level, but other types of actors also participate.

Asynchronous preselection represents the best instance to identify requirements, but it is also necessary that attractive offers derive from them, which must have the characteristics of being particular, original and difficult to replicate. In this way, its penetration in the purchase process can be greater because it represents a more complete, specialized offer and, therefore, less disposable. Respondents reported using asynchronous preselection (Table 5), which allows reducing the high administrative costs of receiving, managing and evaluating the number of proposals and quotes that would be received if the entire registry of suppliers were invited, and also allows reducing the uncertainty about the supplier's final performance when there is no historical performance or previous sales. The criteria used by mining companies to preselect a supplier in the asynchronous phase with 41 citations, are to meet the quality parameters and solve an unrecognized problem or suggest improvements; with 34 appointments, to be recommended by a professional of the company; and finally with 31 appointments, to be recommended by another mining company. The other phase that makes up the preselection of suppliers is the synchronous phase that is in tune with a specific purchasing process. It represents the earliest stage of a formal process where users recognize a need and raise a requirement. Respondents reported using synchronous preselection (Table 5), which corroborates the aforementioned in the sense that it allows deciding which supplier will be selected to participate in an established purchasing process. The criteria used in the synchronous phase with 41 citations are; positive evaluation of their technical skills, ISO 9001 certification, ISO 14001 certification and OSHAS 18001 certification. With 40 appointments, positive evaluation of their technical skills. With 28 appointments, the positive evaluation of your financial situation; and lastly, with 20 appointments, enrollment in external supplier qualification records. These results are consistent with the research by Dickson (1966), and especially with the research by Zimmer, Frohling and Schultmann (2016) on the environmental and social criteria for the selection of sustainable suppliers.

Supplier selection criteria

Once the suppliers and their offers have gone through the pre-selection processes, a small group of suppliers between 3 and 5 moves on to the next stage, where the decision criteria are considered within an evaluation and administrative process that takes the form of a tender. or contest. As previously stated, the supplier selection criteria presented to the respondents is based on the supplier selection criteria obtained by Dickson (1966) and Zimmer, Frohling and Schultmann (2016). In the survey of mining company managers on the criteria for selecting goods suppliers,

Table 5. Supplier pre-selection criteria

Does your company use asynchronous pre-selection of suppliers?			
Yes	Not		
100%	0%		
What are the criteria to be considered a supplier in the asynchronous preselection?			
Meet the quality parameters	Recommended by a professional of the company	Recommended by another mining company	Troubleshoots
41 quotes	34 quotes	31 quotes	41 quotes
Does your company use synchronous pre-selection of suppliers?			
Yes	Not		
100%	0%		
What are the criteria to be considered a supplier in synchronous preselection?			
Registration in external supplier qualification records			
20 quotes			
Positive evaluation of your financial situation			
28 quotes			
Positive evaluation of your technical skills			
41 quotes			
Positive assessment of your business skills			
40 quotes			
ISO 9001 certification			
41 quotes			
ISO 14001 certification			
41 quotes			
OHSAS 18001 certification			
41 quotes			

Source: Author

they are asked to select from the list of criteria those they consider relevant according to their knowledge and experience. Then, they must perform a forced ranking where the first they choose is the most important and the last they choose the least important. The aforementioned forced ranking is expressed through the simple average of the accumulated scores assigned by each of the respondents, considering the $n = 41$ that corresponds to the number of managers of the mining companies surveyed. The results obtained allow us to appreciate in the first instance that all the respondents chose the selection criteria mentioned in the Dickson (1966) study, in addition to the criteria of occupational safety management, occupational health management and environmental management mentioned in Zimmer's research., Frohling and Schultmann (2016) (Table 6). The results show that the selection criteria for goods suppliers most valued by the respondents are quality first, delivery on time second, price third, historical performance fourth, fifth place previous sales and sixth technical capacity, and the rest of the evaluation criteria indicated in Dickson's research (1966). These results are consistent with the existing literature, since they correspond to the economic criteria for the selection of sustainable suppliers from the research of Zimmer, Frohling and Schultmann (2016).

Table 6. Selection criteria for goods suppliers

N°	Selection criteria	Average
1	Quality	1,0
2	Delivery	2,85
3	Price	2,93
4	Performance history	4,78
5	Amount of past business	5,83
6	Technical capacity	7,98
7	Geographical location	8,83
8	Operational controls	10,66
9	Production facilities and capacity	10,68
10	Reputation and position in industry	11,37
11	Financial position	11,46
12	Occupational safety management	12,15
13	Warranties and claims	12,22
14	Occupational health management	13,15
15	Environmental management	14,15
16	Impression	14,61
17	Management and organisation	16,34
18	Relationship closeness	18,22
19	Attitude	18,68
20	Labour relations	18,85
21	After sales services	19,39
22	Conflict resolution	20,24
23	Training aids	22,37
24	Reciprocal arrangements	23,27
25	Packaging ability	24,22
26	Communication system	25,12

Source: Author

In the survey applied to the managers of mining companies on the criteria for selecting service providers, the same procedure is followed above. Respondents selected the criteria mentioned in the Dickson (1966) study, in addition to the criteria for occupational safety management, occupational health management and environmental management mentioned in the research by Zimmer, Frohling and Schultmann (2016) (Table 7).

The results show that the criteria for selecting service providers most valued by the respondents are first; management in occupational safety, in second place; management in occupational health, thirdly; environmental management, fourth; quality, in fifth place; the price, in sixth place; delivery on time, seventh; technical capacity; and later; the rest of the selection criteria indicated in Dickson's research (1966). These results are consistent with the existing literature, since they correspond to the environmental and social criteria for the selection of sustainable suppliers from the research of Zimmer, Frohling and Schultmann (2016) (Table 6). Already in the bidding process itself, the technical criteria evaluated may include: quality of services, the company's experience in the field, the profile of the staff, the equipment and tools to perform the service, and the work methodology. In addition, to include a safety evaluation that analyzes the accident rate and the operational risk matrix, an occupational health and hygiene evaluation that includes the

Table 7. Selection criteria for service suppliers

N°	Selection criteria	Average
1	Occupational safety management	1,00
2	Occupational health management	2,07
3	Environmental management	2,98
4	Quality	4,29
5	Price	5,90
6	Delivery	7,12
7	Technical capacity	7,37
8	Performance history	9,24
9	Production facilities and capacity	10,66
10	Financial position	11,63
11	Amount of past business	11,95
12	Labour relations	12,85
13	Geographical location	13,98
14	Operational controls	15,95
15	Warranties and claims	16,10
16	Management and organisation	16,24
17	After sales services	16,44
18	Training aids	16,56
19	Reputation and position in industry	17,34
20	Attitude	17,83
21	Conflict resolution	18,12
22	Communication system	21,15
23	Relationship closeness	21,15
24	Reciprocal arrangements	22,49
25	Impression	25,10
26	Packaging ability	25,41

Source: Author

analysis of occupational diseases and physical design of the work environment; and lastly, an environmental assessment that considers an assessment of the polluting agents and the degree of exposure of the workers.

Conclusions

The copper mining supply chain in Chile uses economic, environmental and social criteria in the pre-selection and selection processes of sustainable suppliers, which are consistent with the research carried out by Dickson (1966) and Zimmer, Frohling and Schultmann (2016). Notwithstanding the foregoing, the differentiation that mining companies make in evaluating criteria when it comes to suppliers of goods or service providers stands out as an important finding. In the case of suppliers of goods, economic criteria are valued more preferably, such as: quality, delivery on time, price, historical performance and previous sales. On the other hand, when it comes to service providers, environmental and social criteria, such as: occupational health and safety management and environmental management, are valued with greater importance. This differentiation made by mining companies is explained by the fact that the goods are inputs and finished products that are purchased for the production process and are manufactured in the supplier's facilities outside the mining

operation. Instead, the services are carried out inside the industrial premises, which implies that the suppliers must maintain their own personnel, machinery and equipment in the mining company's premises. Due to the above, the indicators of occupational safety management, occupational health management and environmental management of service providers, directly affect the management and productivity indicators of the company. In Chile, mining companies must report their indicators in occupational health and safety management, as well as environmental management at a consolidated level, that is; the company's own indicators plus the indicators of the service providers.

The first recommendation from the point of view of the sustainability of the mining business in the long term, is that mining companies implement the selection of sustainable suppliers through the standardization of selection criteria based on economic, environmental and social criteria. in their supply chains. The second recommendation from the point of view of the development of local suppliers is to encourage and support them to implement management systems and continuous improvement as it will allow them to be more productive and competitive, adding more value to the companies' supply chain. mining companies. This innovation will be a positive signal for investors, shareholders, the community and authorities because it demonstrates world-class business management, guaranteeing the delivery of quality products and services, in a sustainable way, taking care of the environment and protecting the integrity and health of its workers.

Chile being the third largest copper producer in the world, a limitation to the work carried out is knowing what are the criteria for selecting suppliers in the first two countries to contrast or to be able to generalized the conclusions reached in this study.

References

- Arias, M., Atienza, M. y Cademartori, J. (2014). Large mining enterprises and regional development in Chile: Between the enclave and cluster. *Journal of Economic Geography*, 14(1), pp. 73-95.
- Amindoust A, Ahmed S, Saghafeinia A, Bahreininejad A. (2012). Sustainable supplier selection: A ranking model based on fuzzy inference system. *Appl. Soft. Comput.* 12(6):1668-77.
- Awasthi, A., Chauhan, S.S. y Goyal, S.K. (2010). A fuzzy multicriteria approach for evaluating environmental performance of suppliers. *Int. J. Prod Econ.* 126(2):370-8.
- Azimifard, A., Moosavirad, SH. y Ariafar, S. (2018). Selecting sustainable supplier countries for Iran's steel industry at three levels by using AHP and TOPSIS methods. *Resour Policy*.
- Bai, C. y Sarkis, J. (2010). Green supplier development: analytical evaluation using rough set theory. *J. Clean Prod.* 18(12):1200-10.
- Bustos-Gallardo, B. y Prieto, M. (2019). Nuevas aproximaciones teóricas a las regiones commodity desde la ecología política. *EURE* (Santiago). Vol 45, número 135. <http://doi.org/10.4067/S0250-71612019000200153>
- Büyükoçkan, G. (2012). An integrated fuzzy multi-criteria group decision-making approach for green supplier evaluation. *Int. J. Prod. Res.* 50(11):2892-909. 10.1080/00207543.2011.564668
- Çifçi, G. y Büyükoçkan, G. (2011). A fuzzy MCDM approach to evaluate green suppliers. *Int. J. Comput Intell Syst.* 4(5):894-909. 10.1080/18756891.2011.9727840
- Dickson, G. (1966). An analysis of vendor selection systems and decisions. *Journal of Purchasing and Supply Management*, 2(1), pp. 5-17. 10.1111/j.1745-493X.1966.tb00818.x
- Dou, Y., Zhu, Q. y Sarkis, J. (2014). Evaluating green supplier development programs with a grey-analytical network process-based methodology. *Eur. J. Oper Res.* 233(2):420-31. 10.1016/j.ejor.2013.03.004
- Ghadimi, P., Dargi, A. y Heavey, C. (2017). Making sustainable sourcing decisions: practical evidence from the automotive industry. *Int. J. Logist.* 20(4):297-321. 10.1080/13675567.2016.1227310
- Ghayebloo S, Tarokh MJ, Venkatadri U, Diallo C. (2015). Developing a bi-objective model of the closed-loop supply chain network with green supplier selection and disassembly of products: the impact of parts reliability and product greenness on the recovery network. *J. Manuf. Syst.* 2015;36:76-86. 10.1016/j.jmsy.2015.02.011
- Govindan, K., Rajendran, S., Sarkis, J. y Murugesan, P. (2015). Multi criteria decision making approaches for green supplier evaluation and selection: a literature review. *J. Clean Prod.* 98, 66-83. 10.1016/j.jclepro.2013.06.046
- Grzybowska, K. y Gajdzik, B. (2014). Logistic strategies in purchasing process of metallurgical companies. *Metallurgija* 43(1), pp. 127-130. <https://hrcak.srce.hr/104393>
- Hanlin, R. y Hanlin, Ch. (2012). The view from below: Lock-in and local procurement in the African gold mining sector. *Resources Policy* 37(4), pp. 468-474. 10.1016/j.resourpol.2012.06.005
- Kannan, D., Govindan, K. y Rajendran, S. (2015). Fuzzy Axiomatic Design approach based green supplier selection: a case study from Singapore. *J. Clean Prod.* 96, 194-208. 10.1016/j.jclepro.2013.12.076
- Korinek, J. (2013). Mineral Resource Trade in Chile: Contribution to Development and Policy Implications. OECD Trade Policy Papers, 145, OECD Publishing, Paris. 10.1787/18166873
- Mafakheri, F., Breton, M., Ghoniem, A. (2011). Supplier selection-order allocation: A two-stage multiple criteria dynamic programming approach. *Int. J. Prod. Econ.* 132(1):52-7. 10.1016/j.ijpe.2011.03.005
- Marques-Vieira, L., Laureano Paiva, E., Beheregarai Finger, A., y Teixeira, R. (2012). Trust and Supplier-buyer Relationships: An Arrazola, I. 41 Seguridad Operacional y Logística Aeronáutica Empirical Analysis. *Brazilian Administration Review*, 10(3), pp. 263-280. 10.1590/S1807-76922013005000001

- Mentzer, J. T., Dewitt, W., Keebler, J. y Zacharia, Z. G. (2016). Researchgate.net. t. 10.1002/j.2158-1592.2001.tb00001x
- Pedrosa, A., Blazevic, V., & Jasmand, C. (2015). Logistics innovation development: A micro-level perspective. *International Journal of Physical Distribution & Logistics Management*, 45(4), 313-332. 10.1108/IJPDLM-12-2014-0289
- Shen L., Olfat L., Govindan K., Khodaverdi R., Diabat A. (2013). A fuzzy multi criteria approach for evaluating green supplier's performance in green supply chain with linguistic preferences. *Resour Conserv. Recycl.*, 74, 170-9. 10.1016/j.resconrec.2012.09.006
- Thornton, L.M., Autry, C.W., Gligor, D.M. y Brik, A.B. (2013). does socially responsible supplier selection pay off for customer firms? A cross-cultural comparison. *J. Supply Chain Manage.* 49(3), 66-89. 10.1111/jscm.12014
- Vahidi, F., Torabi, S.A. y Ramezankhani, M. (2018). Sustainable supplier selection and order allocation under operational and disruption risks. *J. Clean Prod.* 174, 1351-65. 10.1016/j.jclepro.2017.11.012
- Wittstruck, D. y Teuteberg, F. (2012). Integrating the concept of sustainability into the partner selection process: a fuzzy-AHP-TOPSIS approach. *Int. J. Logist Syst Manage.* (2):195-226. 10.1504/IJLSM.2012.047221
- Zimmer K, Fröhling M, Schultmann F. (2016). Sustainable supplier management-a review of models supporting sustainable supplier selection, monitoring and development. *Int. J. Prod Res*, 54(5):1412-42. 10.1080/00207543.2015.1079340

Multimetric Analysis of a Simulated Mixed Traffic of Motorcycles and Automobiles: Flow, Energy, CO₂, and Costs

Análisis multimétrico de un tráfico mixto simulado de motocicletas y automóviles: flujo, energía, CO₂ y costos

Fábio Santana Magnani¹, Paulo D'Ávila Garcia Neto², Fernando Wesley Cavalcanti de Araújo³, Alcides Luiz dos Anjos Hora⁴, and Daniel Arraes de Alencar Valença⁵

ABSTRACT

The fleet of developing countries consists of motorcycles and cars. This heterogeneous traffic condition has its advantages and disadvantages, which results in conflicting points of view (e.g., motorcyclists enjoying a higher mobility while car drivers resent their decreased speed). In this paper, we corroborated the notion that traffic evaluation depends on the chosen metric (e.g., vehicle flow, fuel consumption, monthly costs) and the point of view (driver, rider, and policy makers). To this effect, we studied a mixed traffic condition, considering that the vehicle performance is affected by three scales: engine, vehicle, and traffic. We modeled the engine using empirical correlations of power and energy efficiency, the vehicle based on a balance of propulsive and resistive forces, and traffic with a cellular automata model. We simulated 189 traffic conditions and evaluated vehicle flow, average energy consumption, total CO₂ emission of the road, and monthly costs. We also discussed the results from the point of view of the driver, rider, and society. We concluded that the optimal condition depends both on the choice of metric and point of view, and that is not appropriate to use results from homogeneous traffic to analyze heterogeneous traffic conditions, even if both scenarios present the same total vehicle flow.

Keywords: car, motorcycle, traffic, CO₂, costs, cellular automata

RESUMEN

La flota de los países en vías de desarrollo está compuesta por motocicletas y automóviles. Esta condición heterogénea en el tráfico presenta ventajas y desventajas, lo que resulta en puntos de vista conflictivos (por ejemplo, los motociclistas que disfrutan de su mayor movilidad mientras que los conductores de automóviles se resienten con su velocidad disminuida). En este artículo corroboramos la idea de que la evaluación del tráfico depende de la métrica escogida (por ejemplo, flujo de vehículos, consumo de combustible, costos mensuales) y del punto de vista (conductor, motociclista y responsables de formular políticas). Para ello, estudiamos una condición de tráfico mixto, considerando que el rendimiento del vehículo se ve afectado por tres escalas: motor, vehículo y tráfico. Modelamos el motor usando correlaciones empíricas de potencia y eficiencia energética, la del vehículo a través de un equilibrio de fuerzas propulsoras y resistivas, y la del tráfico mediante un modelo de autómatas celulares. Simulamos 189 condiciones de tráfico y evaluamos el flujo de vehículos, el consumo de energía promedio, la emisión total de CO₂ de la vía y los costos mensuales. También discutimos los resultados desde el punto de vista del conductor, el motociclista y la sociedad. Llegamos a la conclusión de que la condición óptima depende tanto de la elección de la métrica como del punto de vista, además de que no es apropiado usar los resultados del tráfico homogéneo para analizar condiciones de tráfico heterogéneo, incluso si ambos escenarios presentan el mismo flujo total de vehículos.

Palabras clave: automóviles, motocicletas, tráfico, CO₂, costos, autómatas celulares

Received: October 23rd, 2019

Accepted: January 7th, 2021

¹Mechanical Engineer, UFSC, Brazil. Dr. Mech. Eng., UFSC, Brazil.

Affiliation: Associate Professor, UFPE, Brazil. E-mail: fabio.magnani@ufpe.br

²Mechatronic Engineer, UFPE, Brazil. M.Sc. Mech. Eng., UFPE, Brazil.

Affiliation: Assistant Professor, IFPE, Brazil. E-mail: pdgneto@gmail.com

³Chemical Engineer, UFPE, Brazil. M.Sc. Mech. Eng., UFPE, Brazil.

Affiliation: Ph.D. Candidate and Chemical Engineer, UFPE, Brazil.

E-mail: fernando.wesley@ufpe.br

⁴Mechanical Engineer, UFPE, Brazil. M.Sc. Mech. Eng., UFPE, Brazil.

Affiliation: Adjunct Lecturer, UFS, Brazil. E-mail: alcidesluiz@gmail.com

⁵Electronics Engineer, UFPE, Brazil. M.Sc. Mech. Eng., UFPE, Brazil.

Affiliation: General Manager, Ameciclo, Brazil. E-mail: dvalenca@gmail.com

How to cite: Magnani, F. S., Garcia Neto, P. D., Araújo, F. W. C., Hora, A. L. A., and Valença D. A. A. (2021). Multimetric Analysis of a Simulated Mixed Traffic of Motorcycles and Automobiles: Flow, Energy, CO₂ and Costs. *Ingeniería e Investigación*, 41(2), e83114. 10.15446/ing.investig.v41n2.83114

Introduction

Most of the fleets of developing countries such as Brazil, Colombia, Malaysia, Pakistan, Thailand, Philippines, and Nigeria consist of cars and motorcycles (WHO, 2015). In those countries, the use of motorcycles is motivated by the poor quality of transit, traffic congestion, and their advantageous cost of acquisition and operation, together with a higher average speed. On the other hand, motorcycle accidents are accountable for economic and social impacts (Koossalapeerom et al., 2019). The conflict between



Attribution 4.0 International (CC BY 4.0) Share - Adapt

advantages and disadvantages addresses the relevance of the metric analyzed when evaluating traffic, which can be an individual one, such as travel time and direct costs; or a collective one, such as indirect costs with road infrastructure and accidents, flow of vehicles, fuel production, and CO₂ emissions (Tranter, 2012).

Traffic is a complex non-linear system affected by internal and external factors (Zegeye, De Schutter, Hellendoorn, Breunese, and Hegyi, 2013) and it depends on instantaneous conditions such as vehicle density and the ratio of different types of vehicles. Homogeneous traffic flow models are unable to faithfully represent mixed traffic conditions, as it happens in developing countries (Agarwal, Zilske, Rao, and Nagel, 2015), in which motorcycles and passenger cars constitute the fleet and are accountable for significant emissions in major cities (Arun, Mahesh, Ramadurai, and Shiva Nagendra, 2017). Several papers claim that total vehicle flow varies for the same total density when mixed traffic occurs, increasing when there are motorcycles on the track, and decreasing when there are trucks, thus reflecting dynamic characteristics (Yang, Qiu, Yu, Sun, and Pu, 2015).

Furthermore, traffic cannot be evaluated only by its vehicle flow. Other metrics such as air pollution, CO₂ emission, direct costs, congestion, cost of changing the infrastructure, and accidents should also be taken into account (Gössling and Choi, 2015). Individual vehicle owners tend to purchase their vehicle based on flexibility and convenience. For motorcycles, low purchase and running costs are essential for the lower income population who acquire them (Koossalapeerom et al., 2019). There is also a growing concern about the global climate change, and CO₂ emissions from the transportation sector is a frequently addressed subject (Ehsani, Ahmadi, and Fadaei, 2016).

This study contributes to the literature with the evaluation and discussion of different metrics such as flow, energy, CO₂, and costs, from the point of view of different stakeholders: drivers, motorcycle riders, and policy makers. Although the results from individual metrics are present in the literature, there is a lack of studies integrating the models and discussing the results. In order to evaluate those metrics, we applied a method that considers three scales: engine, vehicle, and traffic. We studied the engine using an empirical correlation of power and efficiency, the vehicle was studied modeling the propulsive and resistive forces, and the traffic with a cellular automata (CA) model, in which we simulated the traffic for 189 distinct density combinations of cars and motorcycles.

Methodology

The dynamic behavior and energy expenditure of vehicles depend on the engine, powertrain, chassis, traffic, driver/rider driving style, road/weather condition, and traffic laws. In this study, vehicle performance considers the engine, vehicle, and traffic. Other aspects are simplified, such as the driver/rider always trying to reach the maximum speed, the absence of traffic lights and intersections, and the road being a one-way

straight line (Figure 1). This track model is based on the one proposed by Meng, Dai, Dong, and Zhang (2007), and it represents a single-track road for cars, with enough space for motorcycles to split and filter through them.

The engine is modeled by two empirical correlations. The cubic curve of the maximal power ($P_{\max,eng}$), Equation (1), is given by Ni and Henclewood (2008), and it is a function of engine speed (Ω). This model needs the following inputs: peak power, engine speed at peak power (Ω_p) and engine speed at peak torque (Ω_t).

$$P_{\max,eng}(\Omega) = \frac{P_{\max,eng} 3\Omega(\Omega_p - \Omega_t)}{2\Omega_p^2} - \frac{P_{\max,eng} \Omega(\Omega - \Omega_t)^2}{2\Omega_p^2(\Omega_p - \Omega_t)} \quad (1)$$

The efficiency map in Equation (2) is described by Ben-Chaim, Shmerling, and Kuperman (2013), and it reports engine efficiency (η_{eng}) based on the engine's maximum efficiency ($\eta_{eng,m}$), as well as considering factors related to engine speed (μ_r) and throttle usage (μ_a). A detailed explanation regarding the integration of both models can be found in Andrade, Araújo, Santos, and Magnani (2020).

$$\eta_{eng}(\Omega, \alpha) = \eta_{eng,m} \mu_r \mu_a \quad (2)$$

Table 1 lists the parameters employed in this study to represent cars and motorcycles, reproducing characteristics of the usual Brazilian models. In average, Brazilian cars are lighter and less powerful than American and European cars.



Figure 1. Based on Meng et al. (2007).

Source: Authors

Table 1. Engine and vehicle parameters employed in the simulation

Parameter	Car	Motorcycle
Peak power ($P_{\max,eng}$)	53,69 kW	8,53 kW
Engine speed at peak power (Ω_p)	6 250 rpm	8 250 rpm
Engine speed at peak torque (Ω_t)	4 500 rpm	6 000 rpm
Minimum engine speed	900 rpm	1 400 rpm
Max engine efficiency ($\eta_{eng,m}$)		30%
Rolling resistance coefficient (C_R)		0,02
Vehicle + driver mass (m)	1 010 kg	175 kg
Transmission efficiency (η_{trans})		0,95

Source: Authors

The dynamic behavior of the vehicle is based on the balance of propulsive and resistive forces (Equation 3) (Cossalter, 2006; Jazar, 2014). On the left-hand side of the equation

is the inertia, where m is the total mass (vehicle + driver), V is vehicle speed, and t is time. Tractive force considers $\alpha P_{\max, \text{eng}}$ as the actual power of the engine, and η_{trans} is the transmission efficiency. Throttle usage, α , is the ratio between the actual power and the maximum possible power at a specific engine speed. The braking force has β as the braking factor, μ as the friction coefficient between tire and road, and θ as the road grade. The aerodynamic drag force considers the constant k_A (i.e., $1/2\rho AC_D$) with ρ as fluid density (air), A as the frontal area, C_D as the vehicle shape, and W is the wind speed. In the equation, rolling resistance, C_R , is also considered, as well as the gravitational resistance (mg), both related to road grade.

$$m \frac{dV}{dt} = \frac{\alpha P_{\max, \text{eng}} \eta_{\text{trans}}}{V} - \beta \mu mg \cos \theta - k_A (V - W)^2 - C_R mg \cos \theta - mg \sin \theta \quad (3)$$

The finite difference method is used to solve the balance of forces in Equation (3). For every time step t , this Equation is employed to calculate factors α (throttling) and β (braking) to obtain the desired speed (restricted by the traffic condition, i.e., the speed and position of nearby vehicles, as well as pilot preferences, who may always try to reach the maximum allowed speed as soon as it is physically possible). Thus, those calculated α and β values (limited to the range [0-1]) are reused in Equation (3) to determine the actual instantaneous speed V (in opposition to the original desired speed). As α and β are limited (modelling the limits of the acceleration and braking powers), the actual vehicle speed will not always be equal to the desired one. With the evolution of α (related to the throttle opening) during the vehicle movement, it is possible to calculate the vehicle energy expenditure during a time interval Δt using Equation (4):

$$e = \int_0^{\Delta t} \frac{\alpha P_{\max, \text{eng}}}{\eta_{\text{eng}}} dt \quad (4)$$

Modelling the vehicle (Equations 3 and 4) depends on the engine model and the desired speed, which must result from the traffic model. In this study, the employed traffic model is a cellular automata (CA) model based on Meng et al. (2007). This microscopic traffic model considers the individual movement and interactions of each vehicle in heterogeneous traffic conditions. The CA model is discrete for position and time, but, even with its simplicity, it is able to reproduce complex traffic phenomena, e.g. the start-stop waves that appear in congested traffic. The CA model is also known as the NaSch model, an abbreviation from the researchers that first employed the model: Nagel and Schreckenberg, in 1992. This model was successfully improved and is still employed by several researchers (Chen and Wang, 2016; Hua, Yue, Wei, Chen, and Wang, 2020; Lan and Chang, 2005; Lan, Chiou, Lin, and Hsu, 2010; Lv, Song, Liu, and Ma, 2013; (Sean) Qian, Li, Li, Zhang, and Wang, 2017; Ruan, Zhou, Tu, Jin, and Shi, 2017; Yang, Qiu, Yu, Sun, and Pu, 2015; Zeng et al., 2021).

The modeled track has 2 000 cells with a length of 3,75 m each, totaling 7,5 km. Cars have 11 speeds from 0 to 135

km/h, and motorcycles have 5, from 0 to 54 km/h. Cars can travel on the left side of the lane and motorcycles can travel on both sides; therefore, motorcycles can split the lane with cars and other motorcycles. Additionally, this model attempts to represent the motorcycle's notable ability to weave through traffic at lower speeds (Figure 1).

The traffic simulation has five steps, similar to the one proposed by Meng et al. (2007). Those steps are proposed both to manage the lateral and longitudinal movement and to provide safety for the vehicles, avoiding collisions. Table 2 lists the parameters and variables employed during the procedure.

Table 2. Summary of variables and parameters employed in the traffic model

Variable	Description
$v_{\max}^{(m)}$	Maximum velocity of the motorcycle
$v_{\max}^{(c)}$	Maximum velocity of the car
p	Deceleration probability
d	Number of spaces the vehicle look ahead
$x_n^{(m)}$	Position of the nth motorcycle
$x_n^{(c)}$	Position of the nth car
$v_n^{(m)}$	Velocity of the nth motorcycle
$v_n^{(c)}$	Velocity of the nth car
g_+	Gap on the target lane in front of the motorcycle
g_-	Gap on the target lane behind the motorcycle
$d_n^{(c)}$	Gap between the nth car and the vehicle ahead
$d_n^{(m)}$	Gap between the nth motorcycle and the vehicle ahead
$g_{-}^{(mc)}$	Gap between the nth motorcycle and the nearest car behind it
v_{ll}	Velocity of the vehicle on the left lane considering d
v_{rl}	Velocity of the vehicle on the right lane considering d

Source: Based on Meng et al. (2007)

To summarize, motorcycles decide if it is worth changing sides depending on traffic conditions. In the second and third steps, all vehicles accelerate or decelerate respecting the non-collision rule and their maximum speed. In the fourth step, a braking probability is introduced for all vehicles ($p = 0,10$), in an attempt to represent driver's distraction in real traffic. Without this step, all vehicles would move together with the same speed, as train wagons. We consider that the vehicles leaving the track return to the beginning to maintain constant densities (periodical boundary condition). In the final step, all vehicles move as previously evaluated.

Step 1: Verify the lane-changing procedure (if positive, the motorcycle changes lane)

a. From the right to the left lane:

$$\text{if } v_n^{(m)} \leq g_+ \text{ and } g_- \geq v_{\max}^{(c)} \text{ and } v_{rl} \leq v_{ll} \text{ and } v_{rl} \leq v_n^{(m)}$$

b. From the left to the right lane: if $(v_n^{(m)} \leq g_+ \text{ and } g_- \geq v_{\max}^{(m)})$ and $(g_{-}^{mc} = 0 \text{ or } v_{rl} \geq v_n^{(m)} \text{ or } v_{rl} \geq v_{ll})$

Step 2: Acceleration of the vehicles

- a. Cars: $v_n^{(c)} \rightarrow \min(v_n^{(c)} + 1, v_{\max}^{(c)})$
- b. Motorcycles: $v_n^{(m)} \rightarrow \min(v_n^{(m)} + 1, v_{\max}^{(m)})$

Step 3: Deceleration of the vehicles

- a. Cars: $v_n^{(c)} \rightarrow \min(v_n^{(c)}, d_n^{(c)})$
- b. Motorcycles: $v_n^{(m)} \rightarrow \min(v_n^{(m)}, d_n^{(m)})$

Step 4: Randomization (with the probability p)

- a. Cars: $v_n^{(c)} \rightarrow \max(v_n^{(c)} - 1, 0)$
- b. Motorcycles: $v_n^{(m)} \rightarrow \min(v_n^{(m)} - 1, 0)$

Step 5: Movement of the vehicles

- a. Cars: $x_n^{(c)} \rightarrow x_n^{(c)} + v_n^{(c)}$
- b. Motorcycles: $x_n^{(m)} \rightarrow x_n^{(m)} + v_n^{(m)}$

The traffic model receives the inputs from the engine and vehicle models and calculates two important factors in every time step: the speed of every vehicle i , $v_{i,t}^{(m,c)}$ (m = motorcycle, or c = car), and the energy consumed by each vehicle, $e_{i,t}^{(m,c)}$. The densities of the vehicles: motorcycles ($\rho^{(m)}$, [motorcycle/m]) and cars ($\rho^{(c)}$, [car/m]), are calculated through Equation (5):

$$\rho^{(m,c)} = \left(\frac{n^{(m,c)}}{L_{\text{sim}}} \right) \quad (5)$$

where $n^{(m,c)}$ is the number of motorcycles ($n^{(m)}$) or cars ($n^{(c)}$), and L_{sim} is the length of the simulated track (7500 m). A double average is applied to decrease the influence of the initial condition, one on time and other between simulations. Similarly, the average speed of the vehicles, $V^{(m,c)}$ [m/s], Equation (6), is given by the double average among all the vehicles on the track in the last 1000 seconds of 30 simulations.

$$V^{(m,c)} = \left(\frac{\sum v_{i,t}^{(m,c)}}{n^{(m,c)}} \right) \quad (6)$$

The flow of occupants for each type of vehicle, $Q^{(m)}$ [motorcycle occupant/s] and $Q^{(c)}$ [car occupant/s] is given by Equation (7), as the product of the occupancy rate $o^{(m,c)}$ [occupant/vehicle], the vehicle density $\rho^{(m,c)}$, and the average speed $V^{(m,c)}$. In this study, the occupancy rate for cars and motorcycles is considered equal to 1.

$$Q^{(m,c)} = o^{(m,c)} \rho^{(m,c)} V^{(m,c)} \quad (7)$$

The total flow of occupants on the track Θ (occupant/s), Equation (8), is the sum of the flow of motorcycle and car occupants.

$$\Theta = Q^{(m)} + Q^{(c)} \quad (8)$$

In this study, new metrics are introduced in relation to (Meng et al., 2007), which is possible with the use of the engine and vehicle models. The average consumed energy by vehicle by distance, $E^{(m,c)}$ [J/vehicle·m] is given by Equation (9).

$$E^{(m,c)} = \frac{1}{V^{(m,c)}} \left(\frac{\sum e_{i,t}^{(m,c)}}{n^{(m,c)} \Delta t} \right) \quad (9)$$

The total consumed energy, by time and space, Ξ (J/m·s) is given by the sum of the consumption of motorcycles and cars, as provided by Equation (10). From the energy consumption, it is possible to estimate the CO₂ emissions since they are proportional. We consider the combustion of each MJ of C₈H₁₈ to emit 0,07 kg of CO₂.

$$\Xi = E^{(m)} V^{(m)} \rho^{(m)} + E^{(c)} V^{(c)} \rho^{(c)} \quad (10)$$

Table 3. Financial considerations

Parameter	Car	Motorcycle
Engine displacement	1 000 cm ³	125 cm ³
L_m , monthly distance [km]		315 km
λ , monthly interest rate		0,01
κ , number of months		48
S_m , monthly wage [US\$]		580
H_m , monthly hours of work [h]		168
V_p , vehicle acquisition [US\$]	8 200	1 600
V_s , vehicle reselling [US\$]	5 700	1 200

Source: Authors

Table 3 lists the Brazilian financial parameters employed in the calculation of monthly costs, $C^{(m,c)}$ (US\$/occupant·month), Equation (11). In this Equation, the first term on the right-hand side represents the monthly value relative to the vehicle acquisition, V_p . To compare monthly equivalent values, the corrected number of months μ is employed, which is calculated by Equation (12) (Stoecker, 1989) and considers the monthly interest rate λ and the number of financed months κ used in the analysis. The second term of Equation (11) represents the monthly equivalent of the reselling value of the vehicle, V_s . The third term calculates the operational cost with fuel, considering a fuel tariff σ (US\$/J), the monthly traveled distance L_m , and a factor ε to consider taxes, maintenance, and parking. The last term considers time lost in traffic, while taking the monthly wage S_m into account, which the occupant earns for working H_m hours.

$$C^{(m,c)} = \frac{V_p}{o^{(m,c)}\mu} - \frac{V_s}{o^{(m,c)}\mu(1+\lambda)^\kappa} + \frac{(1+\varepsilon)\sigma E^{(m,c)}}{o^{(m,c)}} \frac{L_m}{V^{(m,c)}} + \frac{S_m}{H_m} \frac{L_m}{V^{(m,c)}} \quad (11)$$

$$\mu = \frac{(1+\lambda)^\kappa - 1}{\kappa(1+\lambda)^\kappa} \quad (12)$$

The complete simulation can be summarized in three steps. First, the vehicle model (Equation 3) is linked to the engine model (Equations 1 and 2) to calculate energy consumption (Equation 4) for all possible situations of traffic (constant speed, acceleration, and braking). In the second step, the traffic simulations are performed (five steps procedure), where 189 traffic conditions were studied, with 27 car densities (0 to 130 cars/km, as well as motorcycle densities (0 to 213,3 motorcycles/km). In the last step, the traffic and the energy vectors are united (Figure 2) to calculate vehicle flow (Equation 7), energy consumption (Equation 9) and financial costs (Equation 11) for each traffic condition. Other relevant parameters managed during the simulation process include vehicle gear (j), which is related to the engine speed (ω) based on the simulated vehicle gear ratio, and lane (l). In this study, all equations are described in SI units. However, in figures and tables, numbers are displayed in more usual units.

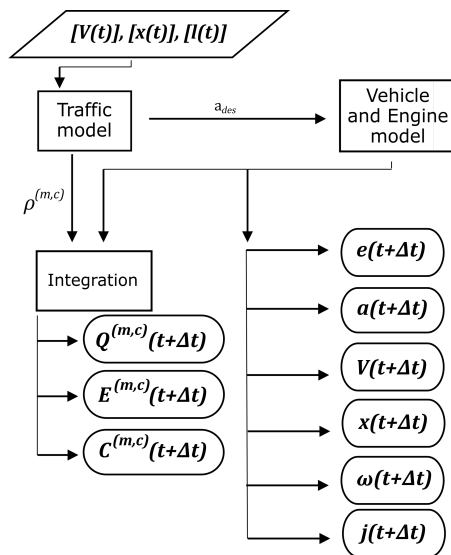


Figure 2. Summary of the Integration between the models.
Source: Authors

Results and discussion

The fundamental diagram of cars (Figure 3) presents the results of our computational algorithm reproducing Meng et al. (2007). Examining the curve for $\rho^{(m)} = 0$ (no motorcycles), as car density $\rho^{(c)}$ increases, car flow (Equation 7) increases up to $\rho^{(c)} = 20$. Car flow decreases from critical density until jam density is $\rho^{(c)} = 130$. This occurs because, under low-density conditions, cars are free to move at the maximum desired

speed. However, as the number of cars increases, their movement is disturbed, thus reducing flow. The maximum car flow is 2 404 cars per hour, and it happens in absence of motorcycles ($\rho^{(m)} = 0$), as well as at a low car density ($\rho^{(c)} = 20$). In addition, examining motorcycle influence on car flow, as the density $\rho^{(m)}$ increases, car flow decreases. This happens because motorcycles can travel on both lanes of the road, which disturbs car flow.

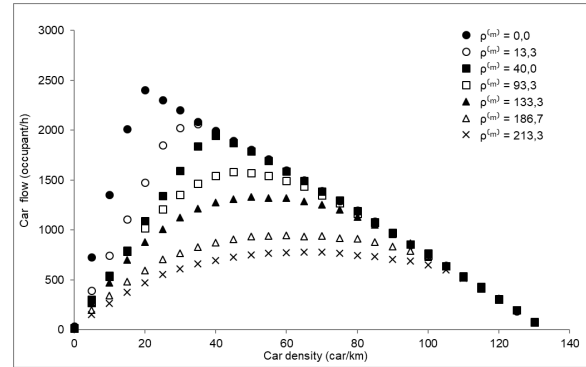


Figure 3. Fundamental diagram for cars.
Source: Authors

Figure 4 displays the total vehicle flow (Equation 8) as a function of the total density. When traffic is seen from this point of view, a higher density of motorcycles increases the total flow of vehicles up to 93,3 motorcycles/km. Figure 3 indicates that motorcycles can increase the passenger flow as high as 78% per lane, from 2 404 (cars only) to 4 291 vehicles per hour (cars and motorcycles).

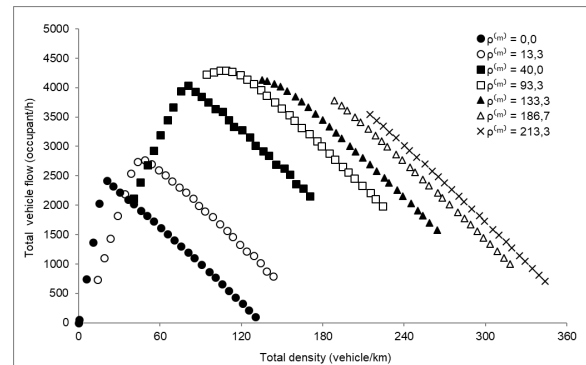


Figure 4. Fundamental diagram for vehicles (cars and motorcycles).
Source: Authors

It is possible to calculate the average speed from Figures 3 and 4 using Equation (7). From the fundamental diagram, it can be seen that the speed for cars is maximum until critical density is reached; and decreases to zero at maximum density, following the pattern described by Daganzo (1994). For motorcycles, when density is low, their average speed is constant for all car densities. As expected, their average speed decreases when motorcycle and car density increases further.

In the next phase of the study, energy consumption Equation (9) is analyzed. Having performed a scale analysis on

Equation (3), it can be concluded that energy consumption is predominantly a function of inertia (re-acceleration) and aerodynamic drag (speed). The force of gravity can also be crucial, but, in this study, we have a null inclination. The behavior of energy consumption for cars per km (Figure 5) is explained by two phenomena: as the density increases, the average speed decreases, hence diminishing drag resistance and increasing the time spent for the same displacement. It also increases the frequency of accelerations.

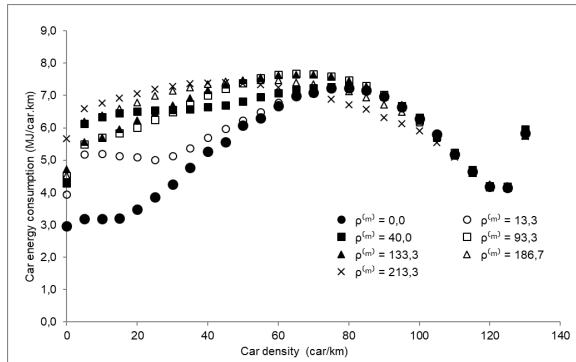


Figure 5. Car energy consumption.

Source: Authors

The increased energy consumption for cars until car density reaches $\rho^c = 80$ is caused by the increase in the frequency of re-accelerations (drag is almost constant). When $\rho^c > 80$, the decrease of car energy consumption occurs both because of the decreasing average speed and decreasing re-acceleration frequency. For very high car densities ($\rho^c > 130$), another increase in consumption is noticed, which is caused by the large amount of time spent in the traffic jam. In Figure 5, it is seen that modifying the motorcycle density for the same car density affects the average car fuel consumption, that is, increasing the motorcycle density also increases the car energy consumption.

Figure 6 presents the results of energy consumption for motorcycles. For lower motorcycle densities ($\rho^m = 13,3$ and $\rho^m = 40,0$), consumption is not affected by cars or other motorcycles in the track. For medium and higher motorcycle densities, consumption qualitatively follows the reacceleration frequency.

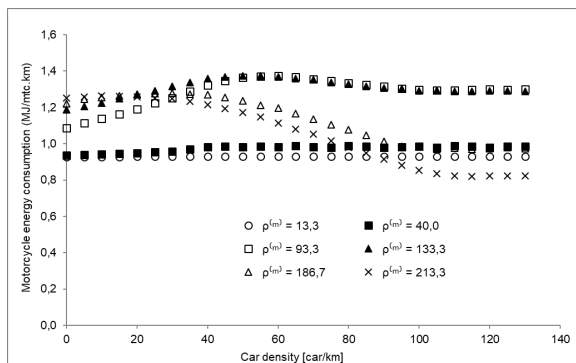


Figure 6. Motorcycle energy consumption.

Source: Authors

While examining the total energy consumption (Figures 7 and 8), some trends can be noticed. First, for the same total flow, it is better to have a higher proportion of motorcycles, since motorcycles are more fuel-economic than cars. Second, in the region of higher total flow ($\rho^m = 93,3$, $0 < \rho^c < 50$), increasing car density can triplicate the energy consumption (consequently, CO₂ emission) with insignificant benefit to the total vehicle flow. Another effect that is worth to discuss, it that for $\rho^m < 93,3$ (Figure 7), an increase in car density tends first to increase the total flow up to its maximum value. On the other hand, for densities $\rho^m > 93,3$ (Figure 8) an increase in the number of cars always decreases the total flow for the same motorcycle density.

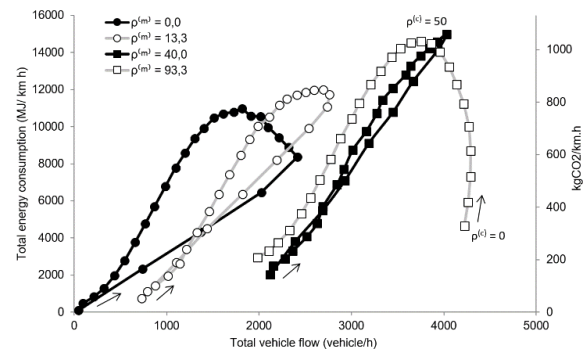


Figure 7. Total energy consumption ($0 \leq \rho^m \leq 93,3$).

Source: Authors

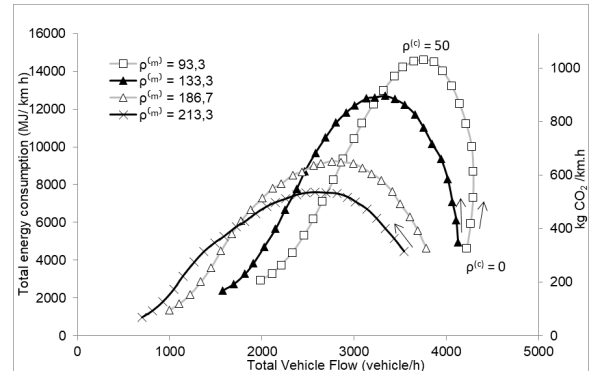


Figure 8. Total energy consumption ($93,3 \leq \rho^m \leq 213,3$).

Source: Authors

The last metric to be analyzed is individual cost, considering the purchase and reselling of the vehicle, fuel consumption, maintenance, taxes, parking, and the cost of the time spent in traffic (Equation 11) according to the financial considerations informed in Table 3. Figure 9 presents the individual costs for cars in function of the densities of cars and motorcycles. It is possible to notice that the higher the number of cars, the higher is the monthly cost. This happens because of two reasons. First, for the same motorcycle density, as car density increases, the average speed decreases, hence increasing the time spent in traffic. The second effect is fuel consumption (Figure 5). From zero to intermediate densities, consumption increases with car density. For higher densities, consumption decreases with car density, but it is not enough

to compensate for the time lost. A higher motorcycle density increases car costs.

Figure 10 presents the individual costs for motorcycles. By comparing them with the monthly car cost (Figure 9), it is possible to notice that the costs for motorcycles are always lower, since they are cheaper and their fuel consumption is lower. Cars do not strongly influence motorcycle costs for low and medium motorcycle densities.

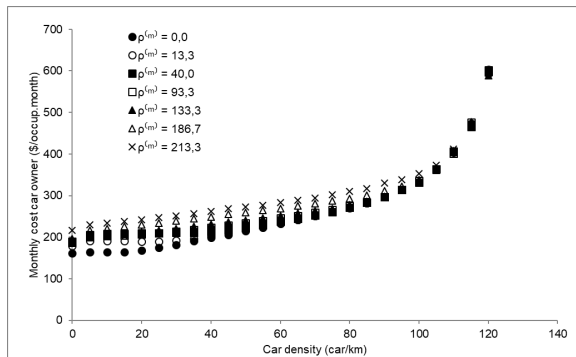


Figure 9. Monthly car cost.

Source: Authors

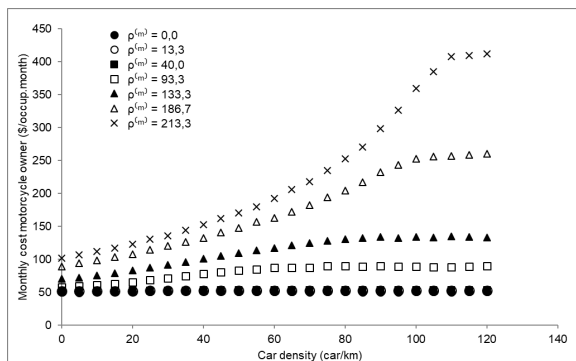


Figure 10. Monthly motorcycle cost.

Source: Authors

Conclusions

According to this analysis, the best scenario can be determined from each point of view. For car drivers, considering the objective of travelling at a higher average speed, the best scenario occurs in the absence of motorcycles ($\rho^m = 0$) and with a low car density ($\rho^c < 20$). Considering individual costs, car drivers would rather have an empty road, without other cars ($\rho^c = 0$) or motorcycles ($\rho^m = 0$). For motorcycle riders, from the point of view of average speed, a low motorcycle density ($\rho^m \leq 40$) would be compelling because they would travel through traffic at maximum speed. The same condition also is interesting financially, since for motorcycles the cost due to lost time is the more relevant.

For society, the metrics should be others. From the point of view of vehicle flow, it would be interesting to have few cars ($\rho^c = 15$) and an intermediate presence

of motorcycles ($\rho^m = 93,3$), with a total density of $\rho = 108,3$, as seen in the fundamental diagram for vehicles (Figure 4). Considering CO₂ emissions as proportional to energy consumption (Figures 7 and 8) for a determined flow, a higher motorcycle proportion is responsible for lower the consumption on the track, since motorcycles are more fuel-economic. This study concludes that, for the same total flow, the relative density of cars and motorcycles can have a huge impact on the total CO₂ emissions of the road.

As hypothesized in the introduction, we conclude that the best traffic conditions depend on the metric (e.g., average speed, flow, CO₂, and costs) and on the point of view (individual or social). It is shown that that the percentage of motorcycles and cars strongly influences the metrics. These results inform that it is not feasible to use results from one study (e.g., richer countries with homogeneous traffic conditions and a small motorcycle fleet) to analyze another one (e.g., developing countries with a mixed traffic of cars of cars and motorcycles), even though both may have the same total flow of vehicles.

Acknowledgements

The authors would like to thank the Coordenação de Aperfeiçoamento de Pessoal de Nível Superior (CAPES) for their scholarship support.

References

- Agarwal, A., Zilske, M., Rao, K. R., and Nagel, K. (2015). An elegant and computationally efficient approach for heterogeneous traffic modelling using agent based simulation. *Procedia Computer Science*, 52(1), 962-967. 10.1016/j.procs.2015.05.173
- Andrade, G. M. S. de, Araújo, F. W. C. de, Santos, M. P. M. de N., and Magnani, F. S. (2020). Standardized Comparison of 40 Local Driving Cycles: Energy and Kinematics. *Energies*, 13(20), 5434. 10.3390/en13205434
- Arun, N. H., Mahesh, S., Ramadurai, G., and Shiva Nagendra, S. M. (2017). Development of driving cycles for passenger cars and motorcycles in Chennai, India. *Sustainable Cities and Society*, 32(March), 508-512. 10.1016/j.scs.2017.05.001
- Ben-Chaim, M., Shmerling, E., and Kuperman, A. (2013). Analytic modeling of vehicle fuel consumption. *Energies*, 6(1), 117-127. 10.3390/en6010117
- Chen, Q. and Wang, Y. (2016). A cellular automata (CA) model for motorized vehicle flows influenced by bicycles along the roadside. *Journal of Advanced Transportation*, 50(6), 949-966. 10.1002/atr.1382
- Cossalter, V. (2006). *Motorcycle Dynamics* (2nd Ed.). Morrisville, NC: LULU.com
- Daganzo, C. F. (1994). The cell transmission model: a dynamic representation of highway traffic consistent with the hydrodynamic theory. *Transportation Research Part B: Methodological*, 28(4), 269-287. 10.1016/0191-2615(94)90002-7

- Ehsani, M., Ahmadi, A., and Fadaei, D. (2016). Modeling of vehicle fuel consumption and carbon dioxide emission in road transport. *Renewable and Sustainable Energy Reviews*, 53, 1638-1648. 10.1016/j.rser.2015.08.062
- Gössling, S. and Choi, A. S. (2015). Transport transitions in Copenhagen: Comparing the cost of cars and bicycles. *Ecological Economics*, 113, 106-113. /10.1016/j.ecolecon.2015.03.006
- Hua, W., Yue, Y., Wei, Z., Chen, J., and Wang, W. (2020). A cellular automata traffic flow model with spatial variation in the cell width. *Physica A: Statistical Mechanics and Its Applications*, 556, 124777. 10.1016/j.physa.2020.124777
- Jazar, R. N. (2014). *Vehicle Dynamics* (2nd Ed.). New York, NY: Springer-Verlag. 10.1007/978-1-4614-8544-5
- Koossalapeerom, T., Satiennam, T., Satiennam, W., Leelapatra, W., Seedam, A., and Rakpukdee, T. (2019). Comparative study of real-world driving cycles, energy consumption, and CO₂ emissions of electric and gasoline motorcycles driving in a congested urban corridor. *Sustainable Cities and Society*, 45(September 2018). 10.1016/j.scs.2018.12.031
- Lan, L. W. and Chang, C.-W. (2005). Inhomogeneous cellular automata modeling for mixed traffic with cars and motorcycles. *Journal of Advanced Transportation*, 39(3), 323-349. 10.1002/atr.5670390307
- Lan, L. W., Chiou, Y. C., Lin, Z. S., and Hsu, C. C. (2010). Cellular automaton simulations for mixed traffic with erratic motorcycles' behaviours. *Physica A: Statistical Mechanics and Its Applications*, 389(10), 2077-2089. 10.1016/j.physa.2010.01.028
- Lv, W., Song, W. G., Liu, X. D., and Ma, J. (2013). A microscopic lane changing process model for multilane traffic. *Physica A: Statistical Mechanics and Its Applications*, 392(5), 1142-1152. 10.1016/j.physa.2012.11.012
- Meng, J., Dai, S., Dong, L., and Zhang, J. (2007). Cellular automaton model for mixed traffic flow with motorcycles. *Physica A: Statistical Mechanics and Its Applications*, 380, 470-480. 10.1016/j.physa.2007.02.091
- Nagel, K. and Schreckenberg, M. (1992). A cellular automaton model for freeway traffic. *Journal de Physique*, 2, 2221-2229. 10.1051/jp1:1992277
- Ni, D. and Henclewood, D. (2008). Simple engine models for VII-enabled in-vehicle applications. *IEEE Transactions on Vehicular Technology*, 57(5), 2695-2702. 10.1109/TVT.2008.917229
- Qian, Z., Li, J., Li, X., Zhang, M., and Wang, H. (2017). Modeling heterogeneous traffic flow: A pragmatic approach. *Transportation Research Part B: Methodological*, 99, 183-204. 10.1016/j.trb.2017.01.011
- Ruan, X., Zhou, J., Tu, H., Jin, Z., and Shi, X. (2017). An improved cellular automaton with axis information for microscopic traffic simulation. *Transportation Research Part C: Emerging Technologies*, 78, 63-77. 10.1016/j.trc.2017.02.023
- Stoecker, W. F. (1989). *Design of Thermal Systems* (3rd Ed.). New York, NY: McGraw-Hill.
- Tranter, P. (2012). Effective Speed: Cycling Because It's "Faster." In J. Pucher and R. Buehler (Eds.) *City Cycling (Urban and Industrial Environments)*. Boston, MA: MIT Press.
- WHO (World Health Organization). (2015). *Global status report on road safety*. http://apps.who.int/iris/bitstream/10665/189242/1/9789241565066_eng.pdf
- Yang, D., Qiu, X., Yu, D., Sun, R., and Pu, Y. (2015). A cellular automata model for car-truck heterogeneous traffic flow considering the car-truck following combination effect. *Physica A: Statistical Mechanics and Its Applications*, 424, 62-72. 10.1016/j.physa.2014.12.020
- Zegeye, S. K., De Schutter, B., Hellendoorn, J., Breunese, E. A., and Hegyi, A. (2013). Integrated macroscopic traffic flow, emission, and fuel consumption model for control purposes. *Transportation Research Part C: Emerging Technologies*, 31, 158-171. 10.1016/j.trc.2013.01.002
- Zeng, J., Qian, Y., Mi, P., Zhang, C., Yin, F., Zhu, L., and Xu, D. (2021). Freeway traffic flow cellular automata model based on mean velocity feedback. *Physica A: Statistical Mechanics and its Applications*, 562, 125387. 10.1016/j.physa.2020.125387

The Gender Gap in Engineering Programs in Colombia

La brecha de género en los programas de ingeniería en Colombia

Nancy E. Hamid-Betancur¹ and María C. Torres-Madronero²

ABSTRACT

In Colombia, engineering is an unattractive field for women. As of 2018, 63,7% of undergraduate engineering graduates were men, and only 36,3% were women. This gap has not changed significantly between 2001 and 2018. This paper analyzes the gap between women and men who obtain undergraduate or graduate engineering degrees in Colombia. The analysis is based on data from the Labor Observatory for Education (OLE) and the National Information System for Higher Education (SNIES) between 2001 to 2018, and it is presented according to degree levels (undergraduate, master and Ph.D.), regions, specific fields of engineering, and salary. The data show a clear difference between the number of women and men graduating from engineering programs at all levels. This gap disappears in programs related to environmental, biomedical, and chemical engineering, where more than 50% of the graduates are women; but, in programs such as electrical, electronic, and mechanical engineering, the gap is more critical, with less than 20% of women's representation. To propose public policies or national programs to improve this situation, this paper also presents a review of international initiatives that have succeeded in improving the representation of women in engineering programs.

Keywords: gender gap, engineering, undergraduate program, graduate program

RESUMEN

En Colombia, la ingeniería es un campo poco atractivo para las mujeres. Para 2018, 63,7 % de los egresados de los programas de pregrado en ingeniería eran hombres y solamente el 36,3 % eran mujeres. Esta brecha no ha cambiado significativamente entre el 2001 y el 2018. Este artículo analiza la brecha entre mujeres y hombres graduados de programas de ingeniería tanto a nivel de pregrado como posgrado en Colombia. El análisis se basa en datos disponibles en el Observatorio Laboral para la Educación (OLE) y el Sistema Nacional de Información de Educación Superior (SNIES) entre 2001 y 2018, y se presenta de acuerdo con el nivel de formación (pregrado, maestría y doctorado), región, campo específico de ingeniería y salario. Los datos muestran una clara diferencia entre el número de mujeres y hombres graduados de programas de ingeniería en todos los niveles. Esta brecha desaparece en programas relacionados con las ingenierías ambiental, biomédica y química, donde más del 50 % de los graduados son mujeres; pero, en programas como ingeniería eléctrica, electrónica y mecánica, esta brecha es más crítica, con menos del 20 % de representación de mujeres. Para proponer políticas públicas o programas nacionales que ayuden a mejorar esta situación, este artículo también presenta una revisión de iniciativas internacionales que han logrado mejorar la representación de mujeres en programas de ingeniería.

Palabras clave: brecha de género, ingeniería, pregrado, posgrado

Received: April 29th, 2020

Accepted: December 15th, 2020

Introduction

Gender equality is considered a keystone for prosperous and modern economies, according to the Organization for Economic Cooperation and Development (OECD). In 2010, the OECD created the Gender Initiative to promote gender equality in education, employment, and entrepreneurship among its members. This initiative aims to reduce the underrepresentation of women in STEM (Science, Technology, Engineering, and Mathematics), which is evident in member countries, where only 18% of new engineering students are women (OECD, 2017). This institution acknowledges the need for policies and initiatives to encourage young women to pursue STEM careers, as well as initiatives to build confidence in their mathematical skills. Colombia became a member in 2018, so it is necessary to align its policies with OECD standards. However, in order to propose new policies, it is necessary to be aware of the real situation of women in STEM programs in Colombia. To this end, this paper presents an analysis based on the statistics of the Labor

Observatory for Education (OLE) and the National Information System for Higher Education (SNIES) regarding women who have graduated from engineering programs between 2001 and 2018.

Previous works have shown the gap in engineering degree programs in Colombia. Quintero (2016) presented a study

¹Systems Engineering, Universidad San Buenaventura, Colombia. MSc. Management of educational technology, Universidad de Santander, Colombia. Affiliation: Adjunct professor, Instituto Tecnológico Metropolitano, Colombia. E-mail: nancyhamid@itm.edu.co

²Electronics Engineer, Universidad Nacional de Colombia, Colombia. M.Sc. Electrical Engineering, University of Puerto Rico, Puerto Rico. Ph.D. Computing and Information Sciences and Engineering, University of Puerto Rico, Puerto Rico. Affiliation: Associate Professor, Instituto Tecnológico Metropolitano, Colombia. E-mail: mariatorres@itm.edu.co

How to cite: Hamid, N. E. and Torres-Madronero, M. C. (2020). The Gender Gap in Engineering Programs in Colombia. *Ingeniería e Investigación*, 41(2), e86758. 10.15446/ing.investig.v41n2.86758



Attribution 4.0 International (CC BY 4.0) Share - Adapt

about the exclusion of women at Universidad Nacional de Colombia. This study highlighted that the largest public university of Colombia had only 37% of women students in 2017, women's participation in STEM careers was under 30% during that year, and the rate of absorption of men duplicates that of women. Similar gaps were identified in math programs in Colombia (Gonzalez-Gutierrez, Sepulveda-Delgado, and Espejo-Lozado, 2018). However, this is a worldwide reality (García-Holgado *et al.*, 2020); women hold only 26% of jobs in technology companies, and this percentage is as low as 28,8% in science. In Latin America, statistics are alarming; for example, in 2015, only 17% of engineering researchers were women in El Salvador, 17% in Honduras, 30% in Costa Rica, 39% in Paraguay, 40% in Venezuela, 31% in Uruguay, 19% in Chile, 25% in Colombia, 19% in Panama, and 25% in Bolivia (Arredondo *et al.*, 2019). Several studies described the gender gap in STEM programs around the world. In the U.S., there is one woman for every four men enrolled in physics, engineering, and computer science degrees (Cimpian, Kim, and McDermott, 2020). In France, the number of women in STEM programs in higher education is only 30% (Breda, Grenet, Monnet, and Van Effenterre, 2020). Finland has a 12,39% of women students in STEM programs (García-Holgado *et al.*, 2020). In contrast, countries such as Spain have similar enrollment indexes to South America, with 33% of women in STEM programs (García-Holgado *et al.*, 2020). In countries such as the U.S., the gender gap is accentuated in the workplace, where women earn less than men in STEM-related occupations (Sterling *et al.*, 2020).

There are proposals to reduce the gender gap in STEM. For instance, the joint effort between educational institutions, the industry, and the government to create national policies oriented towards supporting women in STEM areas shows promising results (García-Holgado *et al.*, 2020). The exposure of girls at an early age to role models encourages selecting STEM careers and is recognized as an essential step to reduce the gender gap (Breda *et al.*, 2020). However, there is still a long way to go in this regard, considering the gender gaps between teachers and researchers in the STEM areas (Rodríguez-Rodríguez, Rodríguez, Ramallo-González, and Elizondo-Moreno, 2020). It should be noted that women's performance in STEM areas is no longer considered a factor in the existing gender gap. Previous studies showed that women in these areas could perform equally or better than men (Rodríguez-Rodríguez *et al.*, 2020), and that women with higher performance at the schools are the ones who select STEM as a career path (Cimpian *et al.*, 2020).

In this paper, analysis of the gender gap in engineering programs in Colombia for three levels: undergraduate, master, and Ph.D., as well as an analysis according to regions, specific fields of engineering, and salary. This analysis is based on statistical data from the OLE and SNIES between 2001 and 2018. Finally, we review international programs and initiatives to reduce the gender gap in engineering programs, highlighting possible solutions to reduce it in our country.

Analysis of gender gap

The data were obtained from the National Information System for Higher Education (SNIES, 2019) and the Labor Observatory for Education (OLE, 2019), both from the information system of the Colombian Ministry of Education. The data of graduates is available for the period between 2001 and 2018, and the salary information is available until 2016. In this paper, the variables used for the analysis are: (1) number of graduates from undergraduate programs according to gender and graduation year, (2) number of graduates from master's and Ph.D. programs according to gender and graduation year, (3) number of graduates according their regional jurisdictions and graduation year, (4) programs with higher preference according to gender, and (5) salary according to gender. The following sections present each variable and its respective analysis.

Analysis according to degree level

We analyzed the rate of women and men graduates from engineering programs at three levels: undergraduate, master, and Ph.D. We included only the five-year undergraduate or so-called 'professional' programs from public and private higher education institutions. Programs were obtained from 81 universities, 2 professional technical institutes, 6 technological institutes, and 64 universities and related institutions. Table 1 presents the percentages of men and women between 2001-2018 for the different levels. Figure 1 compares the number of women and men graduates from engineering undergraduate programs between 2001-2018 in Colombia. It is clear in this Figure that the ratio between women and men had no substantial changes during these years. The graduates from engineering programs were 63,4% men and 36,6% women in 2001. Likewise, 63,7% of graduates were men, and 36,3% were women in 2018. Figure 2 presents the number of graduates according to gender for master's degree programs. A more significant number of men also graduated from such programs than women. The percentages match those observed for undergraduate programs: for 2001, 30,0% of graduates were women, and, in 2018, this percentage was 32,3%. Figure 3 presents the data for graduates from Ph.D. programs. In this case, we can see a significant increase in women graduates while comparing 2001 and 2018, due to the fact that, in the former, the country's first doctorates were still being consolidated. In this year, 100% of Ph.D. graduates were men. It was only until 2004 that the first women graduated from doctoral programs. As of 2018, the rate of Ph.D. women graduates was 27,5%.

Several countries present similar percentages of women enrolled in engineering programs. For example, women amounted to 31% of the undergraduate and graduate student population in Chile's technological programs (Gándara and Silva, 2016). In the U.S., women account for 38% of the bachelor's degree in 2018 (Charlesworth and Banaji, 2019). Several studies have sought to establish why this gap in STEM still exists. The most frequent reasons are associated with socio-cultural factors (Charlesworth and Banaji, 2019; Barone

and Assirelli, 2020). For example, studies have shown that women find it more difficult to obtain opportunities or to be successful in STEM-related areas. In addition, stereotypes that associate science and mathematics more with men than with women are also highlighted. Furthermore, other studies have found that women do not choose STEM careers because there are not enough mentors or role models to generate an interest in these fields during their early years (Botella, Rueda, López-Iñesta, and Marzal, 2019).

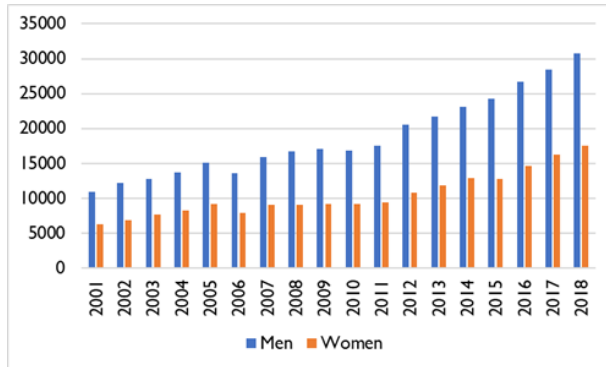


Figure 1. Men vs. women graduates from undergraduate engineering degree program between 2001 and 2018 in Colombia.
Source: SNIES (2019)

Table 1. Percentages of women and men graduates from engineering degree programs between 2001 and 2018 in Colombia

Year	Undergraduate		Master's degree		Ph.D.	
	Men	Women	Men	Women	Men	Women
2001	63,4	36,6	70,0	30,0	100,0	0
2002	64,0	36,0	72,0	28,0	100,0	0
2003	62,7	37,3	72,4	27,6	100,0	0
2004	62,4	37,6	75,1	24,9	84,6	15,4
2005	62,3	37,7	69,4	30,6	87,5	12,5
2006	63,1	36,9	66,8	33,2	70,0	30,0
2007	63,8	36,2	70,6	29,4	91,7	8,3
2008	64,8	35,2	68,9	31,1	66,7	33,3
2009	65,0	35,0	66,7	33,3	85,0	15,0
2010	64,8	35,2	68,3	31,7	80,0	20,0
2011	65,2	34,8	69,8	30,2	77,3	22,7
2012	65,4	34,6	67,2	32,8	72,9	27,1
2013	64,7	35,3	70,0	30,0	81,3	18,7
2014	64,3	35,7	68,5	31,5	66,0	34,0
2015	65,6	34,4	66,4	33,6	68,0	32,0
2016	64,5	35,5	66,5	33,5	66,2	33,8
2017	63,7	36,3	67,0	33,0	71,5	28,5
2018	63,7	36,3	67,7	32,3	72,5	27,5

Source: SNIES (2019)

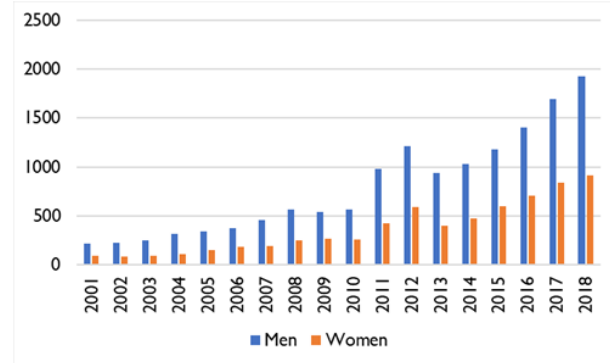


Figure 2. Men vs. women graduates from master's programs in engineering between 2001 and 2018 in Colombia.

Source: SNIES (2019)

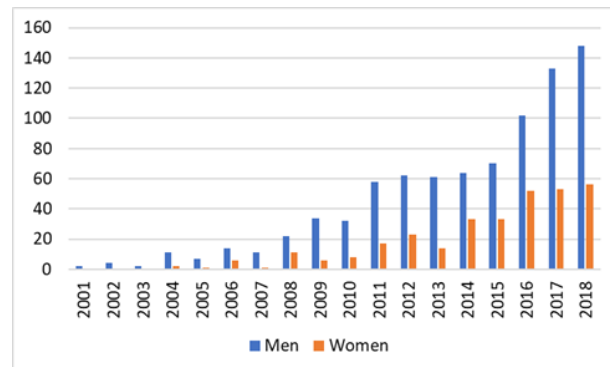


Figure 3. Men vs. women graduates from Ph.D. programs in engineering between 2001 and 2018 in Colombia.

Source: SNIES (2019)

Analysis according to region

In addition to the degree-level analysis, we analyzed the graduation rates of men and women from undergraduate programs according to region. For this, we considered data regarding graduates from engineering programs in Antioquia, Atlántico, Bogotá D.C., Caldas, Santander, and Valle del Cauca. These regions were selected because they have the greatest number of students and higher education institutions. Figure 4 presents the rate of women graduates from undergraduate engineering programs in the selected regions. Women's representation in undergraduate engineering programs ranges from 29% to 45%, depending on the region and the year. For Bogotá D.C., women represented 31% to 35% of graduates between 2001 and 2018, which is similar to the national rate. Atlántico, Caldas, and Valle del Cauca presented a decreasing number of women who earned an engineering degree. In 2005, 41% of engineering graduates were women in Atlántico. However, in 2018, this percentage decreased to 33%.

Similarly, 42% of graduates in Caldas were women in 2003, but there were only 37% in 2018. In Valle del Cauca, the rate of women graduates reached its peak in 2002 with 41%, and women's representation decreased to 33% for 2018. As seen in Figure 4, Santander and Antioquia reported better percentages of women graduates from engineering degree programs. In Santander, 43% of graduates were

women in 2005 and 2017, and 41% in 2018. Although the representation of women engineering graduates declined between 2001 and 2018, it remained above 37% in Antioquia during this period.

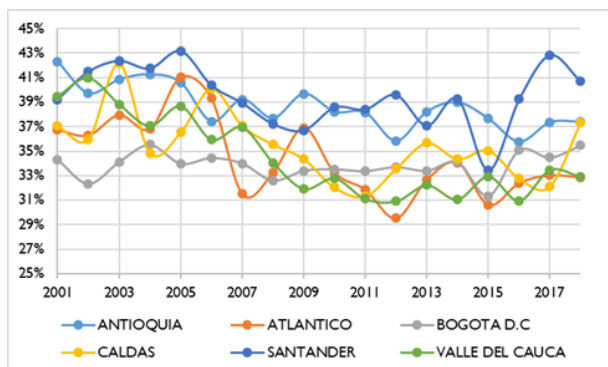


Figure 4. Rate of women graduates from undergraduate programs in engineering between 2001 and 2018 in Antioquia, Atlántico, Bogotá D.C., Caldas, Santander, and Valle del Cauca.

Source: SNIES (2019)

Analysis according to field of engineering

In Colombia, engineering programs are categorized into fourteen areas that encompass the different denominations of undergraduate and postgraduate programs according to the field of study. Using the data from SNIES (2019), we studied the gender gap according to these areas, which is shown in Figure 5. Most women who graduated from engineering programs in Colombia obtained a degree related to industrial engineering (30%). Careers related to systems engineering and telematics graduated 18% of women in the country. 11 percent of women graduated from environmental or sanitary engineering, and 10% from civil engineering graduated. Programs related to agro-industrial and food engineering, electronics and telecommunications engineering, management engineering, and chemical engineering graduated 5% of women each between 2001 and 2018. The lowest proportions of women who earned an engineering degree in Colombia graduated from programs such as agronomy and livestock engineering (2%), mines-metallurgy and mechanical engineering (2%), agricultural and forestry engineering (2%), electrical engineering (1%), and biomedical engineering (1%). Figure 6 presents the proportion of women vs. that of men in each field of knowledge. More women than men graduated from programs like management, environmental, sanitary, biomedical, agro-industrial, food, and chemical engineering programs. A similar number of women and men graduated from programs such as industrial, agricultural, and forestry engineering. However, the gender gap increases in programs like agronomy, livestock, mines, metallurgy, system, telematics, and civil engineering, where the rate of women graduates ranges between 30% and 38%. The worst gender gap is seen in programs related to electronics, telecommunications, electrical, and mechanic engineering where women represent only between 10% and 18% of graduates. These preference by some engineering fields was studied in the literature

(Cheryan, Ziegler, Montoya, and Jiang, 2017; Blosser, 2017). Cheryan *et al.* (2017) describes three reasons for the lower representation of women in computer science and engineering compared to biology and agricultural science: masculine culture, insufficient early experience, and gender gaps in self-efficacy. On the other hand, Blosser (2017) argues that engineering programs related with industry and biology required communication and social skills that attract more women than men. Instead, mechanical, electrical, and electronic engineering are fields where men dominate the workplace, thus decreasing the interest of women students. Similar to the overall gap of women in engineering, the selection of a specific field is related to sociocultural factors and stereotypes.

Analysis of salary according to gender

Another variable studied in this paper is the salary of engineering graduates according to gender. The data was obtained from OLE and was only available from 2007 to 2016. For the comparison, we computed the percentages that represent the difference between the salaries obtained by both women and men. Table 2 presents these percentages, where rows represent the year of graduation, and columns the analyzed years. According to OLE data, there are wage differences between men and women. The average wage gap between men and women between 2007 and 2016 is 15%. These percentage is lower than in other countries. For instance, women in the US earn 21% less than men in STEM careers (Charlesworth and Banaji, 2019). From the table, we can see that the difference in salary between men and women has been decreasing. For example, a woman who graduated in 2001 received 19% less salary than a man in 2007, and 20% less salary in 2016. However, a woman graduated in 2016 had an entry salary 13% lower than a man. This may indicate an improvement in the wage gap at the beginning of the work life, but there is still a need for strategies to address the issue.

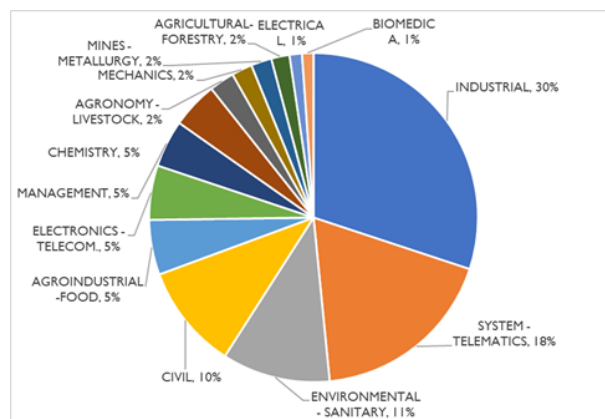


Figure 5. Percentage of women graduated from undergraduate programs in engineering between 2001 and 2018 according to field of engineering.

Source: OLE (2019)

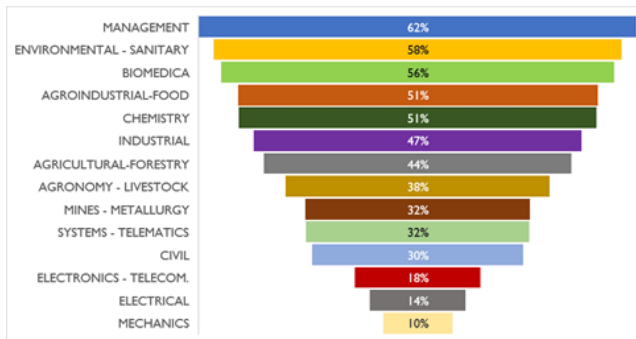


Figure 6. Rate of women vs. men graduates from undergraduate programs in engineering between 2001 and 2018 according to field of engineering.

Source: OLE (2019)

Table 2. Gap between salaries for male and female graduated engineering

Year	2007	2008	2009	2010	2011	2012	2013	2014	2015	2016
2001	19%	20%	22%	21%	22%	22%	20%	22%	21%	20%
2002	18%	20%	20%	24%	23%	25%	24%	25%	23%	24%
2003	17%	19%	18%	20%	19%	20%	19%	19%	19%	15%
2004	13%	16%	14%	18%	19%	19%	20%	20%	19%	19%
2005	14%	14%	12%	14%	15%	16%	16%	17%	18%	17%
2006	11%	14%	11%	15%	15%	17%	15%	17%	16%	17%
2007	15%	13%	10%	10%	10%	11%	13%	14%	15%	15%
2008		13%	12%	14%	13%	13%	14%	16%	18%	17%
2009			11%	11%	9%	10%	9%	13%	14%	14%
2010				12%	12%	11%	11%	11%	15%	13%
2011					9%	9%	10%	10%	11%	9%
2012						12%	11%	12%	14%	12%
2013							13%	12%	12%	14%
2014								15%	14%	12%
2015									16%	11%
2016										13%

Note: Note: Rows correspond to the graduation year.

Source: OLE (2019)

Review of initiative to reduce the gender gap in engineering

The low representation of women in engineering programs is not a phenomenon exclusive to Colombia. At an international level, different initiatives and programs can be found that promote this career path for women. In several studies, the lack of awareness about gender bias at different levels is highlighted. Women, teachers, and mentors often ignore this gap (Charlesworth and Banaji, 2019). In addition, there are several socio-cultural factors that influence the selection of careers among women. The perception that STEM environments are for men (Charlesworth and Banaji, 2019), and that women do not have the same intellectual capacity as men (although studies have shown that this

difference does not exist), are stereotypes that maintain the gender gap in engineering.

Studies suggested that the interest in engineering emerges during the early years (Charlesworth and Banaji, 2019). Therefore, an early orientation in high school can increase the interest in specific fields (Barone and Assirelli, 2020). This approach was applied in several initiatives oriented towards encouraging women to pursue STEM careers through the promotion of engineering programs. Examples of these initiatives are the University of Granada's Technological Campus for Girls, Women TechMaker, Tech & Ladies, IGNITE (Inspiring Girls Now In Technology Evolution), and Engineer Your Life, which are events for girls in their last years of school (Paderewski-Rodríguez *et al.*, 2017). Other initiatives are oriented to develop STEM skills in the early years. For example, Girls Who Code (www.girlswhocode.org) promotes computer science careers in girls through after-school clubs to teach coding, summer immersion in tech jobs, and the creation of communities with other women in college campus. Similarly, Techbridge Girls (www.techbridgegirls.com) promotes all STEM fields in girls through after-school activities.

Other programs are oriented towards improving the performance of women in STEM, based on early mentorship by a faculty researcher. For instance, the AEMES (Achieving Excellence in Mathematics, Engineering, and Science) program of the Smith College in the US (Katz *et al.*, 2017) focuses on the recruitment and permanence of under-represented minorities and first-generation college students. Katz *et al.* (2017) reported that women AEMES students achieved a higher GPA (grade point average) and increased their participation in natural science research.

An interesting case of women enrolled in engineering programs is presented by the United Arab Emirates and Qatar, with 44,5% and 44% of women's representation in engineering programs in 2017, respectively (Ainane, Bouabid, and El Sökkary, 2019). The study presented by Ainane, *et al.* (2019) showed that the main motivations for the increasing interest of women in engineering programs are related with the ideal to serve their community and make their families proud.

Conclusions

The gender gap in engineering and in all STEM areas is a worldwide problem. Colombia is not alien to this phenomenon, which is a consequence of several socio-cultural factors and stereotypes. This article presents the current state of this gap in engineering programs in the country at three levels (undergraduate, master's and doctoral), based on the official numbers of the National Ministry of Education.

The obtained results are alarming. Only 36% of students who graduated from undergraduate engineering programs were women in 2018. The percentages of women graduating from master's and doctoral programs are very similar. However, what is most alarming is that this percentage has not changed significantly since 2001. This indicates a lack of awareness

about the gender gap, as well as a lack of public policies that promote the training of women in engineering in the country. Similar gaps are found at the regional level, but they are wider in some areas such as Bogotá D.C. and Valle del Cauca.

It is also clear that the gender gap in engineering also depends on the field of knowledge. Women represent more than 50% of students in programs such as administrative, environmental, biomedical, chemical, agro-industrial, food, and industrial engineering. However, the gap is drastically increased in careers such as mechanics, electricity, electronics, and telecommunications, where women are less than 20%. This is especially critical when considering the country's policies aimed at promoting 4.0 Industries, where these careers very important.

At a global level and in previous studies, we can find indications to improve this reality. On one hand, it is necessary to implement programs that promote engineering in the early school years, increasing the interest in areas like robotics and programming, as well as educating to eliminate cultural stereotypes. On the other hand, it is necessary to develop mentoring programs that allow girls and teenagers to meet women engineers, thus creating communities that allow women to be the roles to follow. Finally, there is a need for programs that finance female students in engineering careers at all levels.

We must acknowledge that Colombia is far from closing the gender gap. First, it is necessary to recognize that there is a bias, and that all social actors (e.g., schools, universities, teachers, ministry) must propose programs and initiatives to address this issue.

Finally, it is necessary to highlight some of the limitations of this study. The results and analysis presented in this article are limited to the statistical data available in the Ministry of Education databases. To propose programs and strategies to close gaps in Colombia, it is necessary to study the causes and factors that influence the selection of careers for women in the country. Regarding the identification of successful international programs, the analysis can be extended with a systematic review of programs in other countries, which will allow the identification of lessons learned to support the design of a strategy for our country.

References

- Ainane, S., Bouabid, A., and El Sokkary, W. (2019). Factors that influence the high percentage of women enrolled in engineering in the UAE and preparing for careers in the oil and gas industry. *Global Journal of Engineering Education*, 21(1), 62-68. <http://www.wiete.com.au/journals/GJEE/Publish/vol21no1/08-Bouabid-A.pdf>
- Arredondo Trapero, F. G., Vázquez Parra, J. C., and Velázquez Sánchez, L. M. (2019). STEM y brecha de género en Latinoamérica. *Revista de El Colegio de San Luis*, 9(18), 137-158. 10.21696/rcsl9182019947
- Barone, C. and Assirelli, G. (2020). Gender segregation in higher education: an empirical test of seven explanations. *Higher Education*, 79(1), 55-78. 10.1007/s10734-019-00396-2
- Betancur, N. E. H. and Torres-Madronero, M. C. (2015). Acreditación de programas en ingeniería en la región: Análisis comparativo. *Revista Educación en Ingeniería*, 10(19), 80-89. <https://educacioneningenieria.org/index.php/edi/article/view/522>
- Blosser, E. (2017). Gender segregation across engineering majors: How engineering professors understand women's underrepresentation in undergraduate engineering. *Engineering Studies*, 9(1), 24-44. 10.1080/19378629.2017.1311902
- Botella, C., Rueda, S., López-Iñesta, E., and Marzal, P. (2019). Gender diversity in STEM disciplines: A multiple factor problem. *Entropy*, 21(1), 30. 10.3390/e21010030
- Breda, T., Grenet, J., Monnet, M., and Van Effenterre, C. (2020). Do female role models reduce the gender gap in science? Evidence from French high schools (No. 13163). Bonn, Germany: Institute of Labor Economics (IZA). <http://ftp.iza.org/dp13163.png>
- Buse, K.R. and Bilimoria, D. (2014). Personal vision: enhancing work engagement and the retention of women in the engineering profession. *Frontiers in Psychology*, 5, 1-13. 10.3389/fpsyg.2014.01400
- Charlesworth, T. E. and Banaji, M. R. (2019). Gender in Science, Technology, Engineering, and Mathematics: Issues, Causes, Solutions. *Journal of Neuroscience*, 39(37), 7228-7243. 10.1523/JNEUROSCI.0475-18.2019
- Cheryan, S., Ziegler, S. A., Montoya, A. K., and Jiang, L. (2017). Why are some STEM fields more gender balanced than others? *Psychological Bulletin*, 143(1), 1-35. 10.1037/bul0000052
- Cimpian, J. R., Kim, T. H., and McDermott, Z. T. (2020). Understanding persistent gender gaps in STEM. *Science*, 368(6497), 1317-1319. 10.1126/science.aba7377
- Gándara, F. and Silva, M. (2016). Understanding the gender gap in science and engineering: Evidence from the Chilean college admissions tests. *International Journal of Science and Mathematics Education*, 14(6), 1079-1092. 10.1007/s10763-015-9637-2
- García-Holgado, A., Mena Marcos, J. J., García Peñalvo, F. J., Pascual, J., Heikkinen, M., Harmoinen, S., ... and Amores, L. (2020). Gender equality in STEM programs: a proposal to analyse the situation of a university about the gender gap. In IEEE (Eds.) 2020 IEEE Global Engineering Education Conference (EDUCON) (pp. 1824-1830). Piscataway, NJ: IEEE. 10.1109/EDUCON45650.2020.9125326
- González-Gutiérrez, N. R., Sepúlveda-Delgado, O., and Espejo-Lozado, R.L. (2018). Formación matemática en Colombia: una mirada desde una perspectiva de género. *Revista de Investigación, Desarrollo, e Innovación*, 8, 251-264. 10.19053/20278306.v8.n2.2018.7519
- Katz, L. A., Aloisio, K. M., Horton, N. J., Ly, M., Pruss, S., Queeney, K., Rowen, C., and DiBartolo, P. M. (2017). A program aimed toward inclusive excellence for underrepresented undergraduate women in the sciences. *CBE—Life Sciences Education*, 16(1). 10.1187/cbe.16-01-0029

- Mahajan, P. (2017). Engineering a Woman: Marketing Opportunities and Challenges. *The Turkish Online Journal of Educational Technology*, 2017(Special Issue for INTE 2017), 1050-1066. https://www.researchgate.net/publication/326674962_Engineering_a_Woman_Marketing_Opportunities_and_Challenges
- OECD (2017). *The Pursuit of Gender Equality: An Uphill battle*. Paris, France: OECD Publishing.
- OLE (2019). *Vinculación laboral de graduados*. <http://bi.mineducacion.gov.co:8380/eportal/web/men-observatorio-laboral/tasa-de-cotizacion-por-genero>
- Paderewski-Rodríguez, P., García-Arenas, M. I., Gil-Iranzo, R. M., González, C. S., Ortigosa, E. M., and Padilla-Zea, N. (2017). Initiatives and strategies to encourage women into engineering. *IEEE Revista Iberoamericana de Tecnologías del Aprendizaje*, 12(2), 106-114. 10.1109/RITA.2017.2698719
- Parra, L. (2008). Breve recuento histórico de las mujeres colombianas en la ciencia y la ingeniería. *Revista de Antropología y Sociología: Virajes*, 10, 155-166. <https://revistasoj.s.ucaldas.edu.co/index.php/virajes/article/view/805/728>
- Quintero, O. A. (2016). La creciente exclusión de las mujeres de la Universidad Nacional de Colombia. *Nómadias*, 44, 123-145. 10.30578/nomadas.n44a7
- Rodríguez-Rodríguez, I., Rodríguez, J. V., Ramallo-González, A., and Elizondo-Moreno, A. (2020). Percepción del profesorado español de diferentes etapas educativas respecto a cuestiones de igualdad de género en el ámbito docente. *Cuestiones de género, de la igualdad y la diferencia*, 15, 313-340. 10.18002/cg.v0i15.6217
- SNIES (2019). *Estadísticas*. <https://www.mineducacion.gov.co/sistemasinfo/Informacion-a-la-mano/212400:Estadisticas>
- Sterling, A. D., Thompson, M. E., Wang, S., Kusimo, A., Gilmartin, S., and Sheppard, S. (2020). The confidence gap predicts the gender pay gap among STEM graduates. *Proceedings of the National Academy of Sciences*, 117(48), 30303-30308. 10.18002/cg.v0i15.6217